Photoionization, Photodissociation, and Long-Range Bond Formation in Molecular Rydberg States

by

Edward Lees Hamilton

B.A., Calvin College, 1997

A thesis submitted to the

Faculty of the Graduate School of the

University of Colorado in partial fulfillment

of the requirements for the degree of

Doctor of Philosophy

Department of Physics

2003

This thesis entitled:
Photoionization, Photodissociation, and Long-Range Bond Formation in Molecular Rydberg States
written by Edward Lees Hamilton
has been approved for the Department of Physics

Chris H. Greene

John Bohn

Date

The final copy of this thesis has been examined by the signatories, and we find that both the content and the form meet acceptable presentation standards of scholarly work in the above mentioned discipline.

Hamilton, Edward Lees (Ph.D., Physics)

Photoionization, Photodissociation, and Long-Range Bond Formation in Molecular Rydberg States

Thesis directed by Prof. Chris H. Greene

The Rydberg spectra of atoms and small molecules offers an experimentally convenient probe for exploring the exchange of energy between Rydberg electrons and other forms of electronic, vibrational, and rotational excitation. This thesis investigates a series of special topics in the field of molecular Rydberg spectra, using a diverse set of theoretical techniques all designed to take advantage of the computational efficiency of the sorts of scattering parameterizations commonly associated with the field of quantum defect theory. In particular, I consider various mechanisms by which Rydberg electrons participate in the formation (bonding) and destruction (dissociation) of molecular states.

First, I review the methodology of multichannel quantum defect theory in molecular systems, demonstrating its versatility in reducing a complicated set of channel-coupled solutions into a physically observable photoionization spectrum with exceptionally high resolution, even in regions characterized by complex resonant structures with strong energy dependence. The utility of the Fano frame transformation is discussed, two approaches to the problem of extracting resonant effects via the delay of asymptotic boundary conditions are presented, and a case study featuring the molecular hydrogen isotopomer HD is examined in detail.

Second, I turn to the question of Rydberg electrons in the presence of both an ionic core and a neutral perturbing particle, extending certain basic features of the above philosophy to a two-center geometry. This system is predicted to give rise to a potential well that supports bound states, with a potential curve minimum existing at many hundreds or thousands of Bohr radii. The problem is first handled at the

level of a zero-range potential approximation, where the solution can be written by means of degenerate perturbation theory. This approach is compared to a more robust, but computationally expensive, description of the interaction in terms of a finite range model potential, requiring diagonalization of the Hamiltonian with respect to an L^2 basis. Some properties of these states are also noted. Next, a more powerful but difficult formulation using the Coulomb Green's function, subject to limiting boundary conditions at the position of the core and perturber, is derived. Finally, a semiclassical interpretation, corresponding to the trajectories of a point particle electron moving classically in a Coulombic field, is examined in detail.

Third, I return to the case of the diatomic Rydberg spectrum, this time extending the solution to accommodate dissociation pathways through the use of a Siegert pseudostate basis. Previously developed methods of treating the competition between ionization and dissociation are reviewed and evaluated. The Siegert basis is defined, together with an efficient procedure for its calcuation, and some of its unconventional properties are explicitly noted. The Siegert-MQDT method is applied to several reactive scattering or half-scattering processes, including photodissociation, dissociative ionization, and dissociative recombination.

Dedication

To my grandfather, Edward H. Hamilton, who unlike myself was not merely acquainted with electrons, but could also teach them to perform useful tricks.

Acknowledgements

A thesis is not so much the accomplishment of the mind of its author as it is the work of dozens of other minds being filtered through his own. The hope is that, in the course of the filtering, all that other work can directed toward a sharper focus, like water through a funnel or light through a lens.

My initial year at Colorado was challenging, and it seems appropriate to express my appreciation for those who helped me survive it. David Nesbitt, in addition to being a fine teacher (and based on his impromptu in-class barbershop performance, also a fine vocalist!), was a source of early encouragement. Carl Lineberger helped ease my transition by guaranteeing me a position my first summer out, when I was still figuring out where I wanted to go and what I wanted to do when I got there. My office mate Jeff Wright rescued me from certain of the more fiendish problems in Mr. Jackson's famous textbook on rather short notice, and displayed a reassuring combination of humor and good sense when the answers weren't so apparent to either of us.

My research colleagues have provided constant support in both professional, scientific, and personal capacities. Hugo van der Hart deserves credit for introducing me to b-splines, the beginning of a long and profitable relationship. (With the splines, I mean, although Hugo and I get along pretty well too.) Mark Baertschy was always available to explain why my eigenvalues were coming out complex, and other aracane curiosities of linear algebra. I only knew Jeff Stephens for a couple of months, but after using so many of his old codes to help me get off the ground my first year, I feel like I owe him

several years' worth of gratitude. But of the many other associates I could thank, Brian Granger stands out as a talented physicist and a decent person. He was always ready with a whiteboard and marker to walk me through the derivation, or photocopy his old notes from those beautifully organized binders. I owe him a special non-research-related commendation for mailing me a package across country. Trust me, it was important.

Last and foremost, Chris Greene has devoted an enormous investment of time and patience to teaching me just a small corner of his encyclopedic knowledge of AMO physics, and I can't begin to express my thanks for having access to his expertise. He is among the rare academics to have a talent for both instruction and research, without respecting any boundary between them; he lives in both worlds at once, the equivalent of wave-particle duality in academic science. If there is any uncertainty relation enforcing a tradeoff between the quality and scope of his work, then one can only assume that the h-bar that sets its bound must be infinitesimally small.

This research was supported with a grant from the National Science Foundation.

Contents

Chapter

Tables

Table

Figures

Figure

Chapter 1

Introduction

The progress of scientific thought has, at several critical junctures in history, depended essentially on something that can only be regarded, with the advantage of hindsight, as an exceptional stroke of good luck. The theory of celestial mechanics, as first developed by Johannes Kepler, involved several levels of fortunate happenstance: Kepler was lucky to have selected Mars for his studies, with its notably elliptical orbit capable of detection even by the rudimentary measurements of his era; he was lucky that the law he was in the process of discovering involved orbits that traced conic sections, a class of geometric constructs that had been the object of extensive study by the ancient Greeks for purely aesthetic reasons; and he was lucky that the motion of planets in the solar system, due to the mass disparity between them and the sun, could be described so well at the level of approximation as a set of noninteracting two-body systems. Without the benefit of Kepler's good fortune, Copernicus would not have been so quickly vindicated, nor would the foundation for Newton's subsequent development of gravitation been so firmly established.

By coincidence, it would be another researcher named Johannes who, three centuries later, traced Kepler's steps in recognizing an empirical law derived from the same inverse-square force law as Kepler's orbital mechanics– although, like Kepler, Johannes Rydberg had little appreciation of the physical basis for his empirical formula. (Ironically, his doctoral dissertation, written in mathematics before his interests turned to

physics, had been on the subject of conic sections.) As with Kepler's fortuitous choice of Mars, Rydberg had the benefit of several spectral lines of hydrogen (what we now know as the Balmer series) that lay well within the visible region of the spectrum. These lines had in 1885 been identified by yet another Johann, the Swiss schoolteacher Johann Jacob Balmer, as being well-characterized by the formula $\lambda \propto n^2/(n^2 - 2^2)$ [1], although Rydberg was not aware of this at the time he began his study. Rydberg, working from a larger library of spectroscopic data for hydrogen and the alkali metals, was able to successfully generalize Balmer's form of the transition frequency in 1888, with the now-familiar result [2]

$$\frac{n}{N_0} = \frac{1}{(m_1 + c_1)^2} - \frac{1}{(m_2 + c_2)^2}. \tag{1.1}$$

The names of the variables are here intentionally presented using Rydberg's original choice of symbols: n is the wavenumber of the emitted light, N_0 is the eponymous constant named in Rydberg's honor, and m_1 and m_2 are positive integers. The appearance of the additional constants c_i was, happily enough, the **only** modification necessary to extend the hydrogenic formula to the analysis of alkali spectra. And this, of all the providential manifestations of natural simplicity considered thus far, is the one with which this thesis shall be most properly concerned.

It would be an excusable generalization for one to observe that, in practical terms, Rydberg states are the only multiparticle states that are quantitatively understood at anything approaching the celebrated level of success achieved by quantum mechanics for ground state energies and wavefunctions. The tools of quantum chemistry that have so far been developed for the treatment of many particle systems rely chiefly on variational approaches that minimize variables (most commonly the total energy) subject to constraints, and as such generalize poorly to excited states. Only in the last twenty years have techniques for excited state ab initio calculation begun to achieve

reasonable success, and even then only at great computational expense [3]. The Rydberg states arising from a Coulombic potential, uniquely and fortuitously, pass over into a limit which reduces the complex electronic correlations into a simply parameterized form that reflects a nearly-exact integrability of the Schrödinger equation for the electronic potential. As a consequence, even molecular Rydberg spectra with a dizzying array of closely spaced resonances are still naturally tractable with respect to spectroscopic assignment. The more highly excited a Rydberg state becomes, the more it acquires the character of a perturbed hydrogenic state, and thus the more regular and predictable the associated structure is expected to become.

With sufficiently accurate spectroscopic methods, deviations from the general expression given above begin to emerge, reflecting a variety of subtle perturbative effects on the spectrum that would be difficult to detect through other methods. The analysis of Rydberg spectra effectively extracts quantitative information about the spatial distribution of electrons and nuclei in the core, as well as the partitioning of energy between possible modes of core state excitation. One important class of perturbative effects is associated with core anisotropy, arising from either the electrostatic multipole moments of the core geometry or induced polarization of the core electrons. Other small spectroscopic shifts may be attributed to relativistic modification of the motion and interaction of the Rydberg electron, including the so-called Casimir force. These corrections are all manifestations of the alteration of the long-range Coulombic potential, and can be expressed rather intuitively, albeit often non-trivially, as additional terms in the electronic Hamiltonian defining Rydberg motion. While these terms may possess complex tensorial character, they are essentially adiabatic in nature, and thus remain amenable to treatment within the familiar framework of adiabatic approximations.

Another important class of spectroscopic signatures for Rydberg-core interaction involves the sensitivity of the Rydberg electron to short-range many-particle dynamics in the immediate vicinity of the core structure. Due to the disproportionality of the

spatial probability distribution of the highly excited electron relative to that of the (at most weakly excited) core, the volume over which such interactions can contribute is necessarily small. For Rydberg states with more than a few quanta of angular momentum, the resultant centrifugal barrier shields the core entirely, and all short-range effects are buried deep inside of the inner turning point of the effective potential. For any case where the Rydberg wave function extends even slightly into the core volume, however, the core may exert substantial effects on the solution within that volume, and thereby alter the stationary superposition of hydrogenic solution states in the asymptotic Coulomb region as well. Further discussion of the origin of these effects will be deferred until Chapter 2; for the moment, it suffices to note that they require a fundamentally non-Born-Oppenheimer description. When the electron is far from the core, it has relatively little kinetic energy, and its motion cannot be considered "fast" on the time scale of core dynamics; when the electron is close to the nucleus, it has enormous kinetic energy due to proximity to the singularity of the Coulomb potential, and enters and exits the core volume on a time scale much faster than any adiabatic rearrangement of energy within the core. In summary, one may instructively observe that the Rydberg electron lives in one region of space where the Born-Oppenheimer potential is valid but the single particle approximation fails due to strong correlation with the other electrons and coupling with the core degrees of freedom, and one region of space where the single particle approximation is valid but the Born-Oppenheimer approximation fails due to the decoupling of the slow Rydberg electron from the geometry and orientation of the core state.

1.1 Historical development of experimental technique

The separation between lines arising from the manifolds of a hydrogenic energy spectrum diminishes rapidly with increasingly primary quantum number n, as $\frac{1}{n^3}$. The difference between the $n = 99$ and $n = 100$ manifolds is already less than half a

wavenumber. Selective excitation of a particular state either within or near a particular manifold (when, for example, the usual selection rules are broken by the introduction of a small external static electric field) demands even greater control over the energy and linewidth of the incident light. The extraction of detailed structure within the Rydberg spectrum has thus been dependent upon advances in the efficiency with which light can be produced at both high intensity and narrow bandwidth. Prior to the advent of modern laser optics, this required the use of dispersive instruments such as prisms and diffraction gratings to isolate monochromatic components of a broadband source. The task was further complicated by the necessity of working under vacuum conditions due to the strong continuum absorption of common background gas components in the ultraviolet, where Rydberg transitions of atoms and small molecules are most commonly observed. Molecular oxygen becomes opaque below 1850 Å, and molecular nitrogen below 990 Å. (For a survey of some early difficulties of the development of spectroscopy in the VUV, see [4].)

In light of these experimental difficulties, it is understandable that high-resolution Rydberg spectroscopy did not attain sufficient resolution to detect small (i.e., on the order of a wavenumber) structure and shifts until the late 1960s and early 1970s. The earliest high resolution discrete absorption spectrum of molecular hydrogen was that conducted by Herzberg [5], and the first high resolution continuum spectrum was that of Dehmer and Chupka [6]. These results, improving on previous resolution by as much as two orders of magnitude, not only successfully resolved the rotational and vibrational separations of the molecular spectrum with precision better than a fraction of a wavenumber, but also were capable of accurately defining line widths and shapes to an extent that prompted the development of new theory describing strong energy dependence (i.e., resonant effects) of the photoexcitation cross-sections with quantitative rigor.

The emergence of even better experimental methodology in the last twenty years

has continued to improve the quality of Rydberg spectroscopy. Noteworthy examples include the popularization of high-intensity synchrotron radiation sources, permitting even weak features in the spectrum to contribute an observable signal, and the introduction of narrow bandwidth laser sources extending into the far ultraviolet through the use of tunable lasers, frequency doubling, and higher harmonic generation. Laser technology has not only superseded the use of dispersive monochromators, but has also opened the door to exquisitely fine control over the phase and coherence properties of the incident light. Among the many delicate effects now accessible by experimental techniques are the tunneling between the vibrational potential wells of highly excited double-well adiabatic H_2 potential curves [7], the breaking of g-u symmetry in HD, [8], singlet-triplet mixing near the H(n=1)+H(n=2) dissociation limit [9], and competition between dissociation and ionization decay dynamics in the regions of the H_2 spectrum in an energy regime where multiple dissociative fragmentation channels are simultaneously open [10].

1.2 Emerging applications for Rydberg state theory

Much of the appeal of Rydberg states lies in their potential to serve as a bridge between classical and quantum mechanics. Traditionally, the former has been associated paradigmatically with macroscopic systems, and the latter with microscopic systems. In theory, of course, classical mechanics is merely the expression of certain limiting procedures necessary to extend quantum theory to systems with arbitrarily large particle numbers, energies, and state densities. With respect to the boundary between the classical and quantum regimes, one may identify two areas of burgeoning recent research interest: First, techniques to demonstrate explicitly quantum mechanical properties on a macroscopic (or at least mesoscopic) scale, and second, new methods to control or selectively influence the evolution of quantum systems.

Much of the renewed interest in atomic physics generally may be attributed to

rapid improvements in laser trapping and cooling technology. From the standpoint of Rydberg spectroscopy, the ability to cool atoms to temperatures to fractions of a Kelvin is especially appealing, since highly-excited states can survive for long times under such conditions, allowing their evolution over time to be systematically manipulated and externally directed toward a controlled outcome. Possibilities include arranging Rydberg atoms in an orderly spatial geometry, entangling them with one another, constructing Rydberg electron wavepackets that mimic classical particles or display long-time recurrence effects, and exploring the controlled or spontaneous transition of Rydberg atoms into molecules or plasmas.

The range and diversity of such work has been extensive enough that it can only be surveyed here by a selected subset of representative examples. Rydberg atoms have been proposed as a pathway to quantum information processing, either via a dipole blockade effect [11, 12], entanglement in superconducting cavities using microwave photons [13], or half-cycle pulses shaped using optimal control theory [14, 15]. A system of cold trapped atoms excited to high Rydberg levels has been observed to evolve spontaneously into a cold plasma, at temperatures four orders of magnitude lower than any other method of cold plasma generation, in a phase transition postulated to be analogous to the Mott transition in semiconductors [16, 17, 18, 19]. The angular momentum composition of Rydberg wavepackets has been selectively controlled by phase-locked laser pulses [20]. The coherent control of a four-wave mixing signal has been observed as a manifestation of the interference between Rydberg excitation pathways [21]. The collision potentials between Rydberg atoms have been examined in detail, revealing curve crossings at thousands of a.u. capable of supporting bound vibrational levels [22], which may already have been experimentally observed [23]. Finally, Rydberg states have been proposed as a sensitive probe of small electric fields and gas phase ion concentrations, as well as various other measurements of fundamental molecular constants like ionization potentials and ionic energy level structure [24].

Less attention has been paid to what might be termed "Rydberg chemistry", the study of bond formation and dissociation processes facilitated or influenced by the presence of Rydberg electrons. Such applications would define a new field of conceptual overlap between the increasing interest in quantum control of chemical reaction products, in the physical chemistry community, and the atomic Rydberg investigations by the AMO community discussed above.

1.3 Outline of presented topics

In this thesis I explore a number of the properties of molecular Rydberg state solutions, and the calculation and analysis of spectroscopic observables. In the development of new techniques and predictions, one logically begins by working from the simplest cases toward the more complex, and the simplest of all molecules are homonuclear diatomics. I shall consider two varieties of diatomic Rydberg bound states, one being the more conventional case in which the molecular ion is bound by the core electrons, with the Rydberg electron serving as a probe of the core structure and dynamics, and the other being long-range molecules with two distantly separated centers in which the bonding is controlled by the Rydberg electron itself.

In Chapter 2, I introduce the basic concepts and vocabulary of scattering theory in an informal overview. The significance and origin of resonances is considered, with particular attention to their relationship to the different classes of motion that characterize the degrees of freedom that create resonant effects. I specialize to the example of molecular hydrogen, and move on to the consideration of multichannel spectroscopy, and how it can be described from the standpoint of a quantum defect formalism. The spectrum of the molecular hydrogen isotopomer HD is calculated by way of quantum defect theory in conjunction with application of Fano's frame transformation procedure, followed by a critical assessment of the limitations of the approach.

Chapter 3 pursues the separate topic of the perturbed spectrum of a Rydberg

atom in the presence of a ground state atom or molecule. The interaction between the Rydberg electron and the perturbing atom or molecule is first considered at the level of a zero-range interaction approximation, where the particle is described by a delta function potential with a strength proportional to the energy-dependent generalization of the scattering length. This approximation yields an exact analytical result in degenerate perturbation theory for a hydrogenic Rydberg atom, if spin-orbit and other degeneracy-breaking terms can be neglected. The results of this approximation are tested by means of a more detailed finite-range model pseudopotential defined in a way that separates out scattered partial waves non-locally. Properties of the bound state potentials that arise from such interactions are noted and discussed.

Chapter 4 returns to the same problem, but instead treats it using a Green's function formalism. I demonstrate the ability of this method to reproduce the other methods of the previous chapter, both for the hydrogenic and finite quantum defect cases. The case of perturbation of a Rydberg molecule by a weak external electric field is considered, with example calculations. Finally, some relationships between semiclassical closed-orbit theory and the nodal pattern of the quantum wavefunction.

Chapter 5 revisits the diatomic photoionization spectrum, and introduces the complication of competing dissociative processes. The history of methods that treat competition with the dissociative continuum is reviewed, and the advantages and limitations of various methods are observed. As an alternative to these, I propose a new representation of coupling to the continuum, using a discretized pseudostate basis obeying Siegert boundary conditions. The properties of Siegert pseudostates are briefly summarized, and a recently developed method for their efficient generation is described. Using these pseudostates as a finite basis representation for the MQDT-frame transformation technique, it is shown that scattering into the ionization and dissociation continua can be treated simultaneously within a unified formalism.

Chapter 2

General review of molecular MQDT

For over a century, spectroscopy has served as a faithful midwife for the birth of countless new discoveries in modern chemistry and physics. Bohr's theory of the atom was designed to accommodate classical stoichiometric concepts of valency to explain the spectra of hydrogen and alkali atoms. Organic chemists depend on infrared spectroscopy to detect the presence of certain bond types, and the study photoelectron spectra in the visible and ultraviolet regions to draw inferences about the distribution of electrons within those bonds. Biologists utilize the sensitivity of fluorescence decay lifetimes to perturbation by analyte atoms and molecules in order to perform image mapping of cellular structure. The reflectance and emission spectra of rocks and minerals provide clues to geological history, whether of the upheaval of the Earth's crust or of the flow of ancient rivers on Mars. Astronomers rely on spectroscopic observations to determine the composition of stars, as well as their distance, their age, their motion, their temperature, the influence of any extra-solar planets they might support, and the density and composition of the diffuse interstellar matter through which their light subsequently travels. The most accurate clocks in the world depend on spectroscopic standards, as does the definition of the SI unit of length, the meter. The spectroscopic study of distant galaxies and quasars is essential to the pursuit of fundamental cosmological questions regarding the distribution of matter in the universe, its age and early history, and the possible variation of fundamental physical constants over cosmic time scales.

The richness of the information available from spectroscopic analysis is belied by its complexity. The farther removed one becomes from the simple picture of transitions between discrete hydrogenic levels, the more difficult it becomes to make sense of the dense forest of spectroscopic features that encode the details of an atom or molecule's nanoscale structure and dynamics. [1] This onset of complexity may be related to several successive complications of the primitive hydrogenic picture: first, the transition to systems with multiple interacting electrons; second, the passage beyond bound state transitions to the consideration of excitations into the scattering continuum; third, the existence of multiple internal degrees of freedom that may be simultaneously excited, and subsequently exchange energy with one another.

This thesis will be concerned with the resonant continuum spectroscopy of atoms and molecules, for which all three complications are potentially present and important. By the "continuum", we refer to any region of the spectrum that describes complete separation of two fragment particles, either of an electron from its parent atom, molecule, or ion, or of two dissociative fragments that result from the cleavage of a bond in a molecule or molecular ion. Since the potential energy of separating fragments is not subject to quantization, the states of the continuum region are continuously distributed. The spectrum of such a region, however, will in general display quite complex and irregular peak and valley structures that signify the presence of resonant scattering effects. The distribution, shape, width, and intensity of these features reflect the geometric configuration and dynamic evolution of the system during the brief period in which fragmentation occurs. [2]

Throughout this chapter, as well as in chapter 5, molecular hydrogen is used for illustrative purposes, as well as for various example calculations. Molecular hydrogen

[1] The British biologist and Nobel Laureate Francis Crick famously described the interpretation of a complicated biomolecular spectra as being "like trying to determine the structure of a piano by listening to the sound it made while being dropped down a flight of stairs."

[2] The material in this introduction, and the two sections following, is discussed in most introductory graduate level atomic/molecular physics textbooks. See, for example, chapters 9-12 of [25] or chapters 1-3 of [26].

is a homonuclear diatomic, and as such it is characterized by greater symmetry than heteronuclear diatomic or polyatomic molecules. This greatly simplifies the analytical form of many expressions, sacrificing generality for the sake of improved conceptual clarity. For sake of comparison, some discussion and computational results for the more complicated diatomics N_2 and NO can be found in [27], and a recent example of the successful application of quantum defect theory to a simple polyatomic system is presented in [28].

2.1 Degrees of freedom in molecular physics

In a molecular system, there are four classes of motion: electronic, vibrational, rotational, and translational. Since all inertial frames of reference are physically equivalent, the translational motion can be eliminated by a transformation to the rest frame of the molecule, with no effect on the observed spectrum other than an overall Doppler shift. (For a macroscopic sample, of course, translational motion is randomized and these effects are averaged over many atoms, imposing a limit on experimental resolution.) All other motions, however, are fully quantized, potentially spectroscopically active (subject to the relevant symmetry-dependent selection rules), and in general define degrees of freedom in which energy can be stored and potentially transferred by coupling to the other degrees of freedom.

The fact that the motion can be resolved in this way is a consequence of the differing energy scales with respect to which these motions occur. The separation between electronic energy levels is commonly on the order of a few tenths of an atomic unit, at least for the lowest levels, and the associated transitions appear as lines in the visible or ultraviolet. The separation between vibrational levels is on the order of thousandths of atomic units (10^2 to 10^4 cm^{-1}), and appears in the infrared. The separation between rotational levels is on the order of hundreds of thousandths of an atomic unit (10^0 to 10^2 cm^{-1}), extending into the far infrared or microwave. These figures are all approx-

imate, of course, and the vibrational and rotational level splittings depend specifically on the masses of the nuclei; molecular hydrogen and its isotopomers have light nuclei (protons or deuterons), for example, and thus their splittings are increased by an order of magnitude relative to a heavier molecule like NO.

Table 2.1 shows the level spacings for molecular hydrogen relative to the ground state. This data is representative of the literature references used to check the accuracy of the rovibronic energy levels in my own computations. For extended discussion of the techniques used to calculate these and similar quantities, including the absolute dissociation threshold energy of the H_2^+ and HD^+ molecular ions that are used to fix the spectrum relative to threshold in the example calculations, see [29, 30, 31, 32, 33, 34].

Table 2.1: Tabulation of the lowest rovibrational levels for molecular hydrogen, in cm^{-1}, based on the *ab initio* data of [35]. These values reflect the inclusion of both adiabatic and nonadiabatic correction terms beyond the Born-Oppenheimer approximation.

v	J=0	J=1	J=2
0	0.0	118.5	354.4
1	4161.2	4273.8	4497.9
2	8087.0	8193.8	8406.4
3	11782.5	11883.6	12084.8
4	15250.5	15345.9	15535.8
5	18492.1	18581.9	18760.5

The time scale associated with motion in a particular degree of freedom is inversely proportional to its energy splittings, and thus the differences in energy scale can also be interpreted as defining a hierarchy of time scales. Rotational motion is much slower than vibrational motion, and both are slow relative to electronic motion. Conceptually this means that an electron experiences the nuclear structure of a molecule as "fixed in space"; the nuclei, inversely, experience the electron only as a highly averaged spatial distribution of its motion. The result is an approximate separability of the equations of motion governing these two disparate degrees of freedom; when this assumption is taken to be exact, the result is the familiar *Born-Oppenheimer approximation*. To find

a Born-Oppenheimer solution, the nuclei are first frozen in space, and the electronic Hamiltonian diagonalized subject to the potential for that configuration. The electronic calculation is repeated for a systematically varied range of nuclear coordinate values, mapping out variation in energy levels to define associated potential surfaces. The potential surface is then used to define a Hamiltonian controlling the nuclear motion, which is diagonalized for the vibrational energy spectrum and vibrational wavefunctions.

Figure 2.1 shows the lowest electronic singlet *ungerade* potential curves for molecular hydrogen and the Rydberg series limiting curve of the molecular ion, based on data from the *ab initio* calculations of Kolos and Wolniewicz. Notice the avoided crossing in the $4^1\Sigma_u$ curve, resulting from the crossing of a repulsive electronically autoionizing (doubly excited) state potential curve that descends through this region, creating a similar series of avoided crossings with all of the singly excited electronic states higher than n=4.

At the level of the adiabatic approximation, the quantum defect may be defined in the molecular body frame as a function of the internuclear separation R,

$$U_{n\Lambda}(R) = U^{+}_{1s\sigma}(R) - \frac{1}{2}[n - \mu_\Lambda(R)]^{-2}. \tag{2.1}$$

In practice, the quantum defect function $\mu_\Lambda(R)$ has a weak energy dependence, although it rapidly approaches an energy-independent value for increasing principal quantum number n. For energy-independent quantum defect calculations, the quantum defect must be defined either relative to one particular potential curve, or else through some limiting procedure in the energy. As an additional approximation, the curves are here diabatically continued through the avoided crossings, since the the relation in Eq. 2.1 assumes there are no avoided crossings with other electronic states. (This is a reasonable approximation for the *ungerade* states reached in ground state photoionization of H_2, since the avoided crossings appear outside the Franck-Condon region and have little

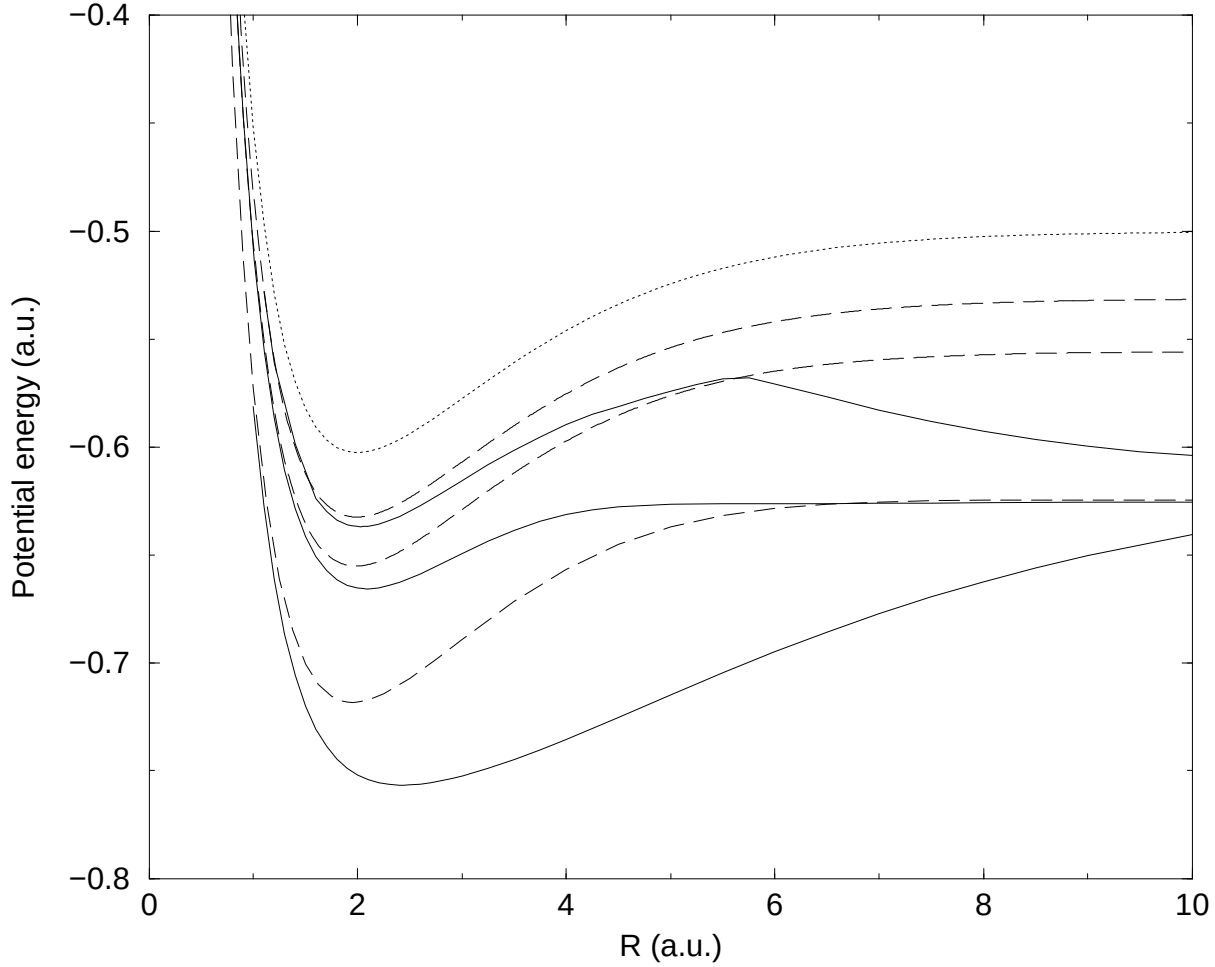

Figure 2.1: Potential energy curves for the Σ (solid) and Π (dashed) symmetries of H_2, together with the ionic potential curve (dotted), based on the *ab initio* calculations of Kolos and Wolniewicz [36].

influence on the preionization spectrum.) For the sake of all remaining calculations in this section, we will use the 5Σ and 6Π potential curves to define the energy-independent quantum defects, as shown in Figure 2.2. The potential curves associated with these defects are shown in Figure 2.3, giving some visual estimation of the extent of the approximation involved in neglecting energy dependence. The most obvious error is the catastrophic failure of the 2Σ state to reach the correct asymptotic limit. The higher Rydberg states that dominate the continuum spectrum, however, are quite well described by the energy independent approximation. Corrections to this approximation are discussed in [37, 38, 39].

The rotation and vibration of a molecule are coupled more strongly than the nuclear and electronic degrees of freedom, by a combination of centrifugal and Coriolis-like terms of the Hamiltonian. In general, one should not speak of separable vibrational and rotational states, but only a fully coupled "rovibrational" state that obeys the entire nuclear Hamiltonian. To a good approximation, however, the energy of such a state is still recognizable as the combination of a rotational excitation and a vibrational excitation, provided the rotational excitation is small.

The coupling between rotation and electronic angular momentum is particularly sensitive to the excitation of the Rydberg electron. The low temperature spectrum of molecular hydrogen is strongly influenced by an l-uncoupling process, whereby the electron undergoes a gradual transition from the low n case of being strongly coupled to the internuclear axis (Hund's case [b], where the approximately "good" quantum number Λ is the projection of the total orbital angular momentum onto the internuclear axis) to the high n case where the electronic angular momentum decouples from the symmetry axis and is instead quantized along the ionic core's axis of rotation (Hund's case [d], where the approximately "good" quantum number N^+ is the rotational angular momentum of the core). In the range n=6-10, the coupling is mixed, and both Λ and N^+ are only meaningful in an approximate sense.

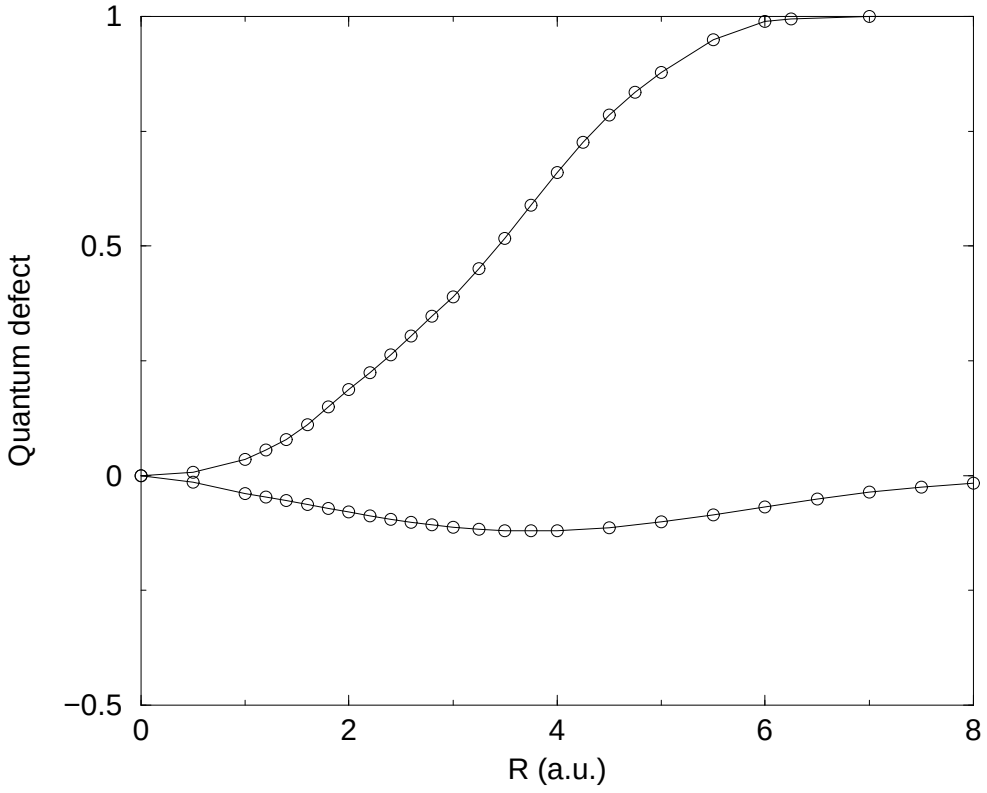

Figure 2.2: Quantum defects for the Σ (solid) and Π (dashed) symmetries of H_2, based on the fittings of Jungen and Atabek [40].

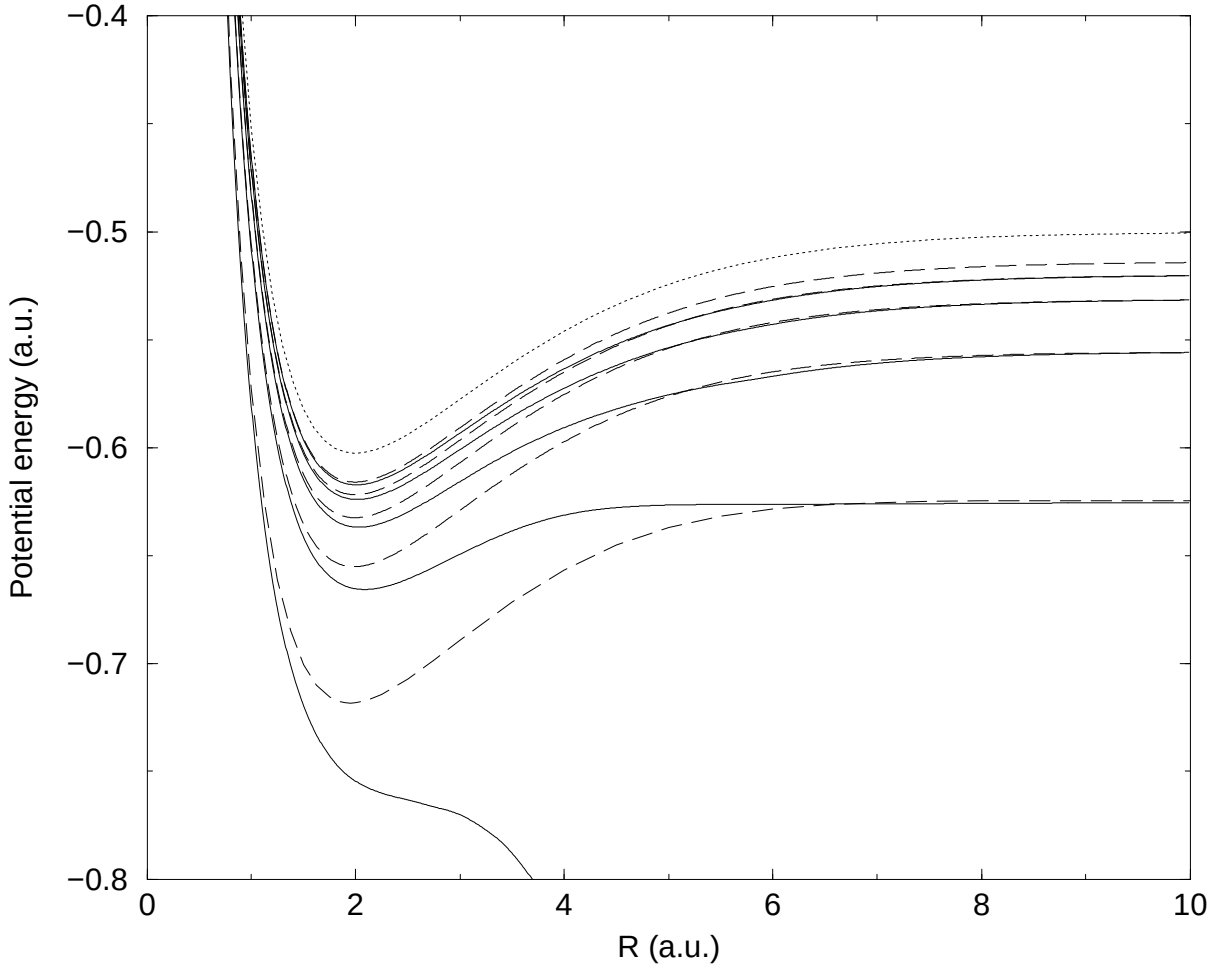

Figure 2.3: Effective energy-independent potential energy curves for the Σ (solid) and Π (dashed) symmetries of H_2, based on the quantum defects in Figure 2.2, together with the ionic potential curve.

2.2 Resonances

In phenomenological terms, a resonance in the continuum scattering behavior of a dynamical system appears as a strong and localized energy dependence. This may manifest itself as either an enhancement or a suppression of the background cross-section. Mathematically speaking, a resonance is associated with the existence of a nearly bound state of the Hamiltonian, an approximate eigensolution that would become a true bound state if the Hamiltonian were modified in some intentional way. Resonances in atomic and molecular physics result in continuum wavefunctions that accumulate probability density in some restricted region of configuration space for which the magnitude of the separation between the scattering particles is "small", such that it resembles the distribution of a bound state wavefunction of the two-particle system. If a state at a resonant energy is initially prepared in a superposition that gives it a spatial distribution localized in this way, it will generally remain localized for a long period of time before slowly decaying into the exterior continuum region; in time dependent terms, a resonance can be described as a decaying nearly-bound state, with an associated lifetime inversely proportional to the strength of its coupling to the surrounding continuum.

Resonances commonly arise from one of two situations. A *shape* resonance occurs when the single-channel potential describing the interaction of two particles has a local maximum separating two regions, and the scattering energy is below the energy of this maximum such that it lies at what would become a bound state in the inner region if the potential beyond the local maximum were replaced by an infinite wall. In the time-dependent picture, a particle must travel back and forth between these regions by tunneling through the potential barrier; since tunneling probability is exponentially sensitive to the height of the barrier, the particle can be effectively trapped inside the inner region for a duration sufficient to complete many cycles of the orbital period appropriate for classical motion within the local potential well. Shape resonances in

electron-atom or atom-atom interactions are commonly encountered as a result of the centrifugal correction to the effective potential arising from the $\frac{(l+1)l}{2r^2}$ repulsive term; attractive interactions are typically shorter-range, and thus the cross-over between the strong but shorter-range attractive potential region and the weaker but longer-range repulsive potential region creates a local maximum close to threshold for scattering states with a finite angular momentum.

A *Feshbach* resonance is the result of coupling between channels associated with the excitation of additional degrees of freedom in a system. For example, the energy associated with two electrons being simultaneously excited to hydrogenic Rydberg states would, in the absence of electron correlation, be a stable doubly excited state. Since one of the two electrons may relax back into the ground state and give up its energy to promote the other into the continuum, the doubly excited state is unstable with respect to autoionization, and the two-particle bound state solution instead becomes a resonance. In molecular systems, autoionizing resonances can also result from coupling to the nuclear degrees of freedom. Because of small terms in the Hamiltonian that violate the Born-Oppenheimer assumptions and introduce coupling between the nuclear and electronic motion, a system excited in both a nuclear and an electron degree of freedom is unstable with respect to transfer of energy from the nuclear excitation into the electron (if it has a total energy greater than the ionization threshold). As a result, the electron is able to escape into the continuum. At the energy of the hypothetically uncoupled doubly-excited state, the continuum will show a *preionization* resonance, a resonance that reflects the existence of a short-lived metastable state that eventually undergoes ionization. Similarly, if the hypothetical doubly-excited system is above the energy required for dissociation, the electron can relax to a lower energy level, transferring its energy to the nuclear motion and yielding a *predissociation* resonance. If both types of continua are energetically accessible at once, then the processes will compete, with relative intensities of the preionization and predissociation spectra at that energy that

correspond to the probabilistic branching ratio between the two processes. (we shall set aside the question of predissociation until Chapter 5, and for the moment limit attention to the preionization spectrum.)

Bound states are characterized by a single intensity parameter, governed (in the limit of the dipole approximation) by the dipole oscillator strength of that transition. The width of a bound state transition line is generally controlled by spectral broadening effects that arise from the finite thermal energy of the sample; as the temperature is decreased, the lines become sharper. Bound state transition lines cannot be made arbitrarily narrow, however, due to the natural linewidth arising from their finite lifetime for decay back to the ground state. Resonances, on the other hand, have a natural width associated with the much faster time scale for energy interchange between coupled degrees of freedom; they can correspondingly display much larger linewidths. The shape of a bound state transition line is usually a symmetric Gaussian, in accordance with the exponential Maxwell distribution of kinetic energies at finite temperature. Resonances, by contrast, have a (potentially asymmetrical) Fano line shape. The asymmetry can be explained by recognizing that the excitation to the continuum can occur either by a direct pathway (just as at non-resonant energies), or by the creation of the intermediate autoionizing state; these two pathways must be summed coherently, and thus could give rise to either destructive interference (suppressing the intensity) or constructive interference (enhancing the intensity). Depending on the value of the lineshape parameter, the peak may even be converted into a window resonance, a nearly symmetric dip in the cross-section.

In the limit of extremely weak coupling (and thus extremely long decay lifetime), resonances strongly resemble bound states. Indeed, as the coupling vanishes, a resonance must pass over smoothly into a true bound state embedded in the continuum. Although the continuum itself is uniformly and densely packed with states, it is possible to imagine taking a carefully arranged linear combination of continuum wavefunctions

(with, in general, complex coefficients) that behaves very much like a discrete eigenstate [41, 42]. In particular, it will display time dependence proportional to $e^{iE_a t}$, where E_a is a complex value; the real part of E_a describes periodic motion within the local quasi-binding potential, and the imaginary part describes the slow leak of electron probability density into the rest of the continuum. This complex energy state is in some sense the optimally discretized eigenstate of the Hamiltonian for representing that particular resonant process; it is a true pole of the scattering Green's function, analytically continued into the complex plane. One can imagine performing the same transformation in the other direction; taking a finite basis of such scattering eigenstates, and using them as a representation of a portion of the continuum. we shall revisit this idea in chapter 5.

For the Coulomb potential of an electron in a neutral molecule, there exists an infinite number of excited electronic Rydberg states. The ionizing electron leaves behind a molecular ion which may be in either the ground state or any energetically accessible rotationally or vibrationally excited state. The residual state, in conjunction with all other quantum numbers needed to describe the escaping electron, is termed a *channel*, and labeled by the appropriate rotational or vibrational quantum numbers of the molecular ion. (The use of asymptotic states to define the channel labels provides a natural connection with the scattering matrix (or S-matrix) representation of the scattered continuum wavefunction– the indices of the S-matrix correspond to the asymptotic channels.) The energy at which a channel becomes energetically accessible, or *open*, is simply the energy of the molecular ion in that rotational and vibrational state. At lower energies, the channel is closed, but still influences the continuum by creating an infinite series of Rydberg resonances. Unlike bound state transitions, which have experimental widths that reflect an incoherent sum over many particles in a sample, resonances can (and frequently do) overlap with one another and produce complicated interference effects. In particular, resonances belonging to a Rydberg series attached to one channel threshold may interact with resonances belonging to a different channel threshold. If the

two series have distinct properties– say, one has broad widths and decays primarily by ionization, and the other is narrow and decays primarily by dissociation– the composite effect on the (coherent) total spectra can be quite complex and difficult to untangle. Surmounting this difficulty is the principal task of theoretical multichannel Rydberg spectroscopy, known more commonly in the literature as multichannel quantum defect theory (MQDT).

2.3 Channel elimination: Traditional and energy-smoothed approaches

Quantum defect theory begins from the assumption that the N_o independent solutions of an N_o-channel Schrödinger equation can be written as an expansion with terms consisting of a product of channel functions (describing the state of the core and all degrees of freedom of the outer electron except the fragmentation coordinate) and a linear combination of radial Coulomb functions. These long range solutions, valid beyond the region where channel coupling remains significant, can be written in more than one representation, but a convenient choice for conceptual purposes is the outgoing wave form

$$\Psi_{i'}^{phys}(E) = \mathbf{A}\sum_{i}^{N_o}\frac{1}{r}\Phi_i(\omega)[f_i^+(r)Sii'^{phys} - f_i^-(r)\delta_{ii'}],\ r\to\infty, \tag{2.2}$$

where the scattering matrix is labeled with the superscript *phys* to denote that only channels which are energetically accessible (open) will contribute to the sum. The Coulomb functions $f_i^{\pm}(r)$ are those that obey incoming and outgoing wave boundary conditions [43], and the operator $\mathbf{A}$ denotes a formal antisymmetrization procedure. In this expression, $\Phi_i(\omega)$ includes the total wavefunction of the core associated with ionic threshold energy E_i, and the spherical harmonics $Y_{lm}(\theta,\phi)$ and spin wavefunction of the outer electron. For the example system of molecular hydrogen, we adopt the approximation that only p-wave scattering contributes to the state probed in total

absorption– even parity states are symmetry forbidden transitions, and f and higher partial waves are unable to penetrate through the centrifugal barrier into the coupling region– and thus the index i describes only the vibrational and rotational states v^+, N^+ of the core. (In fact, for the calculation for HD in the following section the breakdown of *gerade-ungerade* symmetry compromises the accuracy of this approximation, but this is expected to only be significant in the vicinity of the dissociative thresholds of highly excited vibrational states.)

The critical point realized by Seaton, Fano, and other MQDT pioneers is that the asymptotic boundary conditions implied by the above expression need not be enforced until the final stage of the calculation. The short range interactions involved in the creation of auto-ionizing resonances can be fully included by the use of an alternate expansion that incorporates an additional N_c accessible excitation channels, whose Rydberg electron channel energies are below the threshold for ionization. This modified expression is still only accurate beyond some value r_0 bounding the small-r region where coupling occurs, and can be written in the similar form

$$\Psi_{i'}(E) = \mathbf{A}\sum_{i}^{N}\frac{1}{r}\Phi_i(\omega)\frac{1}{i\sqrt{2}}[f_i^+(r)S_{ii'} - f_i^-(r)\delta_{ii'}], r > r_0. \tag{2.3}$$

Here $S_{ii'}$ indicates a quantity familiar in multichannel quantum defect studies, the *smooth, short-range* N-channel scattering matrix.

Roughly speaking, the i'-th independent solution in Eq. (2.3) describes a simple one-step scattering process in which the outermost electron encounters the ionic core while moving inward in channel i', and scatters outward into all channels i. Some of the i channels may be energetically closed at $r \to \infty$, but the finiteness boundary condition has not yet been imposed.

In order to remove unphysical closed-channel divergences, the usual MQDT "channel-elimination" procedure is employed, which amounts to forming an appropriate linear

combination of the solutions in Eq. (2.3) to construct the physical scattering matrix. We write this expression in the form used in Ref. [44], in terms of the Hermitian conjugate of S, partitioned into open and closed sub-blocks:

$$\mathbf{S}^{\dagger phys} = \mathbf{S}^{\dagger}_{\mathbf{oo}} - \mathbf{S}^{\dagger}_{\mathbf{oc}}[\mathbf{S}^{\dagger}_{\mathbf{cc}} - e^{2i\beta}]^{-1}\mathbf{S}^{\dagger}_{\mathbf{co}}. \tag{2.4}$$

The four matrices in the right-hand side of (2.4) are physically open and closed partitions of the smooth, short-range scattering matrix (Hermitian conjugated) from Eq. (2.3),

$$\mathbf{S}^{\dagger} = \begin{pmatrix} \mathbf{S}^{\dagger}_{\mathbf{oo}} & \mathbf{S}^{\dagger}_{\mathbf{oc}} \\ \mathbf{S}^{\dagger}_{\mathbf{co}} & \mathbf{S}^{\dagger}_{\mathbf{cc}} \end{pmatrix}. \tag{2.5}$$

The matrix β is diagonal and of dimension $N_c \times N_c$; its elements $\beta_i = \pi[-2(E - E_i)]^{-1/2}$ are the Coulomb phase parameters in each closed channel. These quantities vary strongly with energy near their respective thresholds, and account for nearly all the energy dependence of the physical scattering process. This allows the expression to correctly describe resonant spectra even while the energy dependence of the smooth, short-range scattering matrix is entirely neglected.

The physical significance of the eigenvalues of the scattering matrix, as first realized by Fano [45], centers on the recognition that $\mathbf{S}$ will be diagonal in the representation where the short-range Hamiltonian is diagonal. That is, there exist $N = N_c + N_o$ solutions, the *eigenchannel* solutions Φ_α, each of which have a common phase shift $\pi\mu_\alpha$ in all physical channels. The scattering matrix can be recovered from the eigenchannel defects μ_α by means of a transformation,

$$S_{ii'} = \sum_\alpha U_{i\alpha} e^{2i\pi\mu_\alpha} (\mathbf{U}^T)_{\alpha i'}. \tag{2.6}$$

The matrix $\mathbf{U}$ is known as the frame transformation matrix as a consequence of its role in transforming from the short-range ("body frame") diagonal representation to the long-range ("lab frame") electron-plus-core representation. In the inner region, the

outer electron is moving fast enough that a definite value of the internuclear separation R and orbital angular momentum along the axis Λ can be defined; in the outer region, the electron is moving slowly on the time scale of nuclear motion, and the system is more appropriately described by the ionization channel indices. The rotational and vibrational components of the frame transformation matrix can be separated to give

$$U_{i\alpha} = \langle i|\alpha\rangle = \langle v^+|R\rangle^{(N^+)}\langle N^+|\Lambda\rangle^{(lJ)}. \tag{2.7}$$

The first factor is simply the vibrational wavefunction for the v^+ state, and the second factor is a rotational frame transformation matrix element defined in [27]. Note that this expression assumes that a single value of the orbital angular momentum l is present. If additional partial waves contribute significantly in the outer region, then the form of this transformation becomes more complicated.

The eigenchannel quantum defects, since they are labeled by quantities that are meaningful in the Born-Oppenheimer limit, can be extracted from the bound state potential energy curves of H_2 through their definition given in Eq. 2.1. The actual use of these quantum defects in a numerical frame transformation is problematic owing to the continuous variable R, which effectively necessitates an infinite number of channels to be included in the scattering matrix. In practice, however, a reasonable approximation to the exact frame transformation can be accomplished by truncating the sum over alpha after a relatively small number of vibrational states (usually of the order of one or two dozen per ionic rotational quantum number in this work). The approximate frame transformation matrix is formed from the eigenvectors of the quantum defect matrix, defined by

$$\mu^{(J')}_{v^+N^+,v^{+\prime}N^{+\prime}} = \sum_{\Lambda}\langle N^+|\Lambda\rangle^{(lJ')}\left[\int dR\langle v^+|R\rangle^{(N^+)}\mu_\Lambda(R)\langle R|v^{+\prime}\rangle^{N^{+\prime}}\right]\langle\Lambda|N^{+\prime}\rangle^{(lJ')}, \tag{2.8}$$

The numerical diagonalization of Eq. 2.8 is generally more convenient than direct construction and diagonalization of the scattering matrix itself.

Because of the weak energy dependence of the quantum defect (see Ref. [37]) a single function for each body frame symmetry, $\mu_\Lambda(R)$, suffices to describe all bound state potential energy curves of the π symmetry, and provides a reasonable approximation to most higher n curves of the σ symmetry. We follow Raoult and Jungen [46] in selecting an eigenquantum defect function derived from fitting to the bound states of the n=6 curve for the σ case, and n=5 for π. Since the $3p\sigma$ state deviates substantially from this simple approximation, and the $2p\sigma$ state also differs qualitatively, peaks associated with resonances in these low-n channels are not expected to be located precisely by this method. Gao and Greene [39] have shown how the frame transformation may be reformulated to account for such energy dependent effects.

The total photoionization cross section is directly proportional to the differential oscillator strength, and is given by the expression

$$\sigma(\omega) = \frac{4\pi^2\omega\alpha}{3(2J_0+1)} \sum_J \sum_j |D_j^{(-)phys}|^2 \tag{2.9}$$

where J_0 is the initial total angular momentum state, J is the final angular momentum state, $D_j^{(-)phys}$ is the reduced dipole matrix element between the j-th physical incoming-wave solution and the molecular ground state, ω is the frequency of the absorbed photon, and α is the fine structure constant. $D_j^{(-)phys}$ can be calculated by a channel elimination transformation analogous to that for the physical scattering matrix above,

$$\mathbf{D}^{(-)phys} = \mathbf{D_o^-} - \mathbf{D_c^-}[\mathbf{S_{cc}^\dagger} - e^{2i\beta}]^{-1}\mathbf{S_{co}^\dagger}, \tag{2.10}$$

using the reduced dipole matrix elements for the long-range solutions $D_j^{(-)}$, which can themselves be found from the body-frame dipole matrix elements by application of the frame transformation coefficients [47, 27]. Note that in a real physical system at finite

temperature, more than one J_0 will typically be present, and a final average must be carried out over the initial statistical distribution.

In traditional MQDT, an analogue of the scattering matrix channel elimination procedure is performed to determine the final solutions used in the dipole matrix elements. As before, this allows the N_o physical D_j^{phys} to be factored into the matrix product of a vector consisting of N weakly energy dependent short-range D_j and an N_o by N matrix containing all of the resonant structure. The cross section may then be convolved over some finite width Γ using (for example) a Lorentzian kernel

$$\sigma_{conv}(\omega_0) = \frac{1}{2\pi}\int d\omega\, \sigma(\omega)\frac{\Gamma}{(\omega-\omega_0)^2+(\Gamma/2)^2} \tag{2.11}$$

to produce a spectrum that approximates the finite resolution achieved in any actual experiment.

Robicheaux [48] showed that this analytical form for the convolution can be rewritten in the suggestive form (suppressing the sum over J)

$$\sigma_{conv}(\omega_0) = -\frac{4\pi^2\alpha}{3(2J_0+1)}\mathrm{Im}\left[(\omega_0+\frac{i\Gamma}{2})\sum_j\int dE\,|D_j^{(-)}|^2\left(E_g+\omega_0+\frac{i\Gamma}{2}-E\right)^{-1}\right] \tag{2.12}$$

where $E = E_g+\omega$ is the energy of the final state and E_g is the ground state energy. The sum and integration can be formally carried out to yield a new formula which involves the Coulomb functions defined at *complex* electron energies $E = E_r + \frac{i\Gamma}{2}$. Robicheaux's original expression for this preconvolved cross section, after rearrangement and the application of a matrix identity, can be written as

$$\sigma_{conv}(\omega_0) = -\frac{4\pi^2\alpha}{3(2J_0+1)}\mathrm{Im}\left[(\omega_0+\frac{i\Gamma}{2})\sum_j D_j^{(-)*}\sum_k\left((S^\dagger-e^{2i\beta})^{(-1)}(S^\dagger+e^{2i\beta})\right)_{j,k}D_k^{(-)}\right] \tag{2.13}$$

Unlike the partitioning scheme for channel elimination (as in Eq. (2.4), this formula treats open and closed channels on an equal footing. In essence Eq. (2.13) relies on the exponential to naturally close a channel every time its argument β (a complex generalization of the phase parameter) switches from being almost real at energies below the channel threshold to having a large imaginary component at energies above the threshold. Although the exact expression derived by Robicheaux for β is complicated to evaluate, the approximation

$$\beta_j = \pi\kappa_j, \quad E_r - E_j < 0 \tag{2.14}$$

$$\beta_j = i\infty, \quad E_r - E_j > 0 \tag{2.15}$$

can be used in its place. Here $\kappa_j = 1/\sqrt{-2(E - E_j)}$ is a complex generalization of the effective quantum number in channel j, with the branch chosen such that Re $\beta_j > 0$ when $E_r - E_j < 0$.

2.4 Application: HD photoionization spectrum

The experimental photoionization spectrum of HD was first observed at high resolution by Dehmer and Chupka [49], and theoretically modeled to a high degree of accuracy by Du and Greene [50]. In this section, we revisit the HD problem using Robicheaux's faster, more direct reformulation of MQDT to generate a much broader range of the photoabsorption spectrum. The decision to return to this system is motivated by several factors. First, high resolution experimental data exists for both the photoionization and photoabsorption cross-sections, and it provides a qualitative measure of the influence of competing dissociation channels or other decay pathways. This allows us to study the anticipated failure of the Ref. [50] implementation of energy independent MQDT. Discrepancies are expected in the neighborhood of strong coupling to the dis-

sociative regions of the potential energy surface, where g-u symmetries become mixed, and where the $1s\sigma$ potential curve may no longer adequately suffice to describe the core electronic state. Second, most of the peaks in the experimental spectrum of HD have remained unassigned, or have only tentative spectroscopic labels, and the present study can identify them with minimal ambiguity. Third, this comparatively straightforward application offers a reasonable opportunity to assess the speed and robustness of the preconvolution variant of MQDT, with the intent of considering it for more general application to other molecular problems in the future.

Below the first ionization threshold, located at 124568.5 cm^{-1}, the spectrum is discrete, consisting of isolated bound states. The preconvolution algorithm describes this region equally well, but owing to our primary interest in the photoionizaton spectrum, discrete photoabsorption will not be discussed further here. At higher energies, the spectrum consists of sets of Rydberg series that converge to thresholds associated with rovibrational states of the residual ion. Because the vibrational levels are more widely spaced than the rotational levels by approximately an order of magnitude ($\sim$2000 cm^{-1} vs. $\sim$200 cm^{-1}), ionization thresholds appear as neighboring pairs, with all allowed transitions corresponding to an ionic rotational state of either $J+1$ or $J-1$ (since the Rydberg electron is restricted to the p-wave solutions excited when an HD ground state electron absorbs a single VUV photon). To simulate the results of a spectrum taken at 78 K, the contributions from the three energetically accessible initial rotational states, labeled by their total angular momentum as J_0=0, 1, and 2 are weighted by the Boltzmann statistical factors 61.9%, 35.8%, and 2.2%, respectively. This results in four distinct thresholds, each with up to three attached series (R, Q, and P branches), which originate from each vibrational state of the core.

Much of the complexity of the photoionization spectrum arises in regions where peaks in one series are perturbed by the lower-n resonances of a higher threshold that lie at roughly the same energy. In such cases, spectral features can become so strongly

mixed as that any formal spectroscopic assignments would be somewhat arbitrary. A common example occurs when a lower-n resonance appears just slightly below a higher-n threshold, such that its width is less than the energy separations of the near-threshold series. In this instance, the low-n resonance will be distributed over many adjacent peaks in the series, causing the total number of such peaks to be increased by one and uniformly enhancing their intensity, yet no one peak can be unambiguously assigned to the perturber.

To a limited extent, the spectrum exhibits repeated patterns attributable to the nearly uniform separation between the first few vibrational levels. As a result, a subsection of the total spectrum that spans one vibrational energy spacing serves to provide a qualitatively representative measure of accuracy over a broader range. We have chosen to focus on the spectrum in the energy regime near the second ($v^+ = 1$) set of rovibrational thresholds, from 125500 cm^{-1} to 127300 cm^{-1}.

Figures 2.4-2.7 show the theoretical results superimposed on the experimental data points. Since the experiment does not provide an absolute normalization for the intensity, we have normalized this data to match the theoretical cross-section at 127000 cm^{-1}. The peaks in Figure 1 have been labeled through the application of a technique detailed in [37] which involves searching for the roots of a determinantal equation and examining the magnitude of the coefficients in each closed channel. As n becomes large ($\geq$10), the coupling (as noted earlier) undergoes a transition from Hund's case b (where the projection of the angular momentum of the Rydberg electron along the internuclear axis Λ is a "good" quantum number) to Hund's case d (where the preferred quantum number is the rotational state of the core). Although this decoupling occurs gradually, we adopt here the convention of describing resonances of n<10 according to the first case, and n>10 in terms of the second.

In Figures 2.4 - 2.7 several peaks are labeled that exhibit some significant discrepancies between theory and with experiment. These discrepancies likely arise from our

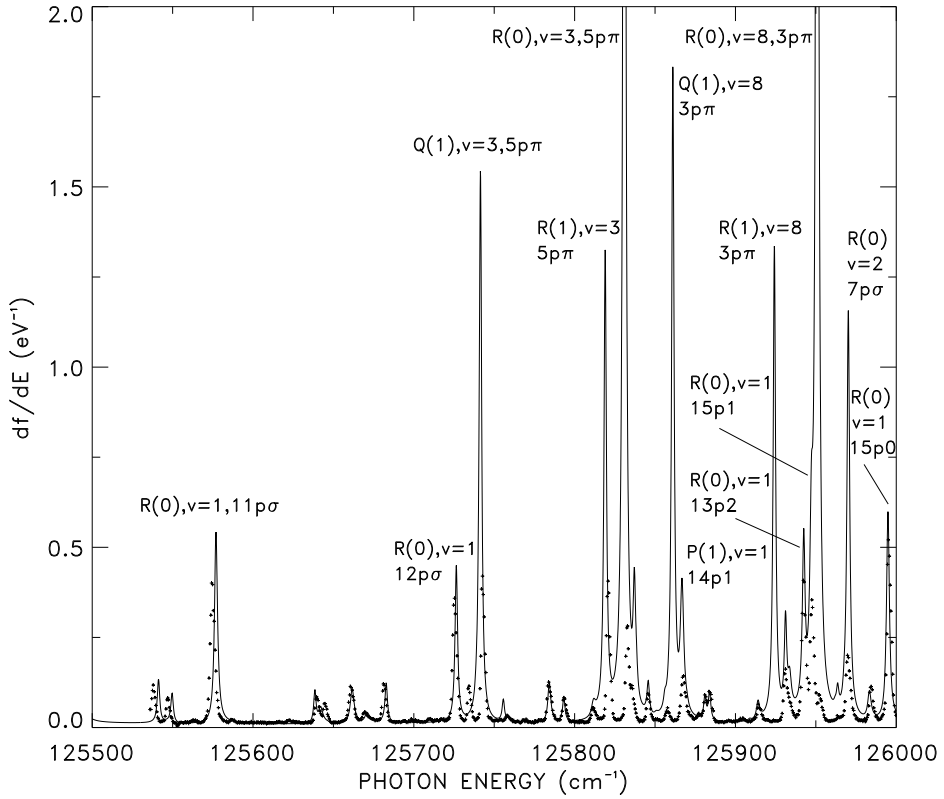

Figure 2.4: Experimental[49] and preconvolved theoretical oscillator strength [51] for HD photoionization between 125500-126000 cm^{-1} photon energy.

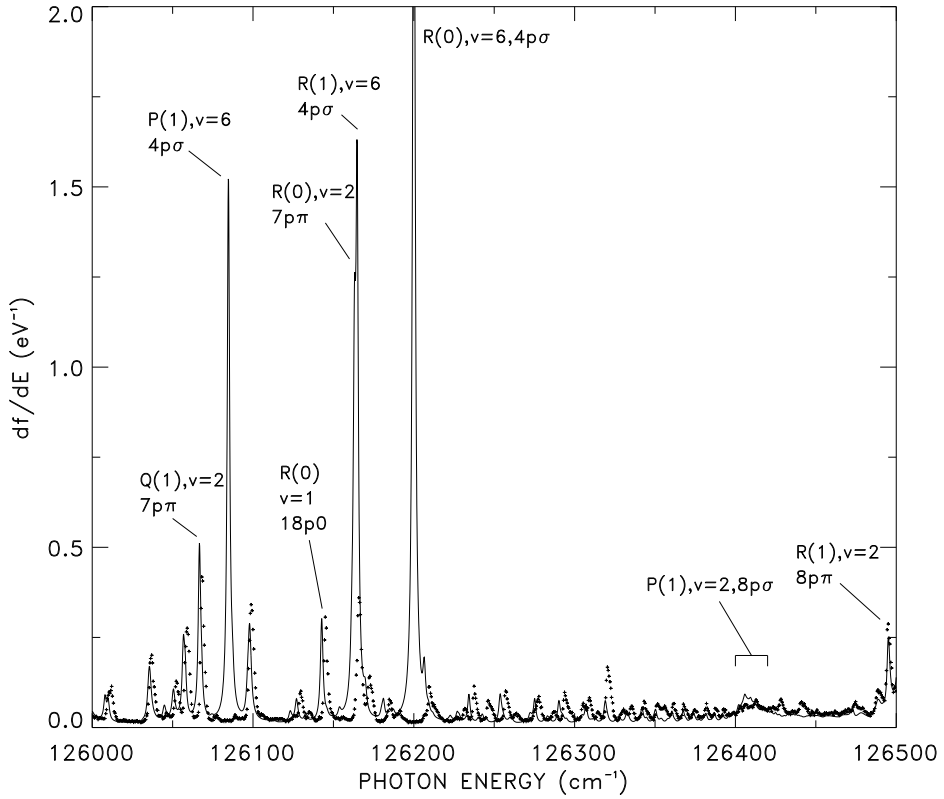

Figure 2.5: Experimental[49] and preconvolved theoretical oscillator strength [51] for HD photoionization between 126000-126500 cm^{-1} photon energy.

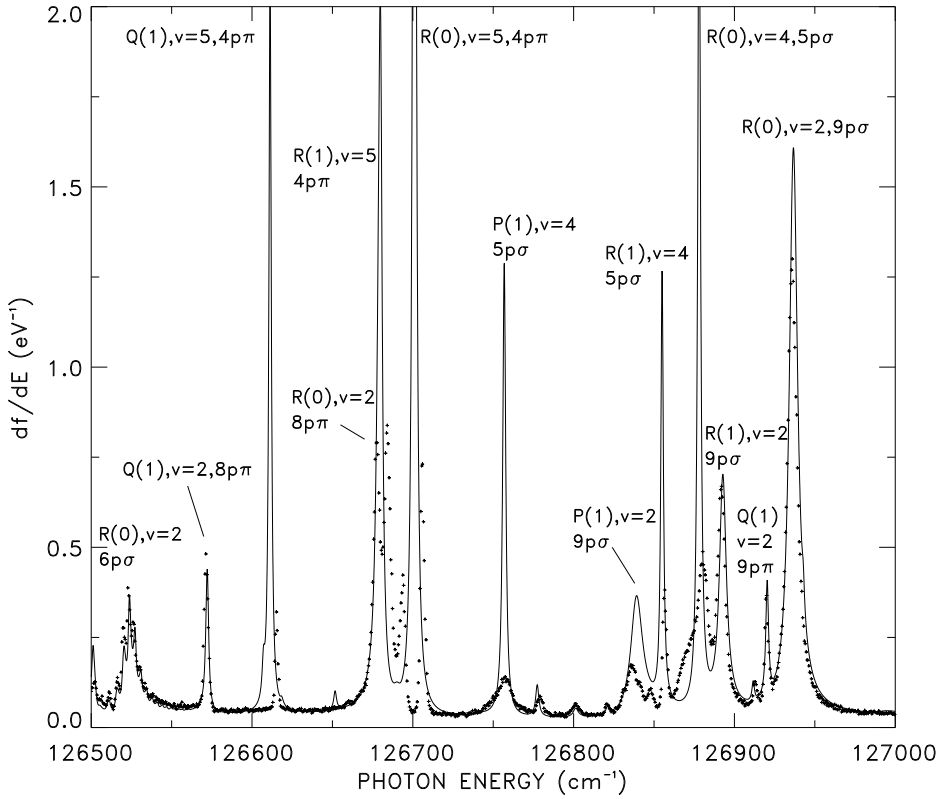

Figure 2.6: Experimental[49] and preconvolved theoretical oscillator strength [51] for HD photoionization between 126500-127000 cm^{-1} photon energy.

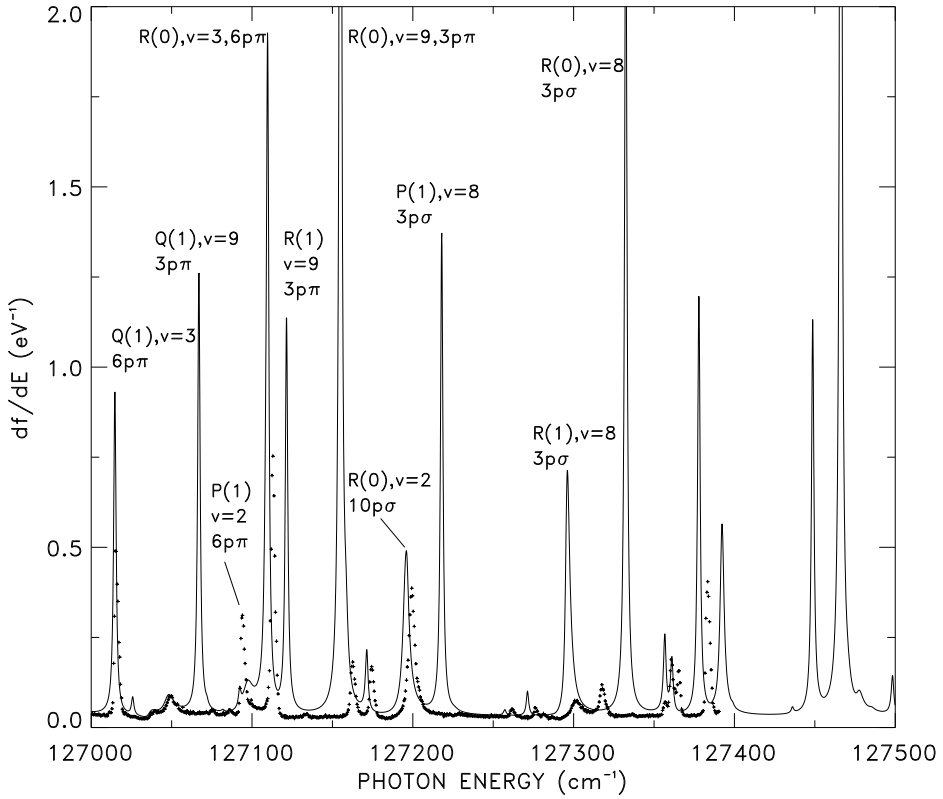

Figure 2.7: Experimental[49] and preconvolved theoretical oscillator strength [51] for HD photoionization between 126000-127500 cm^{-1} photon energy.

neglect of competing predissociation processes in the MQDT calculations. As previously shown by Du and Greene[50], departures from linear absorption in the experiments from photon energies ∼12600 to greater than 12700 cm^{-1} are also a potential problem. Regarding predissociation, for example, the resonances labeled R(0), R(1), and Q(1) that are assigned to perturbers associated with $v = 3 - 8$ ionic cores are likely to be affected by coupling with either the repulsive, dissociative inner wall of the potential energy surface via the Coriolis interaction (for $\Lambda \neq \Lambda'$), or the outer potential regions where nλn'λ' doubly-excited potential curves are known to intersect and strongly perturb the Rydberg potential surface. Such examples of channel interactions are well-documented in H_2 (e.g. the 3pσ-3pπ Coriolis-type predissociation discussed in [52], and predissociation of the 3pπ, $v = 8$ and 4pπ, $v = 5$ states discussed in [53] and [54]). Although these two mechanisms appear to be distinct, MQDT in principle allows a unified description of *joint* Coriolis interactions and electronic core excitations.

Comparison of our results with experiment in Figure 2.4 shows that many of the observed resonances are in good agreement in terms of position and intensity. Most of these resonances are assigned to those classified in the Hund's case d limit and they also have low vibrational excitation. Discrepancies in intensities, however are apparent for the strong v=3 resonances predicted at 125750 and 125830cm^{-1}, as well as the v=8 set between 125860 and 125900 cm^{-1}. These resonances are associated with 5pπ, $v = 3$ interlopers. For HD it is somewhat surprising (but not unprecedented) that Rydberg states attached to ionic cores with vibrational quanta as low as $v = 3$ excitation will strongly sample the dissociative regions of the potential energy surfaces, resulting in a significant competition with the autoionization channel. The increase in the effective, non-adiabatic couplings in HD may therefore be related to the breakdown of the g-u inversion symmetry, particularly near its dissociative limits; for the corresponding peaks in the H_2 spectrum the predissociation is only moderate [55].

Another class of discrepancy in Figure 2.4 is typified by the predicted R(0), $v = 2$,

7pσ interloper at 125970 cm^{-1}, which, while in good agreement in terms of position, is too intense. This may be due to the breakdown of symmetry, or else to the non-linearity of the intensity dependence on the cross section arising from saturation effects [50]. (The results of Glass-Maujean [55] imply that ionization prevails for the 7pσ series in H_2 except in cases where cases where the peaks are strongly mixed with another series.)

Figures 2.5 - 2.7 show a comparison of the present theory with the remaining range of experiment considered here, leading up to 127500 cm^{-1}. Figure 2.5 shows an increasing number of low-n, high-v interlopers predicted by theory with minimal correlation to resonance observed in the experiment. It is also apparent that shifting of many predicted resonances $\sim$3-5 cm^{-1} compared to experiment occurs near the $v = 1$ threshold at 126600 cm^{-1} (shifts of this magnitude are also noticeable for some of the resonances in Figure 2.4 as well). The origin of these shifts is not certain, although Ref. [50] pointed out that they are likely due to our neglect of energy dependence in the quantum defects, or else associated with random slippage errors in the experimental wavelength calibration.

The discrepancies seen in Figure 2.6 are most apparent for the very strong resonances predicted at 126610, 126680, and 126700 cm^{-1}, respectively. These resonances are associated with 4pπ, $v = 5$ interlopers which can predissociate. This resonance and intensity pattern parallels the three predicted 5pπ, $v = 3$ interlopers shown in Figure 2.4, perhaps strengthening the conclusion that those are strongly predissociated as well.

In Figure 2.7 one observes a complete breakdown of agreement between the theoretical predictions and experiment beyond $\sim$127200 cm^{-1}. This must be attributed to my neglect of predissociation processes, particularly since the predicted resonances are associated with interlopers which have very high vibrational excitation, for example, states with 3pλ, $v = 8 - 9$. These states would predissociate primarily through Coriolis coupling with nσ states of comparable total energy.

In summary, disagreement between the MQDT calculations and experiment is probably partly attributable to the neglect of predissociation via the Coriolis interaction and channel-coupling with two-electron excited core states. In limited spectral regions, departures from linearity in the original experimental conditions could also be a source of discrepancy. In chapter 5, approaches to the treatment of predissociation will be reconsidered in greater detail.

Within regions of the spectrum dominated by high-n resonances, however, the frame transformation-based MQDT method remains impressively accurate. The very recent work of Merkt and coworkers [56] provides a persuasive example of the capabilities of the frame transformation to describe even densely spaced resonances in the near-threshold regime. Figure 2.8 shows the experimental photoionization spectrum plotted in a narrow region near the $v = 1$, np0 threshold, where the Rydberg series has many sharp and narrow resonances. Just above the threshold is a complex resonance arising from the perturbation of the $v = 1$, np2 series (converging to a threshold at 789.847 Å) by an interloper attached to the $v = 2$ threshold. Each of the modulated groupings of peaks below the threshold at 790.630 Å can similarly be understood as a complex resonance arising from the mixing of the overlapping $v = 1$, np0 and $v = 1$, np2 series. The theory (b) in 2.8 is a reproduction of the result in [50], calculated at too coarse a mesh to identify any of these high-n structures. Figure 2.9 shows the same spectrum recalculated on a much finer mesh; the positions as well as the intensity modulation and shifting line profiles across the complex resonance sets are all well-described by the theory, aside from a few very weak and broad features in the experimental spectrum. (The disagreement in intensity for the Q(1), $v = 2$ 8pπ peak at 790.07 Å is presumably due to predissociation.)

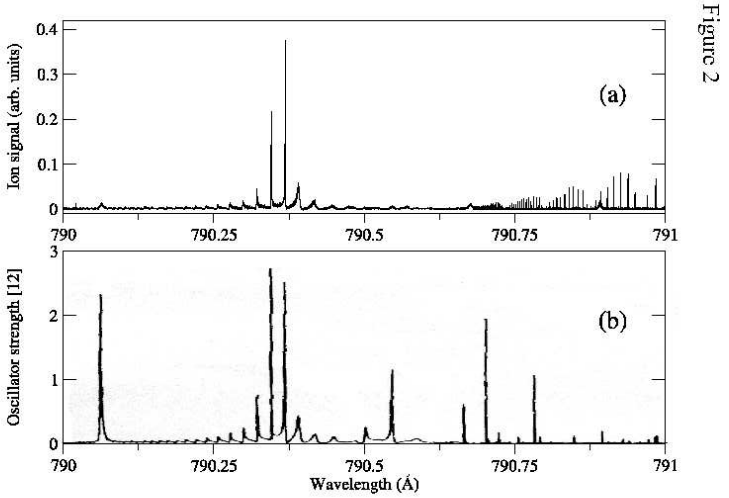

Figure 2.8: Ultra high resolution experimental (a) [56] and theoretical (b) oscillator strength for HD photoionization near the v=1 threshold, using theory from the mid-1980s by Du and Greene [50].

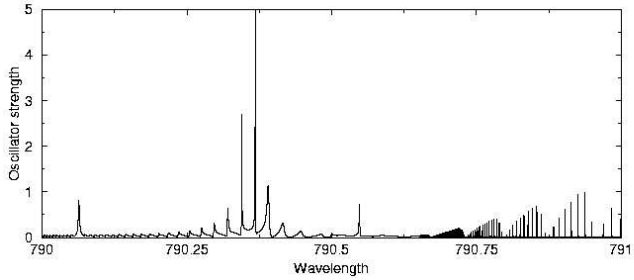

Figure 2.9: Recent recalculation of the theoretical oscillator strength by the same method, on a much finer grid and at a rotational temperature (25 K) appropriate for the newer experiment.

Chapter 3

Long-range Rydberg state: Approximate and model approaches

In the previous chapter, we considered a system consisting of a Rydberg electron attached to a single positively-charged core. Within a small region of space defined by the dimensionality of the core, the electron would experience a complex potential, but outside that region, the behavior of the electron would be well-characterized by some linear combination of bound or continuum hydrogenic solutions. The method of multichannel quantum defect theory was explicitly designed to exploit this natural partitioning of the Hamiltonian into a complicated form in one tightly localized region of space, and a far simpler form everywhere outside of it. Suppose that, instead of a single core, the Rydberg electron had two such regions of "hard physics", well separated from one another, within the volume of space where its probability density was non-vanishing. The philosophy of quantum defect theory would still be highly appropriate for this class of nuclear geometries. The vast majority of the volume in which the electron resided would still be simple Coulombic physics, and the interaction with the isolated and localized regions where the electron was governed by a more complex Hamiltonian could still be conceptualized as scattering centers embedded in a region of far smoother trajectories, like divots in a fairway of a golf course, or bumpers in the playfield of a pinball machine. It would still be fantastically wasteful, from a computational standpoint, to expend effort describing the short-range and long-range interactions using the same approach; any method that would be adequate to describe the difficult many-particle

interactions of the inner regions would entail accounting for all manner of correlations, (anti)symmetrizations, and excitations, and once the method was outside that region, all of this specialized machinery would no longer be essential.

3.1 The Fermi pseudopotential approximation

When an atom in a low-lying excited state or a Rydberg state is brought near a ground state atom or molecule, much of the interaction derives from simple electron scattering off of the ground state species. This picture was developed in a classic paper by Fermi [57], to describe pressure shifts and broadening of atomic Rydberg spectral lines, as well as for the scattering of neutrons by protons in a hydrogen-rich sample [58]. Fermi's approximation, although conceptually crude, was surprisingly accurate for its time, in part because certain effects neglected by his analysis (the "excluded volume" and "wave distortion" corrections) tend to cancel one another [59]. [1] Presnyakov, however, noted that the Fermi model would be difficult to extend to alkali-alkali interactions, due to the electron affinity of alkali atoms [62]; most of them have either true ionic bound states, or else near-threshold resonances.

The outer electron of a Rydberg atom is distributed over a region that extends far from the ionic core. At large radii the Coloumb potential is weak, and varies slowly as a function of position; consequently, the valence electron has low momentum and may be viewed as occupying a 'quasi-free' state. This allows the interaction between a nearby ground state particle (the 'perturber') and the Rydberg atom to be described in terms of isolated scattering events between the electron and perturber and between the electron and the ionic core. In effect, the three-body problem (electron, ion, and perturber) is treated as a combination of two separate two-body interactions.

Ordinarily, the scattering of a low energy electron (such as a Rydberg electron

[1] For detailed reviews of the theory of pressure shifts and broadening, including comparison of the Fermi model with several other methods, see Allard and Kielkopf [60] or Beigman and Lebedev [61].

far from the core) can be well-approximated by including only S-wave scattering. This is a familiar consequence of the Wigner threshold law. When the angular momentum of the scattered electron relative to the perturbing particle is greater than zero, however, the short-range potential may support quasibound negative ion states, i.e., shape resonances. Since the scattering parameters vary rapidly as a function of energy in the vicinity of a shape resonance, such resonance channels can result in the formation of molecular bound states. This situation will be considered later in further detail, and for now we restrict attention to the S-wave case.

The Fermi pseudo-potential appropriate for S-wave scattering is given by

$$V_S(\vec{r},\vec{R}) = 2\pi a_T[k(R)]\delta(\vec{r}-\vec{R}) \tag{3.1}$$

where $\vec{r}$ is the position of the electron, $\vec{R}$ is the position of the perturber, both from the ionic core, $k(R)$ is the valence electron wavenumber, and we define the triplet scattering length for electron-perturber collisions as $a_T = -\tan\delta_0^T/k$. The energy variation of the triplet S-wave phase shift δ_0^T, comes from its implicit dependence on R, according to $\frac{1}{2}k^2(R) = -\frac{1}{2n^2} + \frac{1}{R}$, for a Rydberg electron with principal quantum number n. In general, it is necessary to account for singlet scattering as well, but for Rubidium, the singlet scattering interaction is much weaker and does not give rise to the same bound states, so to a good approximation it may be neglected.

Alternatively, a more general zero-range pseudopotential form appropriate to partial waves beyond $l = 0$ can be formulated using a Green's-function technique that treats the perturber as an additional boundary condition on the atomic solution [63]. Such methods will be considered in further detail in the following chapter. The Green's function approach has been applied fruitfully to the study of electron transfer effects in atomic collisions [64], particularly those in which the collision is assisted by a laser field that excites one of the atoms into a Rydberg state [65, 66]. A second, and fully

equivalent, method applies the zero-range potential as an additional term in the molecular Hamiltonian, consisting of a sum of separable projections for each l-channel onto angular momentum eigenstates [67].

Even before the work considered in this thesis, two particularly noteworthy and relevant predictions have been based on the Fermi approximation. First, Ivanov, in his study of the perturbation of strongly degenerate Rydberg levels, observed that the interaction potential associated with S-wave scattering of the Rydberg electron from the perturber would experience a sign reversal as it passed through the separation radius associated with the Ramsauer minimum of the electron-perturber scattering cross-section [68]. Since the potential vanishes asymptotically, and is attractive at intermediate distances, Ivanov concluded that the potential was sufficiently broad that it must support a bonded complex at large distances. Second, Du and Greene [69, 70] applied a combination of the Fermi method and MQDT to rare gas Rydberg dimers in order to explain features of their photoionization spectra. Even at the level of the Fermi approximation, their potential curves displayed long-range oscillations comparable to those witnessed by de Prunelé.

3.2 Degenerate perturbation theory for the hydrogenic case

In a high Rydberg state, the electron kinetic energy is so low that the electron-perturber scattering is primarily S-wave, and such that the scattering properties of the electron at non-resonant energies are dominated by the S-wave scattering length. Analysis by Greene, Dickinson, and Sadeghpour [71] showed that, in an ultracold gas, the negative ^3S-wave scattering length can produce a new type of ultra-long-range molecule with unusual properties. This model has already been used to predict the existence of two classes of ultra-long-range (i.e. of size 10^2-10^4 a.u.) Rydberg molecular bound states in an ultracold Rb gas; these molecules consist of one excited and one ground state atom [71]. In addition to being much larger than any previously known diatomic ground

state, [2] these molecules are expected to have permanent electric dipole moments in the kdebye range, and lifetimes on the order of tens or hundreds of microseconds (for n in the range 30-70). The Born-Oppenheimer potential curves of these states are oscillatory, with many local minima, each supporting multiple vibrational levels. The second class, the perturbed hydrogenic states [69, 70], also have an unusual valence electron probability distribution resembling a trilobite fossil, which can be viewed as a semiclassical electron interference pattern [73]. Both classes of molecular states, however, are bound only weakly, by just a small fraction of the spacing between adjacent n-manifolds. For $n = 30$, for example, the minimum of the first type of state is approximately 100 MHz, whereas the minimum of the second type is roughly 10 GHz, compared to the 250 GHz separation between the $n = 30$ and $n = 29$ manifolds. All further discussion will be focused entirely on the perturbed hydrogenic states.

For a completely degenerate hydrogenic n^2 manifold, the Fermi S-wave pseudopotential effectively recombines the manifold into n^2-1 states that remain unperturbed and degenerate (and thus have zero amplitude at the perturber position) and one non-degenerate state that maximizes the amplitude at this position. Using first-order degenerate perturbation theory for the delta-function perturbation of Eq. 3.1, the resulting non-degenerate internuclear potential may be written in closed form,

$$U_n(R) = -\frac{1}{2n^2} + 2\pi a_T(k(R)) \sum_{l=l_{min}}^{n-1} \frac{2l+1}{4\pi} R_{nl}(R)^2, \tag{3.2}$$

where R_{nl} is the radial hydrogenic wavefunction and the states below l_{min} are possibly non-degenerate levels that are sufficiently distant from the manifold that their contribution may be reasonably neglected. This formula is exact for a Coulomb potential, and remains reasonably accurate for quasi-degenerate approximations to the level structure of an alkali atom. (For short internuclear distances, the potential must also be ad-

[2] Since the first publication of this prediction, the observation of other classes of diatomics with comparably large internuclear separations, generated by various dipole-dipole interaction effects, has been reported [23, 72].

justed to include the polarization interaction between the ion and the perturber, since the highly excited Rydberg electron no longer shields the ionic core.) A plot of the molecular bound state defined by Eq. 3.2 is shown in Figure 3.1.

This class of potentials supports many vibrationally bound states. The lowest states are confined to individual local potential wells associated with the oscillation of the perturbed hydrogenic potential, while higher states are distributed over multiple minima, or over the entire width of the broad well formed by the energy-dependence of the scattering length. For n=30, the potential supports about 70 vibrational wavefunctions. All of these states are characterized by strongly asymmetrical charge distribution, with the electron density accumulated heavily on top of the perturber in a pronounced peak. This charge separation is the origin of the unusually large dipole moments associated with this class of states, on the order of $D = R - \frac{1}{2}n^2$ a.u.; for states in the vicinity of n=30, the degenerate perturbation theory predicts electric dipole moments on the order of a kdebye (see [74] for a recent calculation of the dependence of the dipole moment on R).

It may seem somewhat peculiar to suggest that a homonuclear diatomic bonded complex could possess a permanent dipole moment. In principle, the solutions should appear in parity eigenstate pairs (*gerade/ungerade*) symmetrized in such a way as to make the nuclei indistinguishable. In any practical application, however, the parity eigenstates are so nearly degenerate as to make such symmetrization irrelevant; even the smallest external perturbation (by stray electric field, say, or a nearby Rydberg atom) is sufficient to break degeneracy and form the charge-separated states calculated above by hybridization of adjacent J states of opposite parity. Equivalently, one could think of preparing the system in a charge-localized state, and estimating the tunneling time necessary for the ground state valence electron on the perturbing alkali to penetrate to the location of the ionic core; even a rough estimate of the parity splitting ($< 10^{-100}$ a.u., from [71]) gives a localization half-life many orders of magnitude longer than the

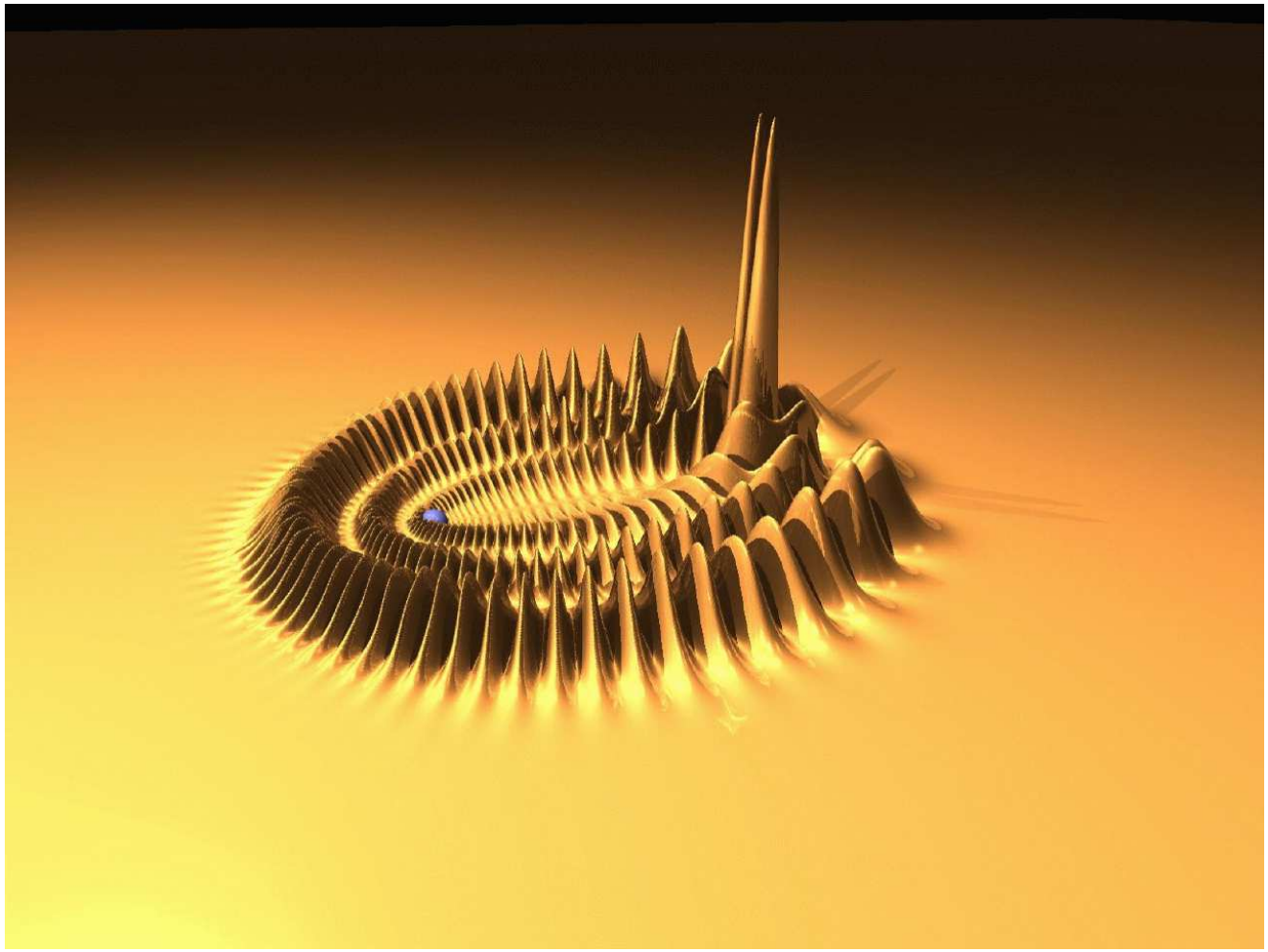

Figure 3.1: A surface plot of the Rydberg electron probability density $\rho|\Psi(\rho,z)|^2$ in cylindrical coordinates for the $n = 30$ $^3\Sigma$ S-wave scattered ("trilobite") state [71]. The perturber is located at the position of the lowest minimum in the potential energy curve (at $R = 1234$ a.u.), and corresponds to the largest peaks in electron density along the axis of symmetry.

entire history of the universe.

3.3 Omont's generalized delta-function approximation

For electron-perturber scattering in partial waves beyond the S-wave case, the strongest contributions are expected to occur when some higher partial wave is resonant. Our treatment of this problem follows a method developed by Omont [75], based on approximating the zero-range pseudopotential with an l-expansion of the R-matrix. For the present results, we shall be content to examine only systems for which the scattering is dominated by the S- and P-wave partial waves, although the same approach should also apply to perturbers with D-wave or F-wave shape resonances (such as N_2 or SF_6.) we will here assume the ^{87}Rb Rydberg atom, whose large ionic core destroys the orbital angular momentum degeneracy and whose heavy mass ensures the existence of many closely-spaced vibrational levels. Rubidium, of course, is a favorite atom utilized in the study of ultracold atomic gases. I shall further assume that experimental ability exists to prepare a Rydberg state containing high angular-momentum components, either by a multiphoton process or by the imposition of a weak electric field that breaks the dipole selection rule.

Following Omont, the matrix element associated with P-wave electron-perturber scattering can be written as

$$\langle \Psi_1 | V_p | \Psi_2 \rangle = -\frac{6\pi \, \tan \delta_1^T}{k^3(R)} \vec{\nabla} \Psi_1(\vec{r}) \cdot \vec{\nabla}' \Psi_2(\vec{r}') \mid_{\vec{r}=\vec{r}'=R} \tag{3.3}$$

where δ_1^T is now the triplet P-wave scattering phase shift. we adopt the *ab initio* calculations of Bahrim *et al* [76, 77, 78], for the S- and P-wave triplet e^--Rb($5s$) scattering phase shifts.

In order to generate a bound state, the perturbation should ideally result in a negative energy shift, though bound states might in some cases result from repulsive scat-

tering lengths. For S-wave scattering, a negative shift occurs when the scattering length $a_T = -\tan\delta_0^T(k)/k$ is negative. For P-wave scattering, the corresponding parameter that must have a negative value is the effective scattering volume, $a_T = -\tan\delta_1^T(k)/k^3$. (Again, in general both singlet and triplet scattering must be included, but for Rb only the triplet P-wave scattering is resonant.) Qualitatively, these pseudopotentials may be viewed as selecting a linear combination of atomic states that maximizes either the value of the wavefunction (S-wave) or of its derivative (P-wave) at the position of the perturber. Note that for the P-wave correction, the derivative acts in all three spatial directions, giving rise to two possible sets of states: those that maximize the gradient parallel to the internuclear axis, and those that maximize the gradient perpendicular to it. The former have a nodal plane perpendicular to the internuclear axis, and thus a Σ molecular symmetry ($m = 0$), and the latter place the nodal plane along the axis, and hence have a Π molecular symmetry ($m = 1$).

3.4 Resonance scattering effects

At the position of a resonance, the tangent of the phase shift diverges, resulting in an unphysical form of the interaction potential. In practice, however, the energy eigenstate is bounded by manifolds corresponding to $n+1$ and $n-1$, and is subject to level repulsion by states of identical symmetry attached to the adjacent manifolds. This permits a diagonalization even at energies close to the resonance energy, circumventing the need to resort to explicit renormalization of the potential. The number of manifolds retained above and below the n-value of interest can be varied to test the eigenvalue stability. In a typical calculation, adequate convergence is obtained with three to seven total manifolds.

The Born-Oppenheimer potential curves (both S- and P-waves) associated with the Σ molecular symmetry are shown in Figure 3.2, and the curve for the Π symmetry state (possible for P-wave only) is shown in Figure 3.3. These results are found by

diagonalization of the Omont psedopotential within a basis of Rb atomic states associated with the included manifolds, including both the high-l quasidegenerate states and the lower-l states with finite quantum defect. The associated S- and P-wave phase shifts, as functions of energy, are shown in Figure 3.4. Recall that the phase shifts at the perturber R are implicit functions of R as a result of the change in the local kinetic energy of the scattered electron. The most prominent qualitative features of the potentials are directly controlled by the energy dependence of the phase shift. For example, the point at which the Σ S-wave potential passes through zero corresponds to the Ramsauer-Townsend zero in the e^--Rb(5s) phase shift at 0.042 eV (around $R = 450$ a.u.) [71].

For the present context, the most notable characteristic of the P-wave potentials is their broad and comparatively deep minimum. As R decreases through the vicinity of the shape resonance around $R = 700$, the associated P-wave potentials detach from the $n = 30$ manifold, pass through a point where the slope of the potential becomes large, and run close to the $n = 29$ manifold for smaller R. In essence, a rise by π in the scattering phase shift due to the P-wave resonance results in a promotion of the associated molecular curve to the next lower manifold. *We emphasize that this effect is quite general; it will occur between any two adjacent n-manifolds, for any partial-wave electron-perturber scattering channel that contains a shape resonance.* This behavior should consistently define the existence of a global minimum in the potential curve, and thus a set of bound vibrational levels. In the inset of figure 3.2 we show the first ten vibrational levels for the P-wave scattered Σ state.

Both sets of potential curves exhibit multiple avoided crossings, with both the hydrogenic energy levels and (in the case of identical molecular symmetry) with each other. Depending on the Landau-Zener parameters for each crossing, sufficiently high vibrational levels may dissociate on a time scale shorter than the natural lifetime of the Rydberg state. Even for states lower in energy than the crossing energy, the possibility

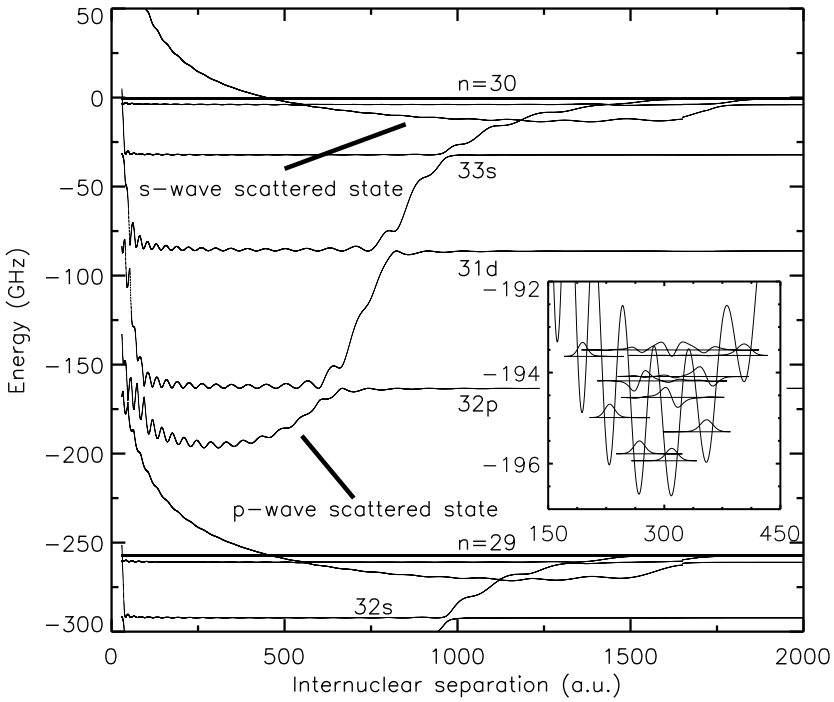

Figure 3.2: $^3\Sigma$ Born-Oppenheimer potential curves for states arising from both S-wave and P-wave scattering [79]. Several of the lowest vibrational levels, along with their associated wavefunctions, are shown in the inset. The zero of the energy axis is taken to lie at the position of the $n = 30$ manifold.

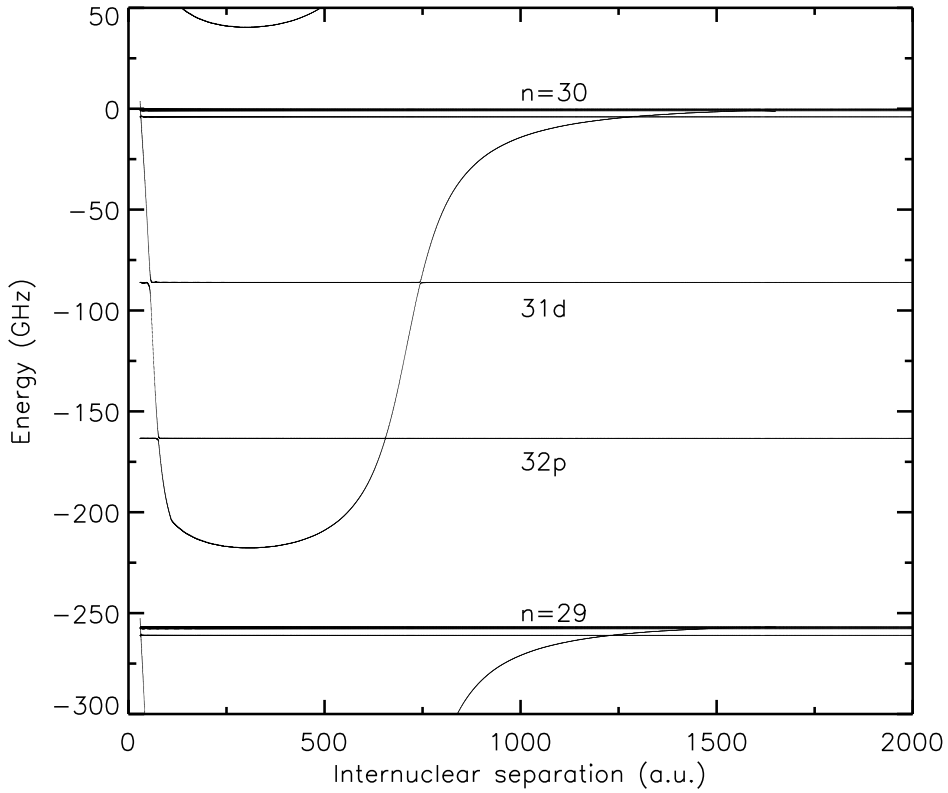

Figure 3.3: $^3\Pi$ Born-Oppenheimer potential curve arising from P-wave scattering [79].

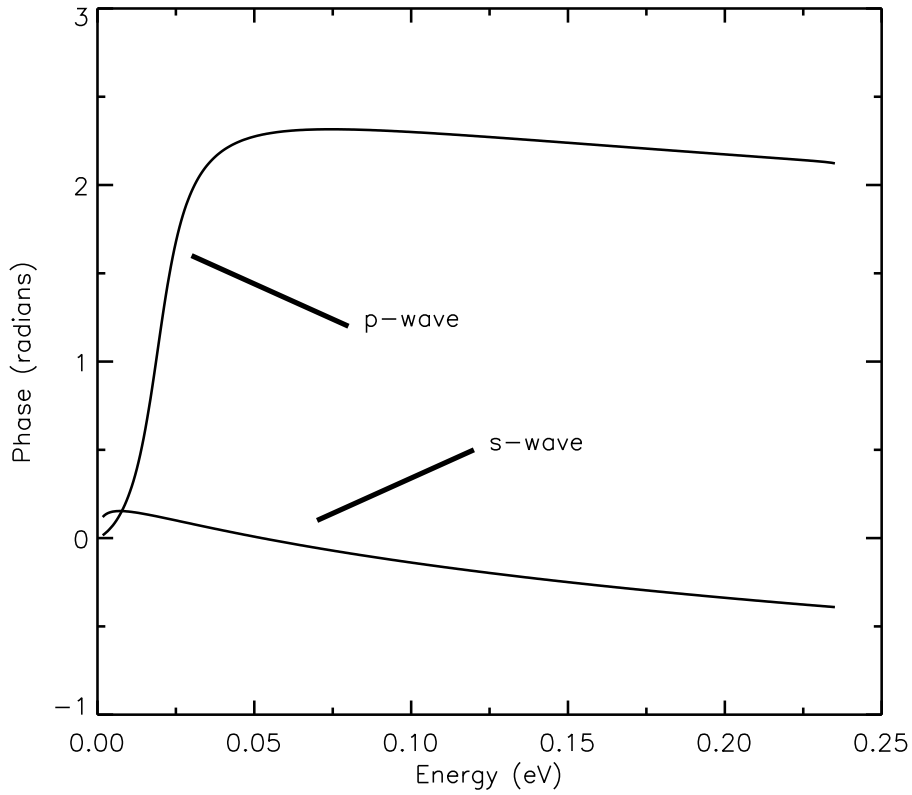

Figure 3.4: Phase shifts for low energy S- and P-wave scattering from ^{87}Rb as a function of energy [79]. The Ramsauer-Townsend zero in the S-wave curve at $E = 0.05$ eV corresponds to the point at $R = 450$ where the S-wave potential crosses through the $n = 30$ manifold. The resonance in the P-wave phase between 0.02 and 0.04 eV controls the rapid rise of the P-wave potential in the range between $R = 500$ and $R = 1000$ a.u.

of tunneling cannot be excluded; this is of particular concern for the crossing between S- and P-wave $^3\Sigma$ states, which occurs close to the S-wave minimum and could potentially destabilize even the lowest vibrational level. Based on this and other anticipated decay mechanisms, including a significant contribution from blackbody radiation, we predict that the lifetime of such states should scale as n^2 [80] and be of the order of $50\mu s$ for $n = 30$. This is longer than the vibrational period of low-lying levels, suggesting the possibility of resolving vibrational substructure in the absorption spectrum.

Figure 3.5 contains a wavefunction of the Σ P-wave scattered molecular state in the vicinity of the minimum of the potential curve. Rather than being distributed over the entire classically allowed region, the electron density is confined to an envelope with the approximate shape of a butterfly. The nodal pattern features two large "wings" of electron density extending to the usual spatial boundary of the atomic Rydberg state, but along the internuclear axis the density accumulates near the position of the perturber.

Like the trilobite states controlled by pure S-wave scattering [71], the P-wave "butterfly" states develop large electric dipole moments, despite the fact that the electron density vanishes at the perturber. The behavior of the dipole moment at the equilibrium separation with n scales roughly linearly with n, and its value for the $n = 30$ states is approximately 1.05 kdebye, rising to 3.91 kdebye for $n = 70$. The Π symmetry states have similarly large dipole moments, but negative, with a value of -1.53 kdebye at $n = 30$. Such large permanent dipole moments can be manipulated by external electromagnetic fields or by dipole-dipole interactions.

3.5 Finite range nonlocal pseudopotential

In order to confirm the accuracy of the zero-range model, we have adopted a short-range nonlocal approximation of the form developed by Pascale [81]. In particular, this allows the model to represent longer-range polarization terms arising from the dipole and

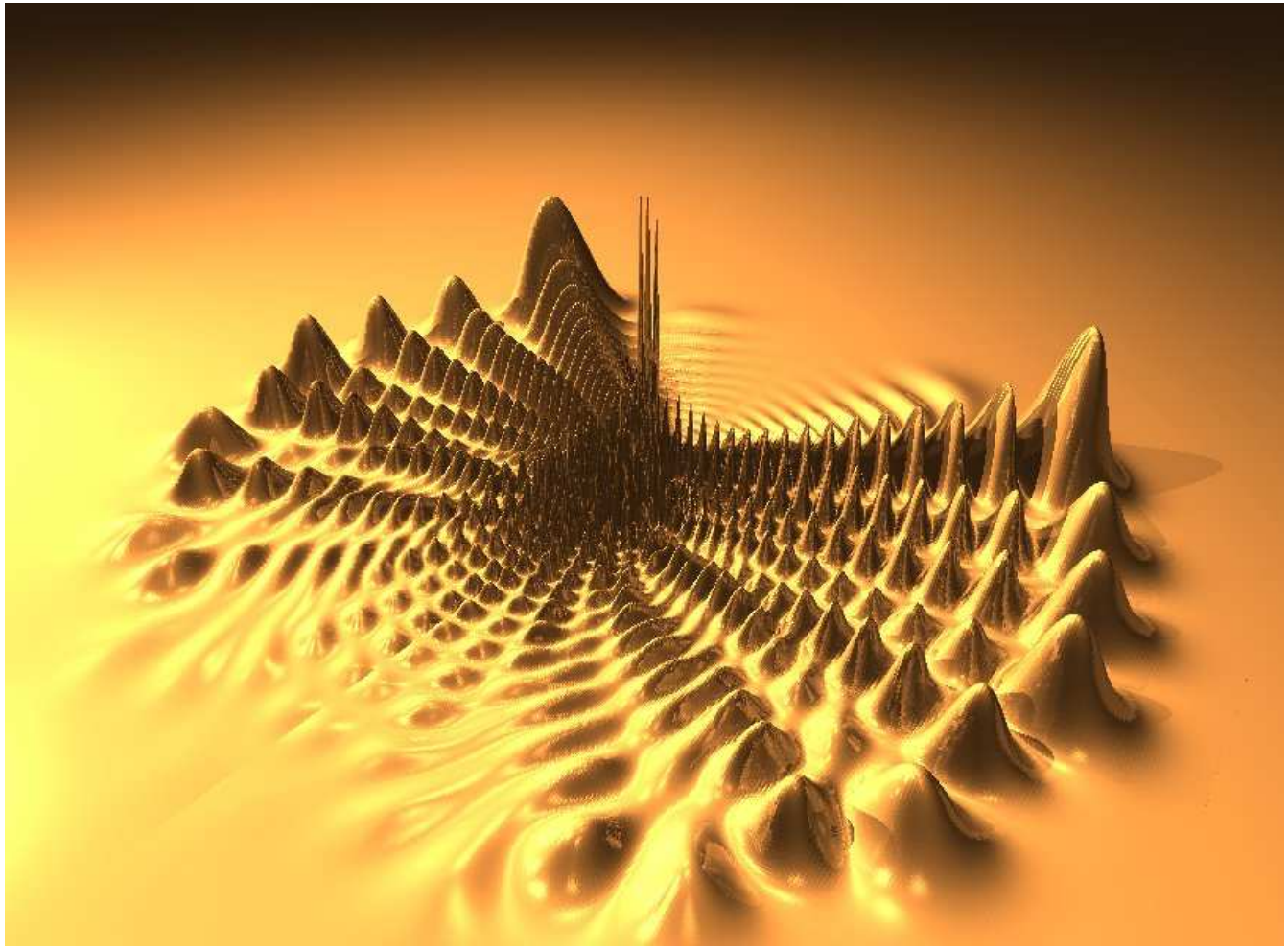

Figure 3.5: A surface plot of the Rydberg electron probability density $\rho|\Psi(\rho,z)|^2$ in cylindrical coordinates for the $n = 30$ $^3\Sigma$ P-wave scattered ("butterfly") state [79]. The perturber is located at the position of the lowest minimum in the potential energy curve (at $R = 308$ a.u.), and corresponds to the largest peaks in electron density along the axis of symmetry.

quadrapole polarizability of the perturber. This technique has been used successfully, for example, in the calculation of adiabatic potential curves for helium-barium collisions [82]. To verify the accuracy of the Omont theory, we performed a full diagonalization on a two-dimensional spline basis set using a nonlocal model pseudopotential with free parameters that could be varied to reproduce the observed phase shifts. (See [83] for a recent example of the application of this method.) As a further test, we also implemented the zero-range potential approximation using a Green's-function technique, as presented in Chapter 4. A comparison of these three methods is shown in Figure 3.6. In each calculation, the overall shape of the P-wave bound state confirms the validity of the extended Fermi model, with quantitative agreement to within a few percent. Note that for the sake of this comparison, the core quantum defects have been set to zero (i.e., an H + Rb system), allowing the use of the exact analytically-known Coulomb Green's-function.

These conclusions can be extended to molecular perturbers, through a generalized version of the same zero-range potential [66]. The simplest such system, a diatomic molecular perturber, introduces a second axis of symmetry into the problem, defining the orientation of the molecule, with the result that states of differing molecular symmetry (i.e., projection of the electronic angular momentum onto the ion-perturber axis) can become coupled. Note, however, that if the perturber has a permanent dipole moment, the longer-range electron-dipole interaction controls the scattering physics, invalidating the assumptions of the zero-range approximation. The large number of shape resonances known in electron-molecule scattering (N_2, SF_6, BF_3, CO_2, for instance) suggests that this class of Born-Oppenheimer potential curves should be observable in many different contexts, ranging from the conventional quantum chemistry of valence states to the Rydberg states of an ultracold gas.

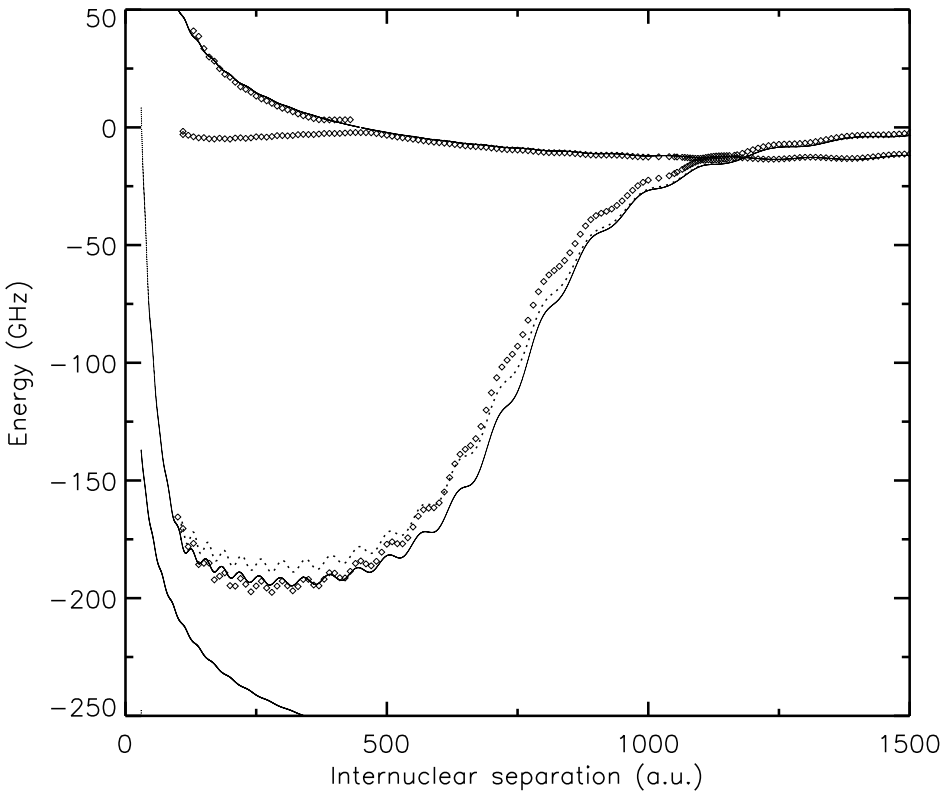

Figure 3.6: Comparison of the Omont generalization of the Fermi pseudopotential (dashed) with the finite-range Pascale-type pseudopotential (points), and the Green's function method (solid) [79].

Chapter 4

Long-range Rydberg states: Green's function method

If requested to derive a method more rigorous than the perturbative or model potential methods discussed in the last chapter, the first inclination of a researcher trained in the tradition of quantum chemistry would be to turn to a variational method. This would be done with the expectation that improving both the volume of the basis set space and the description of electron correlation (by CI or some other method) would result in a solution set converging with arbitrary accuracy to the true energy spectrum. From a computational standpoint, however, applying the standard machinery of quantum chemistry to the system of a separated neutral atom and Rydberg atom entails the acceptance of considerable inefficiencies. The Rydberg electron is distributed over an enormous volume of space, only a small fraction of which is occupied by either the ionic core or the perturbing atom. Apart from these isolated regions of space, the electron experiences only the residual Coulombic potential of the core, completely screened by the core electrons to yield an effective long-range charge of unity. Thus, the system is identical to atomic hydrogen in this region, and must yield a solution assembled by linear superposition of the hydrogenic solutions.

Conceptually, this amounts to envisioning the system as a series of scattering events, with the electron being tossed back and forth from one center to the other, like a ping-pong ball that receives an impulse "kick" and "spin" from the paddle of each player on repeated transits back and forth across the table. If we envision enclosing

all short-range modifications to the asymptotic Coulomb potential within small spheres surrounding the separated centers, the eigenenergies of the system can be found by solving for general solutions locally within each of the three partitioned regions of the electron's motion, and then matching them suitably at the surface of the spheres, to select out appropriate linear combinations of the solutions in each region.

In practice, we still have no interest in actually describing the form of the wavefunction in regions where it interacts strongly with the other electrons. The electron spends only a small fraction of its orbit in these complicated regions, and the net effect of such interactions on the final spectrum is merely to generate appropriate boundary conditions for the "external" Coulombic solutions. In the philosophy of multichannel quantum defect theory, the consequence of such localized boundary conditions is to define a phase shift of the usual hydrogenic solution, which must be accommodated by the formation of a linear combination of the regular and irregular solutions that reproduces that phase shift. The same idea applies in the current context— except that because the system has a boundary condition with symmetry dissimilar to that of the Coulombic potential, the solution will mix not only regular and irregular solutions, but also solutions with different values of angular momenta relative to the core.

Because the solution will be controlled entirely by boundary conditions at a surface, the most computationally advantageous implementation of the solution will involve writing a formal solution in integral form, and then evaluating the effect of phase shifts by means of surface integral corrections to that solution. Surface integrals have reduced dimensionality relative to any method that would involve diagonalization of functions in three-dimensional configuration space, potentially improving the speed of calculations by several orders of magnitude. Moreover, the surface integrals are expected to be over extremely small and localized surfaces, permitting certain natural approximations. The most familiar way of reducing a volume integral solution to surface integral conditions is the application of Green's theorem (variantly known as the "second Green's identity"

in some references), and so we now turn to the task of formulating a Green's function technique for construction of the solution.

4.1 The Coulomb Green's function

The Coulomb Green's function, fortunately, is known since the work of Hostler and Pratt in the 1960s [84, 85, 86] to have an analytic closed form, derived from formally completing the sum over eigenstates in its eigenfunction expansion. To fix the normalization convention, which tends to vary from reference to reference in the literature, we explicitly define the Green's function at energy E, $G_c(\vec{r},\vec{r}\,')$, as the solution to the Coulomb Schrödinger equation

$$\left(\frac{1}{2}\nabla^2 + \frac{1}{r} - \frac{1}{2\nu^2}\right) G_c(\vec{r},\vec{r}\,';\nu) = -\delta(\vec{r}-\vec{r}\,') \tag{4.1}$$

where δ is the Dirac delta function and $\nu = \frac{1}{\sqrt{-2E}}$ is the effective wave number associated with this energy. Then the Green's function can be written in terms of the Whittaker functions $M_{\nu,1/2}(r)$ and $W_{\nu,1/2}(r)$ as

$$G_c(\vec{r},\vec{r}\,';\nu) = \frac{\Gamma(1-\nu)}{2\pi|\vec{r}-\vec{r}\,'|}\left[M'_{\nu,1/2}(\eta)W_{\nu,1/2}(\xi) - M_{\nu,1/2}(\eta)W'_{\nu,1/2}(\xi)\right]. \tag{4.2}$$

The primed functions denote derivatives with respect to the total arguments, which are given by

$$\xi = (r + r' + |\vec{r}-\vec{r}\,'|)/\nu$$

and

$$\eta = (r + r' - |\vec{r}-\vec{r}\,'|)/\nu.$$

Note that these two parameters depend only on the orientation of $\hat{r}$ and $\hat{r}'$ relative to one another, and not the absolute orientation of the entire system, with the result that the entire expression is invariant with respect to rotation, just as one would expect for the solution to a spherically symmetric potential. The fact that the solution can be

reduced to only two dynamical variables, $r + r'$ and $|\vec{r} - \vec{r}|$, instead of three as might be anticipated purely from conservation of angular momentum, is a consequence of the higher symmetry associated with the invariance of the Runge-Lenz vector.

Alternatively, the Green's function can be written as an expansion in spherical harmonics $Y_{lm}(\theta, \phi)$:

$$G_c(\vec{r}, \vec{r}'; \nu) = \sum_{lm} g_l(r, r') Y_{lm}(\theta, \phi) Y_{lm}(\theta', \phi'). \tag{4.3}$$

The one-dimensional radial Green's function for a particular angular momentum l is then

$$g_l(r, r') = \frac{\nu}{rr'} \frac{\Gamma(l + 1 - \nu)}{\Gamma(2l + 2)} M_{\nu, l+1/2}\left(\frac{2r_<}{\nu}\right) W_{\nu, l+1/2}\left(\frac{2r_>}{\nu}\right), \tag{4.4}$$

with $r_<$ defined as the lesser of r and r', and $r_>$ as the greater of r and r'. In terms of the regular and irregular Coulomb functions $f_l(r)$ and $g_l(r)$, the same function is written as

$$g_l(r, r') = -\frac{1}{rr'} \frac{\pi}{\sin \pi(\nu - l)} f_l(r_<) \left(f_l(r_>) \cos \pi(\nu - l) + g_l(r_>) \sin \pi(\nu - l)\right). \tag{4.5}$$

The second factor in the product should be recognized as the linear combination of solutions that vanishes at infinity. (Here and elsewhere, the function g_l with one argument denotes the irregular Coulomb function, whereas g_l with two arguments is the radial Green's function.)

Finally, the most general form of the Green's function (from which equation 4.2 can be derived, and of which 4.3 is a special case) is the eigenfunction expansion,

$$G_c(\vec{r}, \vec{r}'; \nu) = \sum_{nlm} \frac{\Phi_{nlm}(r, \theta, \phi) \Phi_{nlm}(r', \theta, \phi)}{E_n - E(\nu)}, \tag{4.6}$$

with $E(\nu) = -\frac{1}{2\nu^2}$ and $E_n = -\frac{1}{2n^2}$. In principle, the sum runs over both the infinity of bound states and extends as an integral into the continuum, although truncation

to a finite number of bound states often provides a reasonable approximation to the converged sum. The eigenstates are the familiar hydrogenic wavefunctions

$$\Phi_{nlm}(r,\theta,\phi) = \frac{2}{n^2}\sqrt{\frac{(n-l-1)!}{(n+l)!}}\left(\frac{2r}{n}\right)^l e^{-r/n}\, L_{n-l-1}^{2l+1}\left(\frac{2r}{n}\right)\, Y_{lm}(\theta,\phi), \qquad (4.7)$$

defined in terms of the generalized Laguerre polynomial $L_b^a(x)$.

4.2 Hydrogenic solution for S- and P-wave scattering

The use of Green's function-based scattering formalism to derive the perturbation of a Rydberg spectrum has been an object of periodic interest, primarily among Russian researchers, since the mid-1960s. In their classic studies of the zero-range potential, Demkov and Drukarev [87, 88, 63] demonstrated that the effect of a short-range potential well on a weakly bound electron in an external electric (or magnetic) field could be approximated as a zero-range boundary condition on the Green's function solution enforced at a single point. Twenty years later, they revisited the same problem for higher angular momenta [89], replacing the zero-radius potential approximation with a boundary condition on a small sphere. A more powerful implementation of the same ideas was proposed by Andreev and coworkers [90, 91], based on Landau and Lifshitz's classic treatment [92] of the scattering of slow particles by a short-range center. Tkachenko [93] explicitly applied this generalized theory to the Coulombic system in the context of studying charge-transfer complexes (i.e., systems in which the short-range potential has at least one bound state that perturbs the spectrum). The charge transfer process has continued to attract attention, for example, in the consideration of laser-assisted collision complex formation [65, 66], or certain fundamental summation relations [94]. One of the more interesting applications of the Green's function method during this period was that of de Prunelé [67], who observed small oscillations in the potential curves of alkali-He systems at separations as large as hundreds of Bohr radii. Most recently,

the work of Fabrikant, Chibisov, and Khuskivadze [95, 74] applied a Kirchoff integral technique involving the matching of the Green's function solution to a short-range solution calculated by *ab initio* methods. The approach of this section differs somewhat from any of these earlier methods in the detailed derivation, but overlaps importantly with them on the conceptual level, and predicts similar results in the appropriate limits. In particular, we follow the same basic procedure as Fabrikant, but we rely here only on phase shift data, without any need to find a short-range electron perturber solution wavefunction.

To find the eigenspectrum of a perturbed hydrogenic Rydberg atom, we begin by assuming the same geometry and coordinate system as in the previous chapter, with the Rydberg atom nucleus at the origin and the perturber located at a distance R along the z-axis. The dimension of the perturber is again taken to be small on the scale of both the electron wavelength, and the variation of the electron wavelength. This permits the use of the same simple quasi-classical relationship between R and the scattering wavenumber k that appeared in equation 3.1, as a parameter for the energy-dependent phase-shift $\delta_l(k)$.

For the hydrogenic case, we consider a solution $\Psi(\vec{r})$ to the Coulomb Schrödinger equation, valid everywhere outside of a small sphere of radius y around the perturber at $\vec{R}$:

$$\left(\frac{1}{2}\nabla^2 + \frac{1}{r} - \frac{1}{2\nu^2}\right)\,\Psi(\vec{r}) = 0. \tag{4.8}$$

By multiplying 4.1 from the left on both sides of the equation by $\Psi(\vec{r})$, 4.8 by $G_c(\vec{r},\vec{r}';\nu)$, taking the difference, and integrating over the outer region, we find an integral form for the formal solution,

$$\Psi(\vec{r}) = -\frac{1}{2}\int \left\{\Psi(\vec{r}\,')\nabla^2 G_c(\vec{r},\vec{r}\,') - G_c(\vec{r},\vec{r}\,')\nabla^2\Psi(\vec{r}\,')\right\} d^3r'. \tag{4.9}$$

By application of Green's theorem, this then reduces to the desired surface integral:

$$\begin{aligned}\Psi(\vec{r}) &= -\frac{1}{2}\oint\left\{\Psi(\vec{r}\,')\vec{\nabla}G_c(\vec{r},\vec{r}\,') - G_c(\vec{r},\vec{r}\,')\vec{\nabla}\Psi(\vec{r}\,')\right\}\cdot d\vec{a}\,' \\ &= \frac{1}{2}\oint\left\{\frac{\partial\Psi(\vec{r}\,')}{\partial \mathrm{n}'}G_c(\vec{r},\vec{r}\,') - \frac{\partial G_c(\vec{r},\vec{r}\,')}{\partial \mathrm{n}'}\Psi(\vec{r}\,')\right\}da\,'. \qquad (4.10)\end{aligned}$$

The derivative with respect to n' denotes differentiation along a surface normal vector directed outward from the original integration volume, that is, pointing into the spherical surface of integration of radius y surrounding the perturber. After defining a local coordinate system centered on the perturber,

$$r_x = |\vec{r} - \vec{R}|, \quad \theta_x = \arctan\left(\frac{\mathrm{r}\sin\theta}{\mathrm{r}\cos\theta - \mathrm{R}}\right), \quad \phi_{\mathrm{x}} = \phi,$$

and for the primed coordinate,

$$r_y = |\vec{r}\,' - \vec{R}|, \quad \theta_y = \arctan\left(\frac{\mathrm{r}'\sin\theta}{\mathrm{r}'\cos\theta - \mathrm{R}}\right), \quad \phi_{\mathrm{y}} = \phi',$$

the outer solution becomes

$$\Psi(\vec{r}) = \frac{1}{2}\oint\left\{\frac{\partial G_c(\vec{r},\vec{r}\,')}{\partial r_y}\Psi(\vec{r}\,') - \frac{\partial\Psi(\vec{r}\,')}{\partial r_x}G_c(\vec{r},\vec{r}\,')\right\}da\,'. \qquad (4.11)$$

The surface of integration is defined as the spherical set of points for which $r_y = y$, where $y \ll 1$ is a constant.

The inner region solution, defined in terms of the same local coordinate system, can be expanded in terms of a set of spherical harmonics centered on the perturber. The sphere enclosing the inner region is small, and the potential due to the ionic core is varying slowly at this distance. To a good approximation, the solution at the bounding surface (where we also assume that the short-range atom-electron potential is negligibly small) can be written in terms of the radial wavefunctions appropriate to free-electron partial-wave scattering: the regular and irregular spherical Bessel functions, j_l and η_l. In conjunction with the previously discussed quasi-classical approximation that fixes the

local wavenumber as $k = \sqrt{-\frac{1}{\nu^2} + \frac{2}{R}}$, this permits us to write the inner region solution at the boundary as

$$\Psi(\vec{r}) = \sum_{lm} A_{lm}(j_l(kx)\cos\delta_l^{(k)} - \eta_l(kx)\sin\delta_l^{(k)})Y_{lm}(\theta_x, \phi_x), \tag{4.12}$$

where the k-dependent parameter $\delta_l^{(k)}$ is the phase shift for free-electron scattering in the lth partial wave channel. In analogy with y above, x is defined as a parameter fixing the value of r_x, this time with $y < x < 1$. (That is to say, not only is this solution valid on the boundary at y, but we have further assumed that it remains approximately valid even on a larger boundary at x where the solutions will be matched. This assumption can be made without loss of generality, since the r and r' coordinates are symmetric in the Green's function, and will be convenient for use in a future Taylor expansion. The approximation only becomes exact, of course, in the limit as both x and y approach 0, but that limit may still be taken in a way that preserves the ratio between x and y.)

Since the current system displays rotational symmetry around the $\vec{R}$ axis, and the magnetic quantum number m is defined relative to this axis in both coordinate systems, the final solution wavefunction will still have m as a good quantum number. In particular, we expect to find molecular wavefunctions of Σ symmetry for $m = 0$, Π symmetry for $m = 1$, and so forth. For present applications, we will assume that electron-perturber scattering for angular momenta beyond $l = 1$ is negligible, although the method may be naturally extended for scattering states with a d-wave resonance. Thus, just as for the previous methods, we anticipate three types of solutions: a Σ state arising from S-wave scattering, a Σ state arising from P-wave scattering with $m = 0$, and a Π state arising from P-wave scattering with $m = 1$. For geometries in this chapter where this symmetry is preserved, the solution will be written with a subscript, $\Psi_m(\vec{r})$, to specify this symmetry.

In order to reduce the formal solution in terms of a linear system of integral

equations into a numerical problem in linear algebra, the solution must be resolved into components defined in terms of some discrete basis. For the hydrogenic case, the most logical choice for a finite basis is the set of spherical harmonics centered on the perturber, for several reasons. First, the inner region solution is already defined as an expansion in this basis, such that the projection onto spherical harmonics simply picks out a single term in the expansion. Since all but the first few l-values will have vanishing phase shifts (reflecting the absence of any interaction with the core), the matrix elements arising from these higher terms decouple entirely from the molecular states generated by lower angular momentum scattering, and including them in the projection basis gives only trivial solutions that correspond to non-interaction. Thus, the summation in equation 4.12 may be effectively truncated after only the low-l terms. Second, the Green's function varies slowly enough over this distance that it may be expanded in a Taylor series with rapidly diminishing higher-order terms. Third, because the symmetries are controlled by the local behavior of the wavefunction at the perturber, an expansion local to that center will naturally result in a matrix equation with diagonal elements that can be associated with states of the appropriate symmetries, and off-diagonal elements that reflect the coupling between them.

To reduce the integral equation to a matrix equation, we first insert the solution from 4.12 into 4.11, and then project both sides onto spherical harmonics:

$$\begin{aligned} < lm|\Psi_m > &= \oint d\Omega_x Y^*_{lm}(\theta_x,\phi_x)\Psi_m \qquad (4.13)\\ &= A_{lm}(j_l(kx)\cos\delta_l^{(k)} - \eta_l(kx)\sin\delta_l^{(k)})\\ &= \frac{1}{2}\sum_{l'} A_{l'm}\oint y^2 d\Omega_y \Big[I'_{lm}(x,\vec{y})\left(j_l(ky)\cos\delta_l^{(k)} - \eta_l(ky)\sin\delta_l^{(k)}\right)\\ &\quad -I_{lm}(x,\vec{y})\frac{\partial}{\partial y}\left(j_l(ky)\cos\delta_l^{(k)} - \eta_l(ky)\sin\delta_l^{(k)}\right)\Big] Y_{l'm}(\theta_y,\phi_y), \end{aligned}$$

where the function $I_{lm}(x,\vec{y})$ is the projection of the Green's function onto $Y^*_{lm}(\theta_x,\phi_x)$,

$$I_{lm}(x,\vec{y}) = \oint d\Omega_x Y^*_{lm}(\theta_x,\phi_x) G_c(\vec{r},\vec{r}';\nu), \tag{4.14}$$

and $I'_{lm}(x,\vec{y})$ is the partial derivative of this function with respect to x.

The resulting matrix equation may be written in its most general form as

$$\begin{pmatrix} a_{00}(x,y;k) & \cdots & a_{0,l'}(x,y;k) & \cdots & a_{0,l_{max}}(x,y;k) \\ \vdots & \ddots & & & \vdots \\ a_{l,0}(x,y;k) & & a_{l,l'}(x,y;k) & & a_{l,l_{max}}(x,y;k) \\ \vdots & & & \ddots & \vdots \\ a_{l_{max},0}(x,y;k) & \cdots & a_{l_{max},l'}(x,y;k) & \cdots & a_{l_{max},l_{max}}(x,y;k) \end{pmatrix} \begin{pmatrix} A_{0m} \\ \vdots \\ A_{lm} \\ \vdots \\ A_{l_{max}m} \end{pmatrix} = 0. \tag{4.15}$$

For the case $l_{max} = 1$, the resulting matrix equation has dimensionality 2×2 for $m = 0$, with the form

$$\begin{pmatrix} a_{00}(x,y;k) & a_{01}(x,y;k) \\ a_{10}(x,y;k) & a_{11}(x,y;k) \end{pmatrix} \begin{pmatrix} A_{00} \\ A_{10} \end{pmatrix} = 0, \tag{4.16}$$

and 1×1 for $m = 1$, with the form

$$a_{11}(x,y;k) A_{11} = 0. \tag{4.17}$$

Eigenvalues of the Hamiltonian are thereby identified as zeroes in the determinant of the matrix $\mathbf{a}$, as a function of the wavenumber k. For a known eigenvalue k, the linear system 4.14 may be solved, giving the relative values of the unknown coefficients A_{lm} (with their absolute values fixed by the additional constraint of normalization). This process, naturally, must be repeated for varying values of the internuclear separation R in order to map out the internuclear potentials.

One important test of the accuracy of a numerical solution of this equation is that the resulting determinant must be independent of y. This is a consequence of the y-

independence of the inner region wavefunction at the boundary x, as seen in 4.12. This implies that, in taking a Taylor series expansion of Green's function used in the outer region wavefunction expression 4.11, only the leading order terms in y (after accounting for any possible cancellation between the two integrand terms) need be retained.

To evaluate the matrix elements

$$\begin{aligned} a_{ll'}(x,y;k) &= \delta_{ll'}(j_l(kx)\cos\delta_l^{(k)} - \eta_l(kx)\sin\delta_l^{(k)}) \\ &\quad -\frac{1}{2}\oint y^2 d\Omega_y \left[I'_{lm}(x,\vec{y}) \left(j_l(ky)\cos\delta_l^{(k)} - \eta_l(ky)\sin\delta_l^{(k)} \right) \right. \\ &\quad \left. -I_{lm}(x,\vec{y})\frac{\partial}{\partial y}\left(j_l(ky)\cos\delta_l^{(k)} - \eta_l(ky)\sin\delta_l^{(k)} \right) \right] Y_{l'm}(\theta_y,\phi_y), \end{aligned} \tag{4.18}$$

we expand the Green's function in a Taylor series around the point $\vec{R}$. As noted previously, the Coulomb Green's function, although defined in a six dimensional configuration space, depends on only two independent variables as a result of its high symmetry. Although these variables have already been defined as ξ and η above for the sake of a compact notation, it will be more convenient here to define them as

$$u = |\vec{r} - \vec{r}\,'| = \nu\tfrac{(\xi-\eta)}{2}$$

and

$$v = r + r' = \nu\tfrac{(\xi+\eta)}{2}.$$

For $\vec{r}$ and $\vec{r'}$ both in the vicinity of $\vec{R}$, the variable u is close to $2R$, and the variable v is close to 0. After separating out the $1/v$ factor containing the divergence at $\vec{r} \to \vec{r}\,'$, the Taylor expansion of the analytical Green's function, to third order in these variables, yields

$$\begin{aligned} G_c(u,v;\nu) &= \frac{1}{2\pi v}\Phi(u,v;\nu) \\ &= \frac{1}{v} + \Phi_v + \Phi_{uv}(u-2R) + \frac{1}{2}\Phi_{vv}v + \frac{1}{2}\Phi_{uuv}(u-2R)^2 \\ &\quad + \frac{1}{2}\Phi_{uvv}(u-2R)v + \frac{1}{6}\Phi_{vvv}v^2. \end{aligned} \tag{4.19}$$

The subscript notation signifies a partial derivative with respect to that variable; Φ_{uv} designates the partial derivative of $\Phi = 2vG_c(u, v; \nu)$ with respect to both u and v, i.e. $\partial^2\Phi/\partial u\partial v$, always evaluated at $u = 2R$ and $v = 0$. The expansion lacks terms that correspond to first and higher partial derivatives with respect to u only, since all such derivatives of Φ identically vanish.

The expressions for the Φ terms often have a surprisingly simple form, due to the ability to convert higher derivatives into lower derivatives using the Whittaker equation identity

$$M''_\nu(\frac{2R}{\nu}) = -(-\frac{1}{4} + \frac{\nu^2}{2R})M_\nu(\frac{2R}{\nu}) = \frac{\nu^2k^2}{4}M_\nu(\frac{2R}{\nu}). \tag{4.20}$$

The second derivative M'' here is with respect to the total argument, and the wavenumber remains defined as before according to the quasi-classical approximation $k = \sqrt{-\frac{1}{\nu^2} + \frac{2}{R}}$. A series of such identities can be defined recursively to reduce any expression of higher order derivatives to an expression written using only M and W, and their first derivatives. The first few cases required for the p-wave case are given here explicitly for reference:

$$\Phi_{vv} = -k^2 \tag{4.21}$$

$$\Phi_{uv} = -\frac{\nu\Gamma(1-\nu)}{2R^2}M_\nu W_\nu \tag{4.22}$$

$$\Phi_{vvv} = \Gamma(1-\nu)\left\{(\frac{\nu}{2R^3} - \frac{k^4\nu}{2})M_\nu W_\nu - \frac{2k^2}{\nu}M'_\nu W'_\nu + \frac{1}{2R^2}\left(M'_\nu W_\nu + M_\nu W'_\nu\right)\right\} \tag{4.23}$$

$$\Phi_{uvv} = \frac{2}{R^2} \tag{4.24}$$

$$\Phi_{uuv} = \Gamma(1-\nu)\left\{\frac{\nu}{2R^3}M_\nu W_\nu - \frac{1}{2R^2}\left(M'_\nu W_\nu + M_\nu W'_\nu\right)\right\}. \tag{4.25}$$

It is implied that all Whittaker functions and derivatives appearing above are evaluated at the position of the perturber, that is, with the argument $\frac{2R}{\nu}$.

The integrals in Eq. 4.14 may be simplified by noting that the projections onto $Y^*_{lm}(\theta_x, \phi_x)$ will eliminate all terms of the Taylor expansion except those with the proper symmetry, based on the orthogonality of spherical harmonics. To make the symmetry explicit, it is advantageous to expand the variables u and v in the spherical polar coordinate system centered on the perturber:

$$u = 2R + (x\cos\theta_x + y\cos\theta_y) + O(\frac{1}{R}) \tag{4.26}$$

$$v = \left(x^2 + y^2 - 2xy(\sin\theta_x \sin\theta_y \cos(\phi_x - \phi_y) + \cos\theta_x \cos\theta_y)\right). \tag{4.27}$$

Then the Taylor series terms are regrouped according to their angular symmetry with respect to the perturber center:

$$\begin{aligned} G_c(u,v;\nu) = \frac{1}{2\pi}\Big\{ & (\frac{1}{x} + \Phi_v + \frac{1}{2}\Phi_{vv}x + \frac{1}{6}\Phi_{vvv}x^2) \\ & +(\Phi_{uv}x + \frac{1}{2}\Phi_{uvv}x^2)\cos\theta_x \\ & +(\Phi_{uv}y + \frac{1}{2}\Phi_{uvv}xy)\cos\theta_y \\ & +(\frac{y}{x^2} - \frac{1}{2}\Phi_{vv}y - \frac{1}{3}\Phi_{vvv}xy)(\sin\theta_x \sin\theta_y \cos(\phi_x - \phi_y) + \cos\theta_x \cos\theta_y)\ \Big\}. \end{aligned} \tag{4.28}$$

Additional terms proportional to higher spherical harmonics are not shown, but would be relevant if Λ took on values greater than 1 (i.e. Δ states and higher). The ϕ dependence controls which terms survive in the Σ and Π molecular symmetries. For example, in the Σ symmetry, the terms proportional to $\cos(\phi_x - \phi_y)$ will vanish in the projection integral, whereas for the Π symmetry the reverse is true, and all terms except for these will vanish. The spherical Bessel functions are already relative to the perturber center, so it is trivial to expand them in powers of x or y.

Once all of these expansions in the perturber-centered coordinate system are inserted into the determinantal equation 4.15, and the relevant integrals over the Green's function are carried out, the elements of the determinant will be written as expansions in

x or y. For the zero-range approximation, where x and y are assumed to be vanishingly small, only the leading order term is significant, and all higher powers can be neglected. Since the inner region solution 4.12 is independent of y, the determinant matrix elements must also be y-independent to leading order; this provides a consistency check on various cancellations that occur in analytical simplification of the matrix elements, and has also been confirmed numerically. The dependence on x is generally finite (since the spherical Bessels do display x dependence), but should cancel on either side of the equation to give a final equation in ν and R *only*. (Factors of k may also need to be divided out of the entire equation in order to clarify the identity of the scattering length, although this is a purely cosmetic modification.) For the Σ symmetry ($m = 0$), the solution condition from the determinantal equation is

$$\begin{aligned} 0 \quad = \quad & \left\{ 1 - \Phi_v \frac{\tan\delta_0^{(k)}}{k} + (\Phi_{vvv} - 3\Phi_{uuv})) \frac{\tan\delta_1^{(k)}}{k^3} - \right. \\ & \left. (\Phi_v \Phi_{vvv} + 3\Phi_{uv}^2 - 3\Phi_v \Phi_{uuv}) \frac{\tan\delta_0^{(k)}}{k} \frac{\tan\delta_1^{(k)}}{k^3} \right\}. \end{aligned} \tag{4.29}$$

Note that the k dependence could have been entirely rewritten in terms of ν and R, but has been left explicit in order to reveal the energy- dependent triplet scattering length, $a_T = -\tan\delta_0^{(k)}/k$, that appears in the Fermi pseudopotential treatment. A logical factorization of this expression yields the equivalent form

$$\{1 + a_T \Phi_v\} \left\{ 1 + (\Phi_{vvv} - 3\Phi_{uuv}) \frac{\tan\delta_1^{(k)}}{k^3} + \frac{a_T}{1 + a_T} (3\Phi_{uv}^2 \frac{\tan\delta_1^{(k)}}{k^3}) \right\} = 0. \tag{4.30}$$

The final term in the second bracketed factor is numerically "small" under most circumstances, and so this amounts to a near-separation of the total quantization condition into two independent solutions. In fact, the first bracketed factor is immediately recognizable as the result of Demkov [63] for S-wave scattering of a Rydberg electron off a zero-range potential, confirming that the method recovers the predicted S-wave solution

in the limit that P-wave scattering is negligible, as first derived by Dalidchick and Ivanov [96]. The capability to describe higher partial waves in our theory is comparable to the theories of Tkachenko [93] and Dubov and Rabitz [66], both derived by the method of Andreev [90], and the results here agree for the special cases considered in those papers. (To our knowledge, however, no previous study ever applied these results to a system with a scattering resonance in the manner of the current work.) Thus, Eq. 4.30 may be understood as a generalization of the results of [63] and [96], but with the additional capability of describing avoided crossings between the two classes of solution. For the Π symmetry, the equivalent expression is simply

$$1 - \Phi_{vvv} \frac{\tan \delta_1^{(k)}}{k^3} = 0. \tag{4.31}$$

The form of the Taylor expansion coefficients Φ_{xy} provides a source of analytical information about the behavior of the solution potential, albeit without much accompanying physical insight. For example, one can observe that both Φ_v, Φ_{uv}, and Φ_{uuv} all oscillate as a function of R such that they may vanish at particular R values, while Φ_{vv}, Φ_{uvv}, and Φ_{vvv} do not. This implies that the Σ solution potential curves will show oscillations, while the Π curve will be smooth. It also suggests that the coupling between the S-wave and P-wave scattered bound states (which is proportional to Φ_{uv}) will potentially vanish for certain values of R, such that the avoided crossing between the potential curves may become nearly diabatic.

Extension of the above results to a non-hydrogenic case (i.e., for finite quantum defects, as with an alkali Rydberg atom) can be accomplished in one of two ways. First, the Rydberg core can be treated as a second scattering center for the electron, and an equivalent set of surface integrals performed local to its center. Of course, the inner region solution around the ionic center will need to be expanded in terms of Coulomb functions, rather than spherical Bessel functions, but in all other respects the derivation

is identical. Each non-zero quantum defect creates an additional linear equation that must be solved, and increases the dimensionality of 4.14 by one. Alternatively, the Green's function can be expanded in spherical harmonics relative to the ionic core, with the quantum defect explicitly inserted into the radial solution of Eq. 4.5:

$$\begin{aligned} g_l^{Rb}(r,r') &= -\frac{1}{rr'}\frac{\pi}{\sin\pi(\nu+\mu_l-l)}\left\{f_l(r_<)\cos\pi\mu_l - g_l(r_<)\sin\pi\mu_l\right\} \\ &\quad \left\{f_l(r_>)\cos\pi(\nu-l) + g_l(r_>)\sin\pi(\nu-l)\right\}. \end{aligned} \tag{4.32}$$

If the Coulomb Green's function given by the expansion for vanishing quantum defect (i.e., using Eq. 4.5) is subtracted from this expression, the result is a closed form for the correction term, first derived (based on a somewhat different argument) by Davydkin *et al.* [97],

$$G_{q.d.\,corr}(\vec{r},\vec{r}';\nu) = \frac{\pi}{rr'\sin\pi\nu}\sum_{lm}\frac{\sin\pi\mu_l}{\sin\pi(\mu_l+\nu)}\mathcal{W}_{\nu,l+1/2}(r)\mathcal{W}_{\nu,l+1/2}(r')Y_{lm}(\theta,\phi)Y^*_{lm}(\theta',\phi'), \tag{4.33}$$

where the notation $\mathcal{W}$ denotes the Whittaker function normalized according to the same convention as the standard Coulomb f and g, i.e. $\mathcal{W} = f\cos\pi(\nu-l) + g\sin\pi(\nu-l)$. The integrals over this correction term are identical in form to those of the Coulomb Green's function itself, and carried out numerically. (Since the sum cannot be performed analytically, there is no advantage to attempting a Taylor series expansion as before.)

In the actual evaluation of these integrals, numerical stability of the root-find procedure is greatly improved by the analytic removal of singularities. In the Coulomb Green's function, the prefactor $\Gamma(1-\nu)$ is singular at each integer ν, and diverges as $(\sin\pi\nu)^{-1}$; this is expected, since the Green's function has a pole at the hydrogenic solutions. Similarly, the terms in the summation form for the correction for finite quantum defects each diverge whenever $\sin\pi(\mu_l+\nu)$ vanishes; in the absence of the perturber, this would define the set of non-degenerate poles at $\nu = n - \mu_l$.

A plot of the Σ potential curves for the Rb*-Rb long-range molecular Rydberg state in the vicinity of the n=30 manifold are shown in Figure 4.1.

4.3 Solution in the presence of an external field

Because of the unusually large dipole moments of these molecules, even a weak external electric field will be sufficient to align them. For this reason, it is desirable to have some estimate of the effect of an electric field on the level structure of the bound state potential curves. Furthermore, the functional form of the field dependence of the level shifts may prove useful in the experimental distinguishing of Rydberg-ground state interactions like the trilobite state, and Rydberg-Rydberg long-range dipole interactions such as those discussed in [22]. The theory of Rydberg-perturber interactions was already the subject of study by de Prunelé [67], in the context of non-resonant states formed for Rydberg-rare gas dimers (which do not support bound states, but do yield oscillatory long-range potential curves).

In introducing a weak external electric field, we follow the approach of de Prunelé, and consider the form of the correction term from the standpoint of an eigenfunction expansion in the Stark eigenstates. This requires that the Stark spectrum first be expanded in terms of the zero-field spectrum by a full diagonalization. In the hydrogenic case, the results of this transformation are known exactly; the Stark Hamiltonian is exactly separable in parabolic coordinates, and the transformation coefficients for arbitrary field were first derived by Fano and Harmin [98, 99], with strong analogies to the MQDT frame transformation [100]. For an alkali system, the diagonalization must be performed numerically by first-order perturbation theory (see, for example, [101]). The Stark map for several manifolds of Rb in the vicinity of n=15 is shown in Figure 4.2.

Since both the Coulomb Green's function and the Coulomb-Stark Green's function can be expanded in eigenstates, the correction due to the external field is [67]

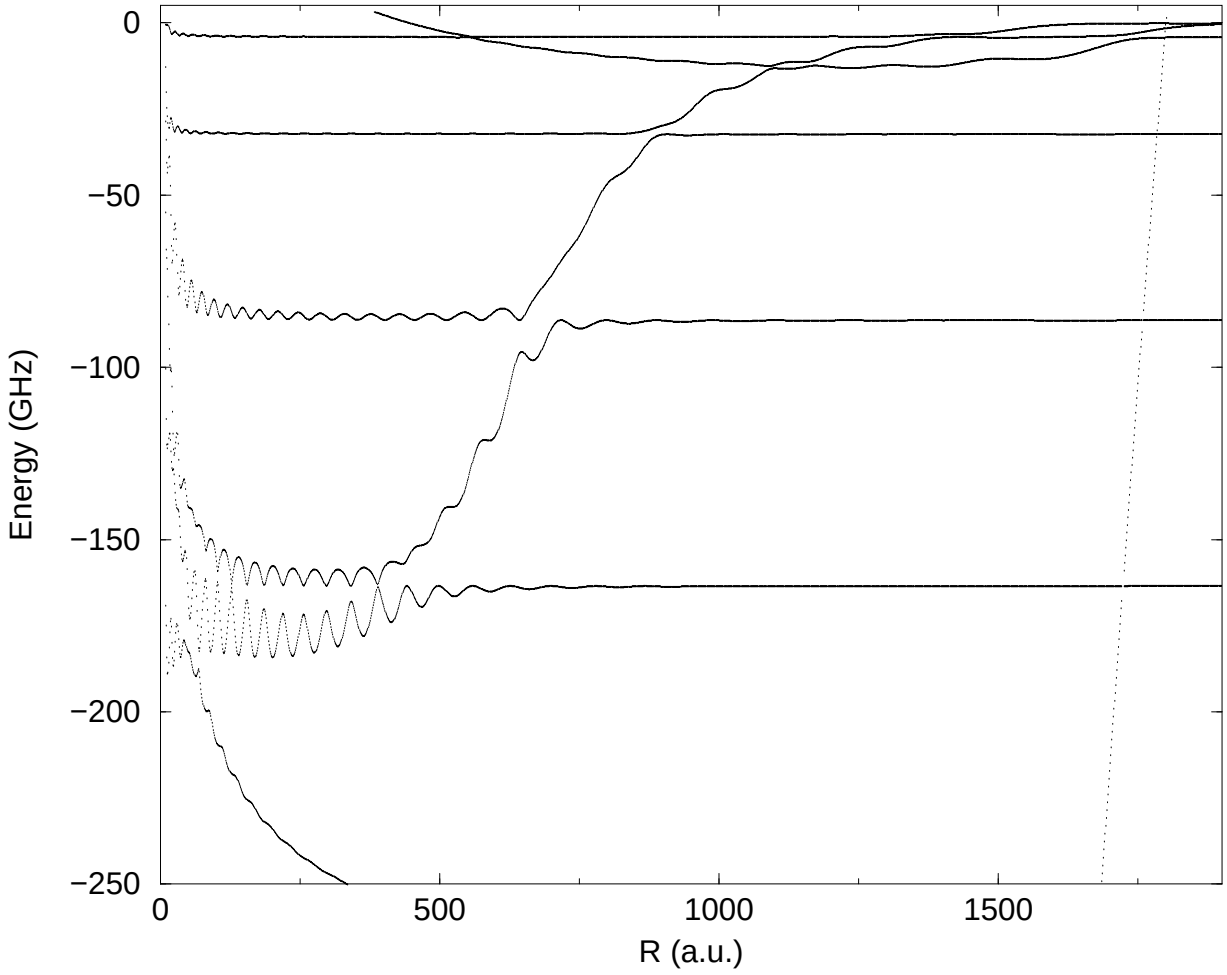

Figure 4.1: $^3\Sigma$ potential curves for Rb*-Rb long-range interaction, relative to the energy of the n=30 hydrogenic manifold. The nearly vertical line of zeroes occurring beyond R=1750 is an artifact of the root finder at the classical turning point k=0.

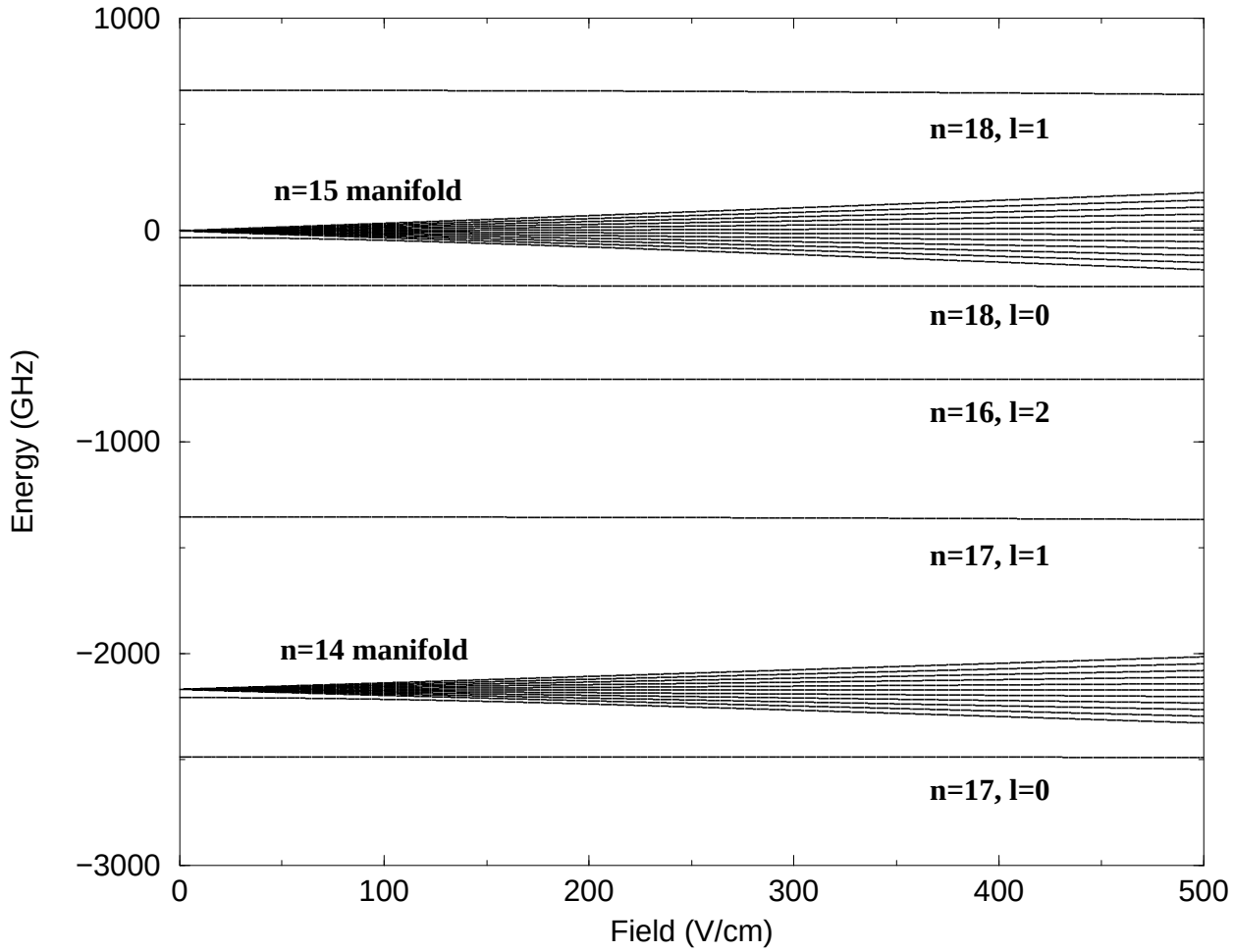

Figure 4.2: Stark splitting for Rb in the vicinity of the n=15 manifold.

$$\Delta G_s(\vec{r},\vec{r}';E) = \langle r| \left(\sum_{\alpha,m} \frac{|\alpha m\rangle\langle \alpha m|}{E-E_\alpha} - \sum_{\nu,l,m} \frac{|\nu l m\rangle\langle \nu l m|}{E-E_{\nu l}} \right) |\vec{r}'\rangle \tag{4.34}$$

In principle, the sum runs over the entire eigenspectrum, including the continuum. For most practical purposes, however, the correction is only important when the terms in the denominator become large, restricting the sum to levels close to the bound state energy of interest.

If this correction term is added to the Green's function in the outer region solution, the matching condition will find solutions for a finite-field Coulomb-Stark Hamiltonian. We will initially assume that the external field is aligned with the internuclear axis. The level structure may be investigated as a function of both the dynamical parameters E and R. Holding E constant and varying R gives the Born-Oppenheimer potential curves for the molecular state. Figures 4.4 and 4.5 show the energy level spectrum at a fixed field strength, as a function of the internuclear separation R.

Alternatively, R may be held constant and the field strength varied, in order to study the Stark effect itself. Figure 4.5 shows the Stark maps for several energy levels at a fixed internuclear separation, as a function of the field strength.

4.4 Semiclassical interpretation

Rydberg states are often celebrated in the literature for their potential to bridge the conceptual gap between the quantum and classical worlds. The motion of a Rydberg electron may be described accurately using semiclassical techniques, which relate the classical closed-orbit trajectories of the spatial potential to the underlying nodal structure of the true quantum mechanical solution. In this section, we discussion the origin of the nodal pattern for the $^3\Sigma$-scattered state. This is a condensed version of the semiclassical interpretation presented in [73], which may referenced for a more extended discussion of these results in terms of the EKB quantization.

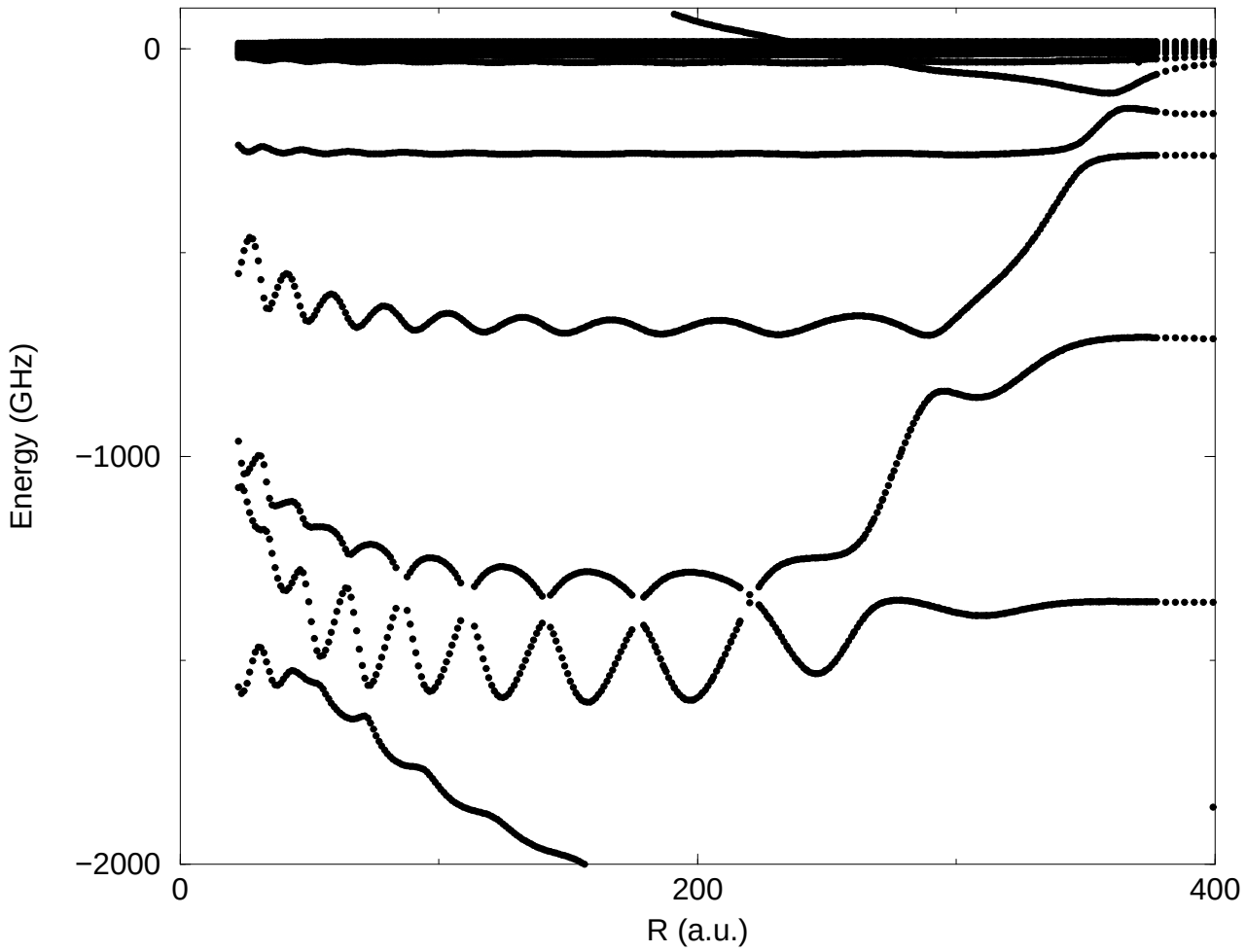

Figure 4.3: Adiabatic energy level spectrum for states of Σ molecular symmetry in the vicinity of then = 15 manifold, for a field strength of 51.42 V/cm. Note that the degenerate manifold has been split in accordance with the linear Stark effect. The avoided crossings between the P-wave scattered molecular state and the atomic P state are partially obscured by artifacts that reflect insufficient sensitivity of the root-finding algorithm.

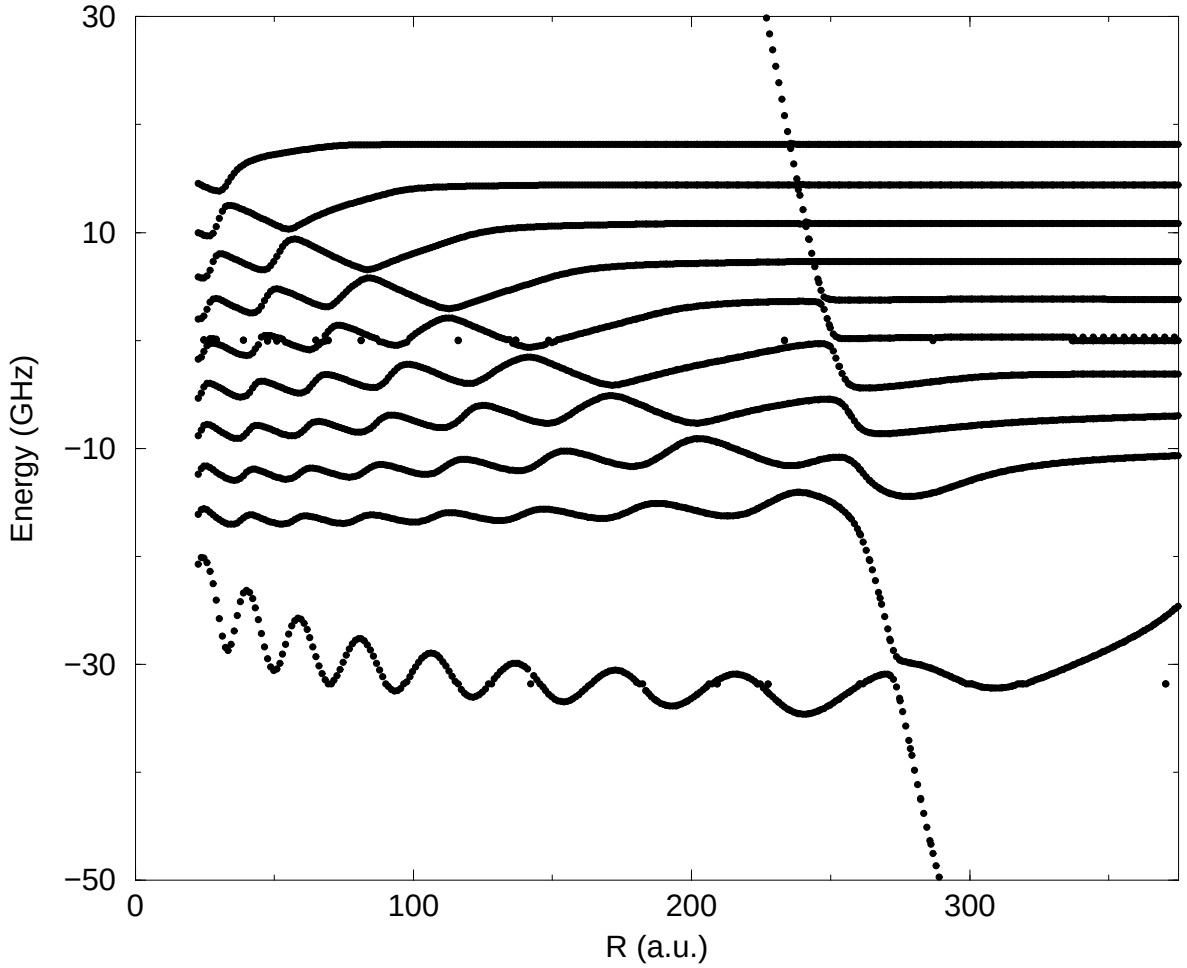

Figure 4.4: Magnified region of the previous plot showing the energy spectrum near the degenerate manifold, with a series of avoided crossings between the trilobite state and high-angular momentum atomic states. Occasional spurious roots appear at the position of the atomic levels, reflecting imperfect cancellation between the Stark correction term and the Coulomb Green's function.

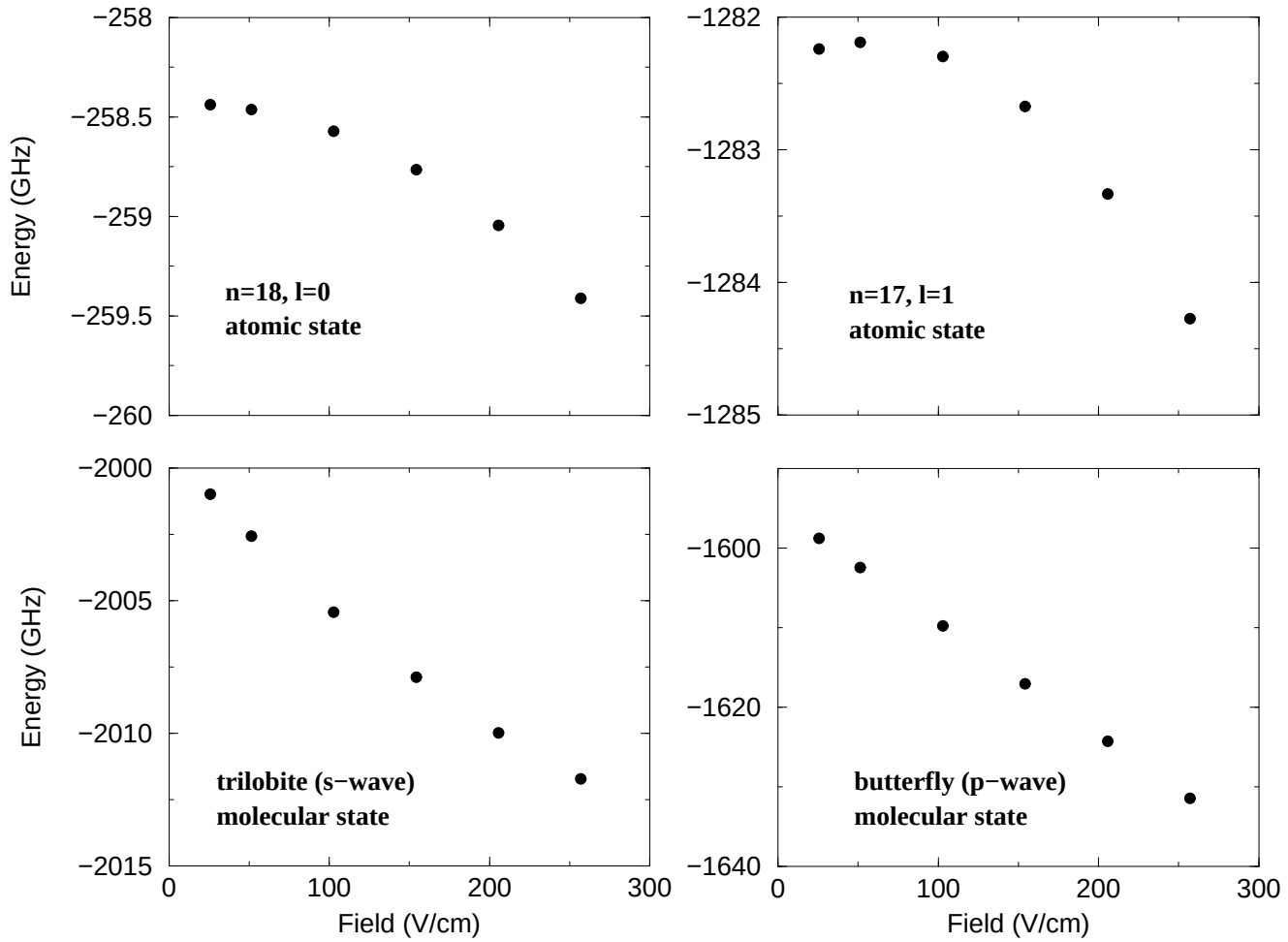

Figure 4.5: Energy dependence of selected atomic and molecular levels with respect to electric field, at an internuclear separation of $R = 157$.

The robust, elliptic nodal structure of the electronic states observed in Figure 3.1 suggests that the problem will simplify in elliptic coordinates. Elliptic coordinates have been used to treat a number of other two center problems such as H_2^+ [102] and atomic hydrogen perturbed by a point dipole [103]. From this standpoint, it is no surprise that elliptic coordinates are useful for the current system. However, it is desirable to understand both why elliptic coordinates seem to be preferred in our system, and exactly how the description is simplified when elliptic coordinates are used.

Guided by the elliptically shaped nodal patterns, we introduce elliptic coordinates, defined with the foci of the elliptical coordinate system placed on the ion (at the origin) and the perturbing Rb atom $(\rho, z) = (0, R)$. If r_1 and r_2 are the distances between the Rydberg electron and the two foci of our coordinate system, the elliptic coordinates are defined as

$$\begin{aligned} \xi &= \frac{r_1 + r_2}{R} \\ \eta &= \frac{r_1 - r_2}{R}. \end{aligned} \tag{4.35}$$

These coordinates are constrained to the ranges $1 \leq \xi < \infty$ and $|\eta| \leq 1$. Next, our unperturbed elliptic eigenstates are introduced.

The elliptic eigenstates we construct here are stationary eigenstates of the hydrogen atom. These states differ from the traditional states of hydrogen (eigenstates of $H, \vec{L}^2, L_z$) through the replacement of $\vec{L}^2$ by a constant of the motion that emerges out of elliptic coordinates. The Schrödinger equation for an electron (in a molecular $L_z = 0$ Σ state) in a Coulomb potential in elliptic coordinates reads [104, 105, 106]

$$\left[-\frac{1}{2}\frac{\partial}{\partial\xi}\left(\xi^2 - 1\right)\frac{\partial}{\partial\xi} - \frac{1}{2}\frac{\partial}{\partial\eta}\left(1 - \eta^2\right)\frac{\partial}{\partial\eta} - \frac{R}{2}(\xi - \eta) - \frac{R^2}{4}E\left(\xi^2 - \eta^2\right) \right] \Psi(\xi, \eta; R) = 0. \tag{4.36}$$

This equation separates into two one-dimensional eigenvalue problems for the elliptic separation constant $B(R)$

$$\left[-\frac{1}{2}\frac{\partial}{\partial\xi}\left(\xi^2-1\right)\frac{\partial}{\partial\xi}-\frac{R}{2}\xi-\frac{R^2}{4}E\xi^2\right]F(\xi,R) = B(R)F(\xi,R) \tag{4.37}$$

$$\left[-\frac{1}{2}\frac{\partial}{\partial\eta}\left(1-\eta^2\right)\frac{\partial}{\partial\eta}+\frac{R}{2}\eta+\frac{R^2}{4}E\eta^2\right]\Phi(\eta,R) = -B(R)\Phi(\eta,R), \tag{4.38}$$

where $\Psi(\xi,\eta;R)=F(\xi,R)\Phi(\eta,R)$. Given a total energy $E=\frac{-1}{2n^2}$ and a distance R, the separation constant $B(R)$ becomes quantized when boundary conditions appropriate for bound states are imposed. We label these states by the number of nodes in the ξ direction, $n_\xi=(0,\ldots,n-1)$. The number of nodes in the angular η direction for this $m=0$ state is then given by the constraint

$$n_\eta = n-1-n_\xi. \tag{4.39}$$

Although analytical power series solutions of these Equations (4.37, 4.38) have been found [104, 105, 106], an efficient way of calculating the solutions is to diagonalize the one-dimensional Hamiltonians in a b-spline basis set. This procedure produces the elliptic Coulomb states $\Psi_{n_\xi}(\xi,\eta;R)$ along with the corresponding values of the separation constant $B_{n_\xi}(R)$. In all of the preceding equations, the internuclear separation R appears as a continuous parameter. However, these equations do not yet include the effect of the perturbing Rb atom. So far, the parameter R only gives the distance between the foci of our elliptic coordinate system.

At least back to Sommerfeld [107], it has been known that the hydrogen atom is separable in elliptic coordinates. Although the separability of the hydrogen atom in elliptic coordinates is not widely known, a number of authors have investigated the properties of the elliptic eigenstates. Erikson and Hill first [108] showed that the elliptic separation constant $B(R)$ was related to the orbital angular momentum about the two

foci of the coordinate system (see also [102, 109]). Figure 4.6 shows contour plots of the electron probability density for four of the degenerate elliptic states in the $n = 30$ manifold. The value of R for the elliptic coordinates underlying these states is 1232 a.u. To our knowledge, the unusual nodal patterns of these states, which range from elliptical $(0, 29)$ to semicircular $(14, 15)$ to wedge $(29, 0)$ shaped, have not been reported in the literature thus far. Next, these states are used as zero order eigenstates in perturbation theory.

To include the effect of the perturbing Rb atom, the perturbation is diagonalized in the basis of elliptic eigenstates. The relevant perturbation matrix is

$$V_{n_\xi n'_\xi}(R) = 2\pi A_T[k(R)] \left\langle n_\xi \left| \delta(\vec{r} - \vec{R}) \right| n'_\xi \right\rangle . \tag{4.40}$$

Because this matrix is separable, only one state splits away from the degenerate n-manifold when it is diagonalized. The total energy of the state can be found analytically, and is given by the expression:

$$E_n(R) = \frac{-1}{2n^2} + \sum_{n_\xi} \left| V_{n_\xi n_\xi}(R) \right|^2 = \frac{-1}{2n^2} + 2\pi A_T[k(R)] \sum_{n_\xi} \left| \Psi_{n_\xi}(1, 1; R) \right|^2 , \tag{4.41}$$

which is used in Figure 4.7 to calculate the Born-Oppenheimer potential curve. The wavefunction is then a linear combination of the elliptic eigenstates $\Psi_{n_\xi}(\xi, \eta; R)$:

$$\Psi_n(\xi, \eta; R) = \sum_{n_\xi} \Psi_{n_\xi}(1, 1; R) \Psi_{n_\xi}(\xi, \eta; R). \tag{4.42}$$

It is clear that both the Born-Oppenheimer potential curve (4.41) and wavefunction (4.42) are determined by the values of the primitive elliptic eigenstates $\Psi_{n_\xi}(1, 1; R)$ at the position of the perturbing Rb atom $(\xi, \eta) = (1, 1)$. In general, the wavefunctions and eigenvalues include contributions from all n elliptic eigenstates in the degenerate manifold. That the molecular states shows a strong elliptic character is seen when the values $\Psi_{n_\xi}(1, 1; R)$ are shown as a function of internuclear separation R. Figure

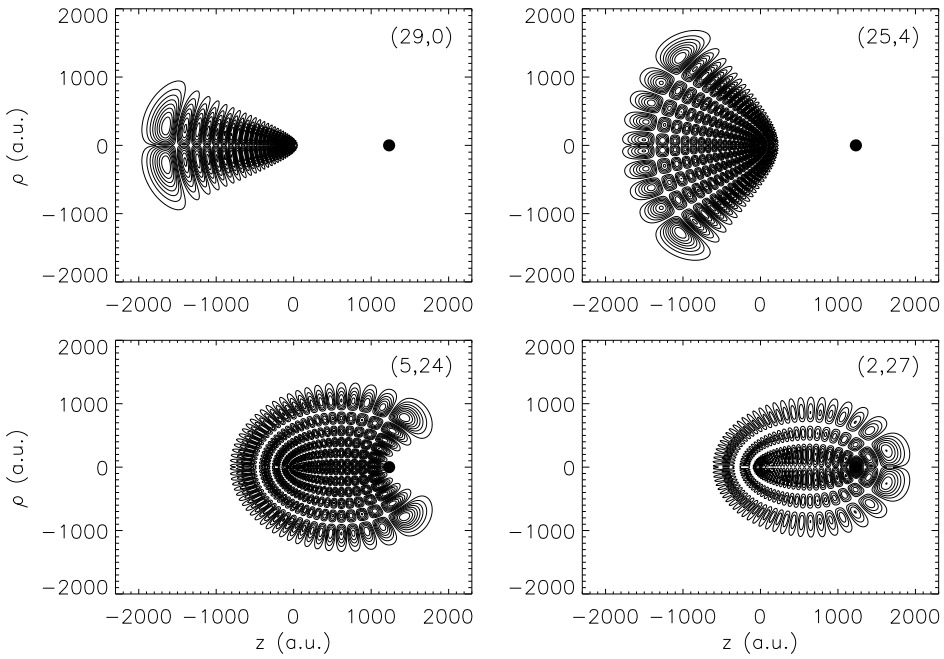

Figure 4.6: Examples of elliptic eigenstates of the $n = 30$ hydrogen atom defined with an elliptic coordinate system where the distance between the foci of the coordinate system is 1232 a.u., and plotted in cylindrical polar coordinates [73]. The foci of the elliptic coordinate system have been placed at the origin and at (ρ, z)=(0,1232) (shown by a small circle).

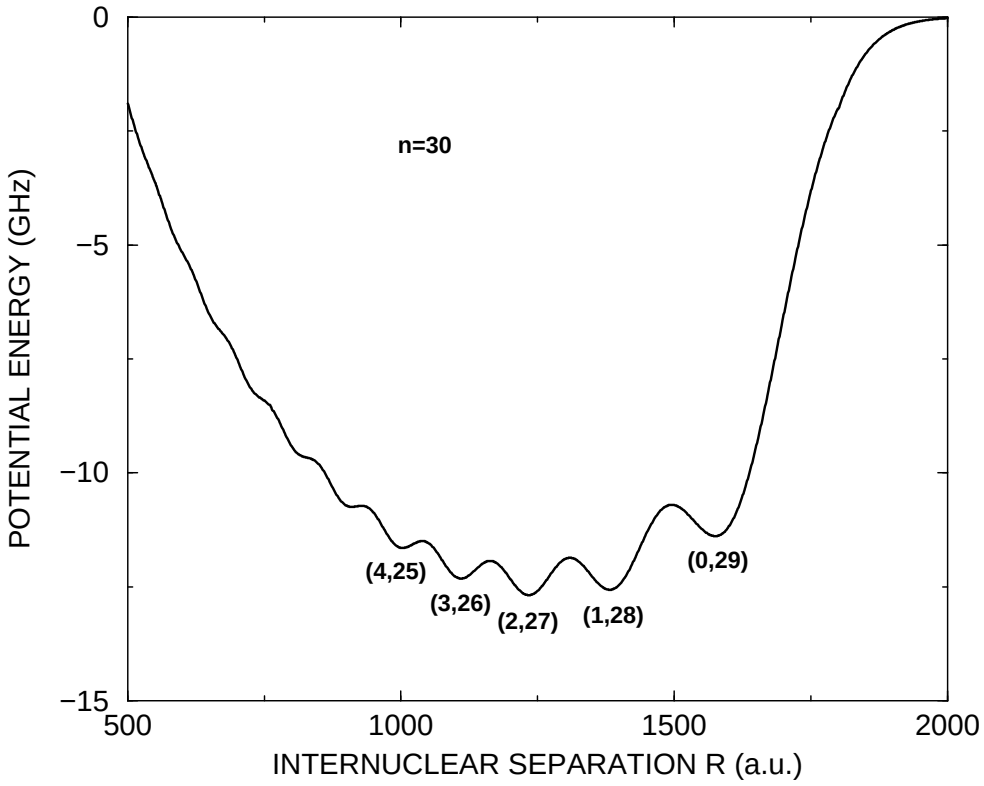

Figure 4.7: Born-Oppenheimer potential curve for a highly polar $n = 30$ Rydberg state of Rb_2 [73]. The approximate numbers of nodes in the electronic wavefunction (ν_ξ, ν_η) are shown below each minima. Note that the effective quantum numbers (ν_ξ, ν_η) evolve continuously as a function of internuclear separation, but are integer valued at the minima.

4.9 shows a plot of the values of $\left|\Psi_{n_\xi}(1,1;R)\right|^2$ $(n_\xi = 0,\, 1\ldots, 10)$ for an unperturbed $n = 30$ state as a function of R. At certain internuclear separations, a single primitive elliptic states dominates the molecular wavefunction (4.42) and Born-Oppenheimer potential curve (4.41). A comparison between the coefficients in Figure 4.9 and the Born-Oppenheimer potential curve in Figure 4.7 shows that the minima in the potential curve occur precisely where a single elliptic state is dominating the molecular wavefunction. This "quasi-separability" of the full wavefunction means that at certain internuclear separations the full Hamiltonian (including the perturbation) is nearly diagonal is the basis of primitive elliptic eigenstates. In some sense, the potential energy is minimized (or maximized, for $A_T > 0$) when the amount a non-separability in elliptic coordinates is the least.

Furthermore, as the internuclear separation is changed, the specific elliptic state that dominates the sums in Equations (4.42) and (4.41) changes. This accounts for the redistribution of the nodes in the molecular wavefunction from the η to the ξ direction as the internuclear separation decreases (see Figures 4.7 and 4.8). Thus, at the outermost minimum ($R = 1575$ a.u.), Figure 4.9 shows a peak in the contribution of the $n_\xi = 0$ state. At the next minimum ($R = 1382$ a.u.), the $n_\xi = 1$ state has come to dominate. As the character of the molecular state evolves from one elliptic state to another the numbers of nodes in the electronic wavefunction (ν_ξ, ν_η) evolve according to the constraint

$$\nu_\xi(R) + \nu_\eta(R) = n - 1. \tag{4.43}$$

The characteristic elliptically shaped nodal pattern is preserved as the nuclei get closer together, but the number of nodes in the two elliptic directions get redistributed from the angular η direction to the radial ξ direction as the internuclear separation is decreased.

Thus we have shown how an unexpected "quasi-separability" in elliptic coordi-

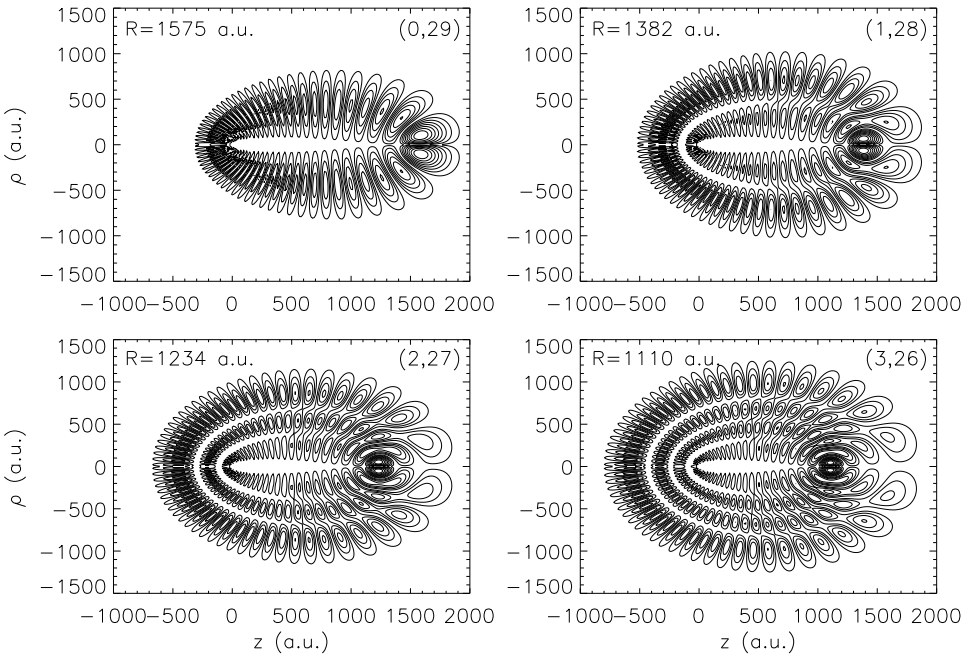

Figure 4.8: Contour plots of $\rho\,|\Psi(\rho,z)|^2$ of the Born-Oppenheimer wavefunctions of a long-range Rb_2 molecule at the energy of an $n = 30$ Rydberg state [73]. Four internuclear separations are shown ($R = 1575, 1382, 1234, 1110$) corresponding to the outermost minima in the oscillating potential curve (see Figure 4.7). These states are labeled by the approximate numbers of nodes (ν_ξ, ν_η) in the two elliptic directions.

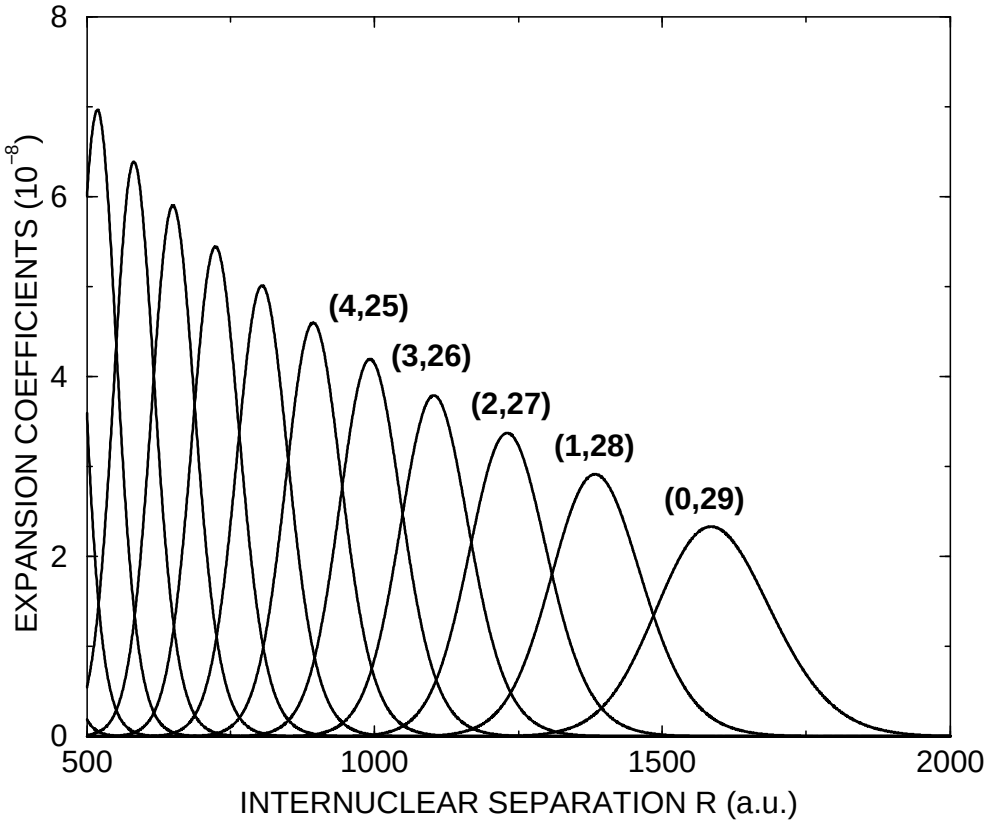

Figure 4.9: The values of the expansion coefficients $\left|\Psi_{n_\xi}(1,1;R)\right|^2$ for a $n = 30$ state [73]. These coefficients determine which elliptic eigenstate of hydrogen (see Figure 4.6) dominates the molecular wavefunction and Born-Oppenheimer potential curve (Figures 4.7 and 4.8) at a given radius. Each peak in the graph is labeled by the elliptic quantum numbers (n_ξ, n_η) of the state the peak represents.

nates emerges at certain internuclear separations. These special internuclear separations are precisely the minima in the Born-Oppenheimer potential curve. That the Born-Oppenheimer Hamiltonian is nearly diagonal in elliptic coordinates at a sequence of internuclear radii is an unexpected simplification that accounts for the elliptical shape of the nodal structure of the molecular states. The evolution of the molecular state with internuclear separation can be viewed as an change in the contributions of the primitive elliptic states that comprise the wavefunction. Now we turn to a semiclassical description of these states.

Semiclassical methods permit a simple interpretation of multidimensional quantum systems [110]. In the absence of the perturbing Rb atom, the long range dynamics of the Rydberg electron are purely Coulombic. Our main challenge is therefore to include the effect of the perturbing Rb atom in a semiclassical treatment. In principle, it would be possible to include the perturbing potential using classical perturbation theory [111]. Rather than this approach, we focus on a more qualitative viewpoint. To include the effect of the perturbing Rb atom semiclassically, we replace its delta-function Fermi potential by an inhomogeneous delta-function source at the perturbing atom. While this is clearly an approximation, we show that this approximation reproduces the solutions from degenerate perturbation (Equation 4.42) theory extremely well. The resulting object of interest is then the Coulomb Green's function with the source placed at the position of the ground state Rb atom. The semiclassical Green's function can be written [110] as a sum over classical trajectories that propagate from $\vec{x}'$ to $\vec{x}$ with energy E:

$$G(\vec{x}, \vec{x}', E) \approx \sum_{traj} A e^{iS(\vec{x},\vec{x}',E) - i\mu\pi/2}.$$

For our purposes the most important quantities in this expression are the classical action $S(\vec{x}, \vec{x}', E)$ and the Maslov index μ of each trajectory, which counts the numbers of sign changes of the amplitude A. The amplitude A is a measure of the stability of each classical path. If the energy E is fixed and the source coordinate of the Green's

function is set to be at the position of the perturbing atom ($\vec{x}' = \vec{R}$) there are only four classical trajectories that contribute to the Green's function $G(\vec{x}, \vec{R}, E)$. These four paths always lie on two Kepler ellipses that intersect the points $\vec{x}$ and $\vec{R}$ and have a Coulomb potential at one focus. An example of these four paths is seen in Figure 4.10. The foci of the elliptic coordinate system (the Coulomb singularity and the perturbing Rb atom) are shown as solid circles. The Green's function is then a coherent sum of the four trajectories that propagate from the ground state Rb atom to the observation point marked by a hollow circle.

Figure 4.11 shows contour plots of both the quantum and semiclassical Coulomb Green's function with the source point placed at the ground state Rb atom $(\rho, z) = (0, 1232)$. The semiclassical Green's function has been constructed as described above, and shows strong agreement with the molecular wavefunction found using degenerate perturbation theory (Figure 4.8) and the quantum Green's function also pictured here. The quantum Green's function shown in Figure 4.11 is based on an analytical expression first derived by Hostler [85, 86]. The good agreement of these three methods (quantum and semiclassical Green's function, and degenerate perturbation theory) show that the inclusion of the perturbing Rb atom through an inhomogeneous source term in the Schrödinger equation is a good approximation for the problem at hand. Additionally, from a semiclassical perspective, then, the nodal structure of these electronic wavefunctions is governed by two things. First, the long range Coulomb physics provides the majority of the dynamical evolution. Second, the ground state Rb atom at $\vec{R}$ selects only Coulomb orbits that pass through this point. From this perspective, constraining the trajectories to pass through the ground state Rb atom is a perfectly sensible way of including the effect of the perturbation in a semiclassical treatment.

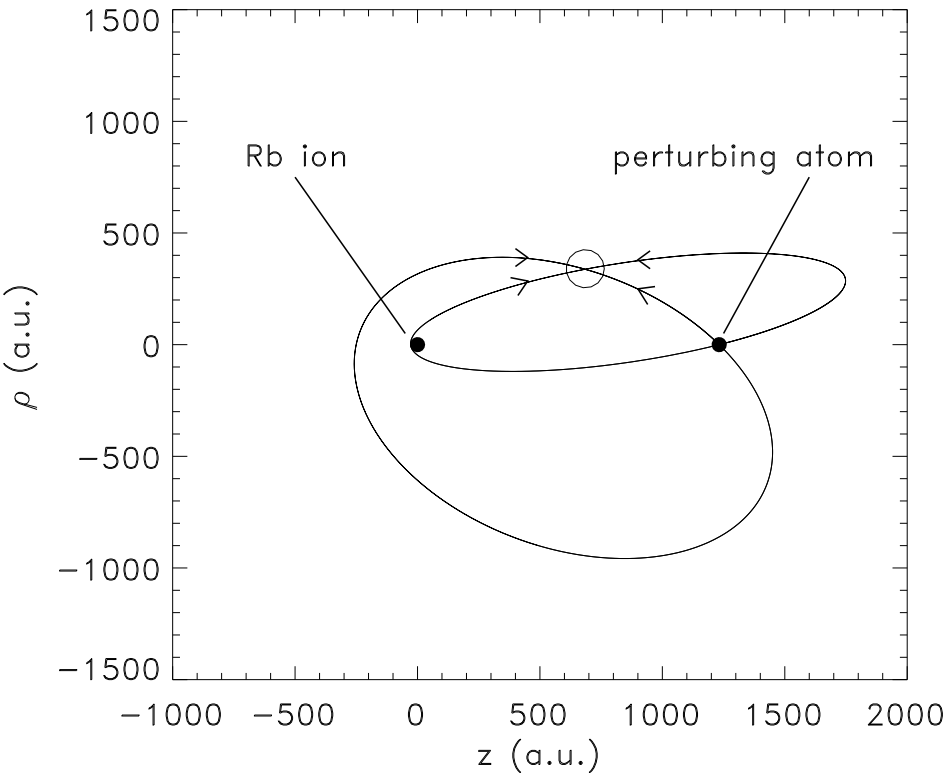

Figure 4.10: An example of the four classical paths lying along the two possible closed-orbit trajectories that contribute to the semiclassical Green's function $G(\vec{x}, \vec{R}, E)$, at the energy of an $n = 30$ Rydberg state [73]. The trajectories lie on two Kepler ellipses intersecting the perturber at $\vec{R}$ (right solid circle) and the observation point $\vec{x}$ (hollow circle). These ellipses are unique when one focus is constrained to be at the Coulomb singularity at the origin (left solid circle).

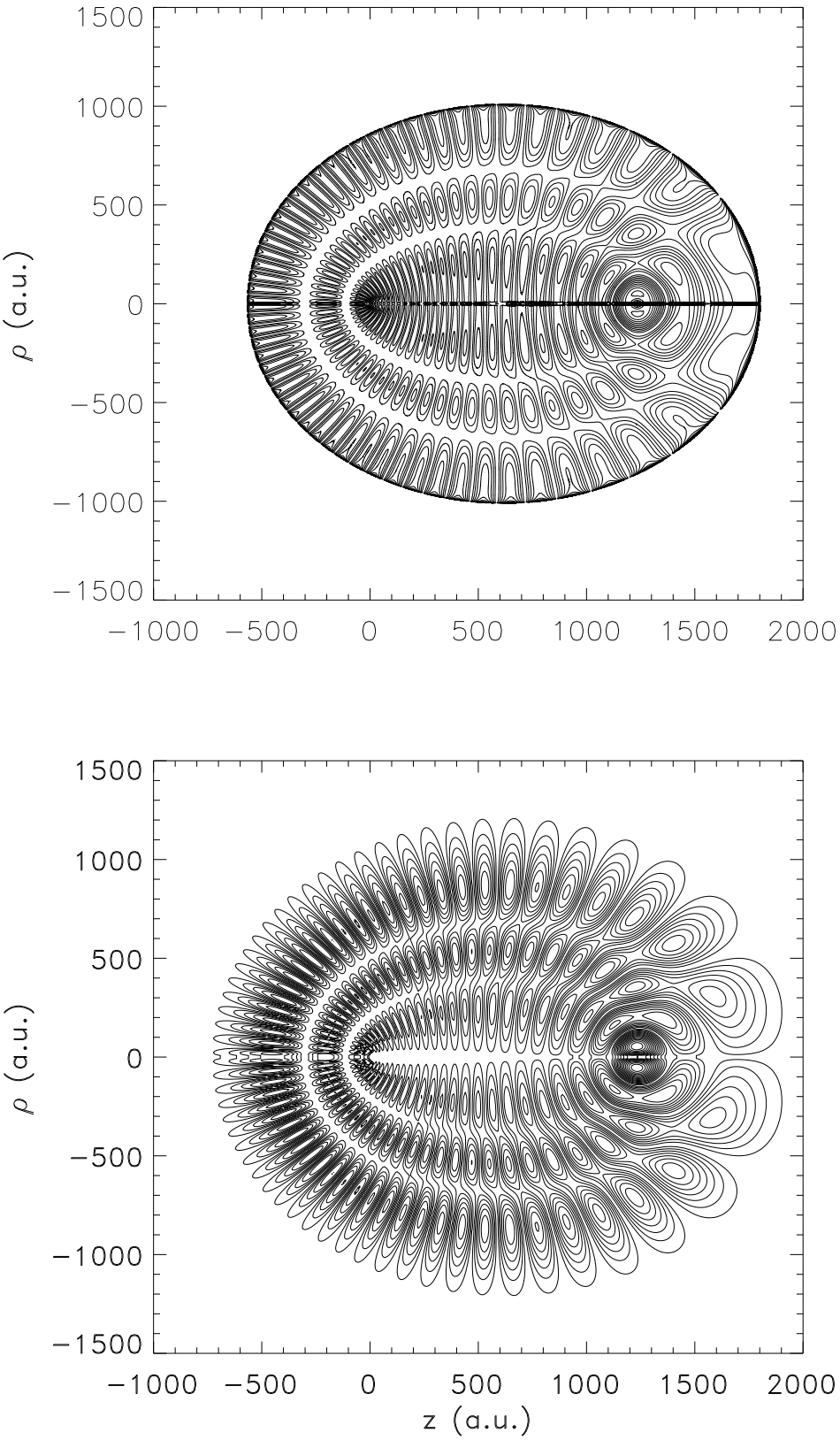

Figure 4.11: Contour plot of the semiclassical (upper) and quantum (lower) Coulomb Green's function with the source coordinate placed at the ground state Rb atom (ρ, z)=(0, 1234) [73]. The semiclassical Green's function has only been shown up to the classical turning point where it diverges unphysically.

Chapter 5

Siegert states

Progress toward a truly general theory of molecular systems excited at continuum energies depends on the ability to describe all accessible continua concurrently. Modern experiments routinely probe energy regimes where multiple channels of both ionizing and dissociative types are in competition [10]. The philosophy of multichannel quantum defect theory outlined in Chapter 2 is naturally suited to the description of physics in the asymptotic region, where channel indices correspond to the quantum numbers of the separated system, and complicated short-range scattering dynamics are reduced to a minimal set of interaction parameters. In principle, the problems of predissociation and preionization are based on exactly the same interaction parameters, since they both hinge on the coupling between the electronic excitation of the Rydberg electron and the rovibronic excitation of the core. In preionization, sufficient energy is transferred from the core to the electron to promote it into the continuum of the separated electron-ion system; in predissociation the reverse process occurs, with energy transferring from the electron into vibrational excitation, dissociating the molecule.

5.1 Dissociative channels in molecular MQDT: General considerations

The extension of quantum defect theory to include a nuclear continuum is not naturally suggested by the form of the channel expansion on which the theory relies,

because the usual theory has only ionization channels represented explicitly (see Eq. 2.2 in Chapter 2). The time-independent Schrödinger wavefunction is conventionally expanded using a solution *ansatz* form that distinguishes the channel states (discrete, and usually calculated numerically) from the asymptotic states of the scattering coordinate (continuous, and usually known analytically at large separations). The necessity of selecting one coordinate set to serve as the "channels" inevitably entails a preimposed bias as to which coordinate should be considered to correspond to the reactive dynamics of the fragmenting particles. From that perspective, the very notion that MQDT could be of utility in double continuum problems may appear on the surface to be questionable.

At the same time, much of the conceptual appeal of quantum defect methods for single continuum studies is retained or even enhanced by the computational challenges of working within a two-continuum problem. The physics of the system is still dominated by a finite set of energetically open channels, and the selection of an expansion form that incorporates those channel states directly will still greatly reduce computational labor. Some coordinates and asymptotically "good" quantum numbers refer to coordinates that obey periodic rather than asymptotic boundary conditions, such as the angular electronic coordinates or the rotational eigenvalues; it would be a great waste of computational resources to solve for wavefunctions already known in advance, such as when the ionization occurs via a few partial waves or into a small number of product rotational states. Moreover, the transition from single continua systems to multiple continua only complicates the necessity of efficiently describing the coupling between metastable resonant states and the continua in which they are embedded. Since the short-range interaction physics to which resonant processes are sensitive is relatively indifferent to the number of different continua or types of continua that are simultaneously open, the same quantum defects and phase shifts that characterize the single-continuum case still ought to contain all necessary information for handling any associated multiple-continuum generalizations of the same system.

5.2 Established methods for handling dissociative channels

The extension of quantum-defect-style techniques to the description of dissociative channel physics was initially pursued in the late 1970s by Schneider, Burke, and other co-workers [112, 113, 114, 115], in the context of electron scattering from neutral molecules. Their calculations were based on the Born-Oppenheimer approximation, and neglected all non-adiabatic coupling effects. This allowed for an adequate handling of dissociative attachment and vibrational excitation processes of neutrals, but could not be extended to electron scattering from positive ions (or the associated half-scattering processes of neutral molecule photoionization and photodissociation), which involve an essentially non-adiabatic coupling interaction with electronic Rydberg states. Still, Schneider *et al.* were able to demonstrate that their R-matrix method gave results formally equivalent to that of the Fano frame transformation formulas (see the concluding discussion of [115]). Other applications of quantum defect theory to the dissociative spectra of diatomic molecules were later developed by Giusti [116] and [117] . These methods are analogous to the standard one-dimensional formulation of quantum defect theory, but with the electronic coordinate replaced by the nuclear degree of freedom. (For an extended discussion of the extension of MQDT to non-Coulombic long-range potentials, see [43, 118, 119].) These methods are rigorous, but naturally involve no reference to electronic physics except at the level of relying on adiabatic or diabatic potential curves.

5.2.1 Jungen eigenphase method

One of the earliest attempts to apply multichannel quantum defect theory to the problem of competing dissociation and ionization processes was carried out by Christian Jungen [53]. Jungen adopted an approach inspired by the utility of Fano's approach [45] in treating the "recoupling" transformation between the short-range interaction of the Rydberg electron with the core, and the long-range Coulombic forces of the Rydberg

states. For escape into an electronic continuum only, the result of this procedure is the orthogonal frame transformation already discussed in Chapter 2. To represent the dissociative physics, the vibrational basis must be augmented in some way that permits a finite value of the wavefunction on the fixed-R boundary between the inner region (where the wavefunction is unknown) and the outer region (where it can be expanded in dissociative channels). R, as before, refers to the internuclear separation, as opposed to r, the radial coordinate of the electron. The assumption is made that the potential in the outer region vanishes except for a constant that defines the channel energy threshold. Note that while the boundary condition of the electronic coordinate r is formally applied at infinity, the boundary condition for the nuclear coordinate R is necessarily imposed at some finite boundary R_0 that delineates the range over which the inner region vibrational basis is defined. Outside the region the solution is a linear combination of the regular and irregular vibrational continuum functions, $F_{n\Lambda}\cos\delta - G_{n\Lambda}\sin\delta$, multiplied by the channel function that describes the state of the dissociating atoms or molecular fragment pair, with the Rydberg electron in a low-n electronic state.

Figure 5.1 shows the inner and outer regions, the boundaries between them, and the form of the solutions in each region, as found in [53]. Solutions with finite amplitude in region II correspond to ionization, and solutions with finite amplitude in region III correspond to dissociation. Solutions in region IV, which would describe dissociative ionization, are not possible in the current version of Jungen's method.

If a vibrational basis for the molecular ion H_2^+ is generated in accordance with a fixed logarithmic derivative boundary condition at R_0, which all functions in the basis must satisfy, then the (discrete) basis consists a ladder of energy levels that begin to resemble the eigenstates of a particle in a one-dimensional box as soon as they rise high enough in energy to exceed the dissociation threshold; they shall be referred to as the "box states", in contrast to the ordinary vibrationally bound states that vanish as $R \to \infty$. For an arbitrary choice of the logarithmic derivative, it is unlikely

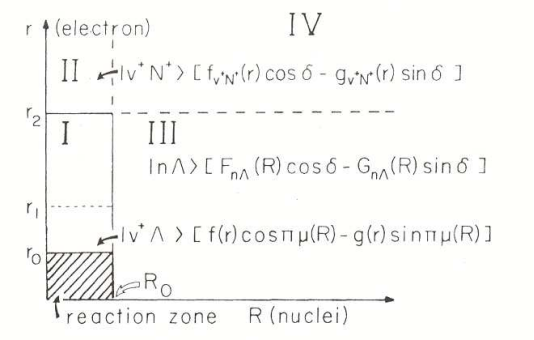

Figure 5.1: Partition of configuration space into inner and outer regions, taken from the work of Ch. Jungen [53].

that the wavefunction expansion constructed using the box states (which all share the same boundary condition) will have an energy at precisely the right value to correspond to the true (energy-conserving) continuum state. The selection of a single logarithmic derivative discretizes the continuum values available for continuum-like H_2^+ channel states, and this also restricts the continuum H_2 states to a finite range of discrete values. Thus, the system must be solved iteratively, with a systematic variation of the logarithmic derivative from $-\infty$ to ∞ that causes the locations of the energy levels to scan across the position of the true dissociative state energy. This is accomplished by casting the eigenequation system normally as for the ionization-only R-matrix approach [120] approach, but including the box state channels as "strongly closed" channels with phase parameters that depend implicitly on the logarithmic derivative. These additional strongly closed channels produce exactly one extra solution, corresponding to the dissociative continuum state of proper energy. This and the other eigenphase solutions are then projected back onto the channel basis, defining the usual smooth, short-range reaction matrix (or scattering matrix). From this point, channel elimination can be performed, usually to close off the "weakly closed" channels associated with the true vibrationally bound states of the molecular ion potential that give rise to the ionization Rydberg series structure.

As originally developed, this method is encumbered by the need to recalculate the eigensolution coupling matrix elements at each new logarithmic derivative. Since the values at which the linear eigensystem possesses an eigensolution are dependent on energy, this means that the system must be solved repeatedly at each energy until the result has iteratively converged to the desired accuracy. Moreover, the method, as originally conceived, functions only for a single dissociative channel per Λ symmetry, and only in the energy regime below dissociative ionization. The reaction matrix contains an explicit channel for dissociation, reflecting the constraint that the solution must vanish either at infinity in all ionization channels, or else at the boundary in the dissociation channel.

More recently [121], Jungen and Ross generalized their method to allow for multiple dissociative channels, and to remove the necessity for iteration. The standard frame transformation calculation is done first for the normal basis set (vanishing at R_0, and it is then repeated with a different logarithmic derivative for each dissociation channel. The eigenchannel solutions for all the different boundary condition choices are combined into a single generalized basis, and the asymptotic boundary conditions then give a generalized eigenvalue problem for the full two-dimensional eigenphases and eigensolution vectors. As before, this gives a short-range reaction matrix with "weakly closed" channels, which may be then eliminated with the usual algebra. This method has provided the most accurate theoretical results currently available, and is in the process of being extended to other systems [122]. It does depend, however, on a physically motivated choice of the "additional" logarithmic derivatives; the accuracy of the results reflects the extent to which an energy in the vibrational basis appears close to the energy at which the calculation is being performed. In effect, this optimization condition amounts to a semi-iterative procedure that must be adjusted "by hand" in different energy ranges. This is easily accomplished for the study of a single peak at some specified energy, but could be potentially quite inconvenient for the calculation of a continuously

energy-dependent spectrum with many peaks over a wide energy range. Moreover, it remains unclear how to extend this method to energies above the dissociative ionization threshold.

5.2.2 Stephens-Greene box averaging method

A more conceptually direct approach to the representation of coupling to a dissociative continuum is that of box size averaging [54]. As in the Jungen method, the dissociative continuum is discretized by allowing the vibrational basis to extend far above the ionic dissociation threshold, to include many box states. Instead of looking at the variation of these state energies with logarithmic derivative, one may instead consider their sensitivity to variations in the box radius R_0. As the box increases in size, the box state levels shift to lower energies, passing smoothly through all continuum energies. The coupling between these fictitious channels and the physical ionization channels provides a measure of the extent to which flux can be expected to pass into those dissociation channels. The positions of resonances with strong dissociative character will be perturbed significantly by the introduction of these additional box states, and the variation in this perturbation as a function of R_0 is thus a measure of the coupling strength between the dissociative continuum and the ionization channel associated with that resonance.

In order to quantitatively interpret this effect, the standard MQDT frame transformation procedure must be performed sequentially for a series of closely spaced box radius parameter values. The cross-sections arising from each individual value of the box radius are then averaged together, giving a cross-section in which the linewidths of dissociation-sensitive peaks have been broadened. The range of R_0 values used in the calculation is determined by the separation between box state energy levels in the vicinity of the energy for which coupling to the dissociative continuum is anticipated to be important; roughly speaking, it is necessary to change R_0 by exactly enough to

shift all the levels down by one cycle, such that the $n+1$-th level is lowered to the position initially occupied by the n-th level. Since the eigenvalues of a particle in a box have a relative spacing itself proportional to n, the selection of an appropriate reference value for n is essential for producing an evenly weighted average. This is a trivial choice at low total energies, where only one dissociative channel is accessible; if there are multiple competing dissociative product channels open at once, however, the criterion becomes more difficult to specify, and if the cycle periodicities are fundamentally incommensurate, potentially impossible.

5.2.3 Two-dimensional R-matrix method

R-matrix techniques derive their name from the original formulation of Wigner and Eisenbud [123], who first recognized that the matrix of generalized logarithmic derivatives on the surface bounding a continuum system of interacting particles could be written as an expansion over resonant terms located at the eigenenergies of the bounded system[1] . This approach demonstrated good utility for the semi-empirical characterization of small collections of known nuclear resonances in terms of a minimal parameter set, but it was not applied widely for *ab initio* computation in its original form, owing to its poor convergence properties. Although it is possible to improve convergence through the inclusion of certain correction schemes, such as the Buttle correction, this can only be accomplished at the expense of some amount of conceptual clarity and computational efficiency.

An alternate version of the R-matrix theory was introduced by Fano and Lee [120], based on transformation to the eigenchannel representation. Rather than selecting a single arbitrary value for the surface logarithmic derivative and solving the Schrödinger equation subject to that condition, the eigenchannel representation provides a set of solutions, each of which has a different logarithmic derivative that is common to all of its

[1] For a review of early applications of R-matrix theory to problems in nuclear physics, see [124].

physical channel components. Since the boundary condition is itself the undetermined eigenvalue parameter, it is permissible to express the matrix equation in a basis set that uses basis functions with a range of different logarithmic derivatives, improving the convergence properties of the final R-matrix expression. This comes at the expense, however, of requiring an iterative solution procedure. For an application of this approach to photoionization, see [125].

The eigenchannel approach may be recast in a noniterative form by means of a variational principle first discovered by Kohn [126]. In contrast to the more traditional bound state applications of the calculus of variations to quantum systems, which apply the Rayleigh-Ritz method to determine a stationary value of the energy for a given basis set, Kohn's principle gives a stationary value for the logarithmic derivative in terms of a fixed scattering energy. For continuum systems this is conceptually advantageous, in that it reflects an awareness that the total energy is typically a controllable input parameter for scattering experiments. This simplification was first proposed for a field-perturbed atomic system by Greene [127], and shortly thereafter extended to molecular photoionization [128]. Although this approach successfully combines the stable convergence of the eigenchannel method with the non-iterative efficiency of the traditional Wigner-Eisenbud theory, it still suffers from the disadvantage of requiring the eigensystem to be solved again at each new energy. This disadvantage may be reduced by use of a modified "streamlined" solution technique for the generalized eigenequation, although for larger basis sets (e.g., such as those commonly required for the two-dimensional R-matrix method), the computational advantage is limited by the inability to efficiently diagonize the Γ matrix in the closed-closed subspace [129, 44]. Additionally, the energy dependence of the R-matrix elements over small energy ranges is frequently smooth enough that they may be interpolated from a limited number of data points, provided sufficient care is taken with respect to the handling of divergences in the logarithmic derivative eigenvalues.

A detailed review of the variational R-matrix method may be found in [129]. Here, we will focus specifically on the specialization of this method to the problem of photoionization and photodissociation in diatomics. For a system with two dissimilar modes of fragmentation, as is the case for competing dissociation and ionization, the variational principle must be adjusted to account for the nonequivalence of the kinetic energy terms of the Hamiltonian. Assume the potential within a two-dimensional box bounded by surfaces at the axes and at $r = r_0$ and $R = R_0$ may be written as $V(r, R)$. Then the time independent Schrödinger equation requires

$$\left(-\frac{1}{2\mu_r}\frac{\partial^2}{\partial r^2} - \frac{1}{2\mu_R}\frac{\partial^2}{\partial R^2} + V(r,R) \right) \psi(r,R) = E\psi(r,R). \tag{5.1}$$

The mass factors μ_r and μ_R denote the reduced masses for electronic and nuclear motion, respectively. The angular degrees of freedom have already been separated in spherical coordinates, such that the full solution in the inner region is given by

$$\Psi(\vec{r}, \vec{R}) = \frac{1}{rR}\psi(r,R)\Phi(\Omega). \tag{5.2}$$

The notation Ω represents all angular degrees of freedom. In general, the possibility of additional electronic symmetries and partial wave components would require a sum over multiple Φ channels, although for the *ungerade* photodissociation spectrum of molecular hydrogen it suffices to assume that only the p-wave channel is active; the R coordinate, however, is strictly confined to s-wave scattering by conservation of momentum. The partition of configuration space that defines the inner region is identical to that of Jungen's work as previously shown in Figure 5.1, with Jungen's radius r_2 corresponding to the box boundary labeled here as r_0.

The mass factors may be temporarily absorbed by a change of variables, $x = \sqrt{\mu_r}r$ and $X = \sqrt{\mu_R}R$, to recast the Hamiltonian in a more symmetric form. Then the differential equation is transformed into the usual matricial form by the taking of an

inner product over the enclosed box volume,

$$E\int dx\,dX\,\psi^*\psi = \int dx\,dX\psi^*\left(-\frac{1}{2}\frac{\partial^2}{\partial x^2}-\frac{1}{2}\frac{\partial^2}{\partial X^2}+\tilde{V}(x,X)\right)\psi \tag{5.3}$$

followed by the application of Green's theorem,

$$\begin{aligned} E\int dx\,dX\,\psi^*\psi &= \int dx\,dX\left(\frac{1}{2}\frac{\partial\psi^*}{\partial x}\frac{\partial\psi^*}{\partial x}+\frac{1}{2}\frac{\partial\psi^*}{\partial X}\frac{\partial\psi^*}{\partial X}\right) && (5.4)\\ &+\int dx\,dX\psi^*\tilde{V}(x,X)\psi && (5.5)\\ &-\frac{1}{2}\int_0^{x_0} dx\,\psi^*(x,X_0)\frac{\partial\psi}{\partial X}|_{x=x_0} && (5.6)\\ &-\frac{1}{2}\int_0^{X_0} dx\,\psi^*(x_0,X)\frac{\partial\psi}{\partial X}|_{X=X_0}. && (5.7)\end{aligned}$$

The logarithmic derivative is defined based on an outward normal with respect to the appropriate scaled variable along each surface,

$$\frac{\partial\psi}{\partial X}|_{X=X_0} = -b\psi, \quad \frac{\partial\psi}{\partial x}|_{x=x_0} = -b\psi.$$

After rearrangement and restoration of the original variables, the variational quantity b may finally be expressed as

$$b = \frac{\sqrt{\mu_r\mu_R}\int dr\,dR\left(2E-\frac{1}{\mu_r}|\frac{\partial\psi}{\partial r}|^2-\frac{1}{\mu_R}|\frac{\partial\psi}{\partial R}|^2-2V(r,R)|\psi|^2\right)}{\sqrt{\mu_r}\int_0^{r_0} dr\,|\psi|^2+\sqrt{\mu_R}\int_0^{R_0} dR\,|\psi|^2} \tag{5.8}$$

Note that the boundary parameter b is not the logarithmic derivative itself, but rather the mass-rescaled logarithmic derivative; to recover the usual logarithmic derivative, b must be multiplied by the appropriate $\sqrt{\mu}$ factor.

Proceeding from this relation, the solution is expanded in a two-dimensional basis,

$$\psi = \sum_i\sum_j c_{i,j}u_i(r)v_j(R)$$

,

to produce the usual generalized eigenvalue equation,

$$\mathbf{\Gamma}\vec{c} = b\mathbf{\Lambda}\vec{c}, \tag{5.9}$$

where $\mathbf{\Gamma}$ is the matrix representation of the numerator of 5.8 and $\mathbf{\Lambda}$ is the matrix representation of the denominator of 5.8 (i.e., the overlap matrix for that basis). Each eigensolution will have a common boundary parameter value b_β on both surfaces. Outside the box boundary, the scattered eigenchannel solutions can be written as a channel decomposition of the regular and irregular solutions [44],

$$\psi_\beta(r,\omega) = \sum_i \frac{1}{r}\Phi_i(\omega)(f_i(r)I_{i\beta} - g_i(r)J_{i\beta}). \tag{5.10}$$

The symbol ω includes all degrees of freedom necessary to describe the channel, including R and all angular coordinates Ω. This wavefunction requires a formal antisymmetrization, but for sufficiently large r_0 this can usually be neglected. For the solutions asymptotic in R, the variable r is replaced by R wherever it appears, and the Coulomb functions f_i and g_i are replaced by the regular and irregular vibrational continuum functions, which can be found by the Milne method [118, 130] or else by similar numerical techniques. The matching condition of continuity for the wavefunction and its derivative permits the determination of $\mathbf{I}$ and $\mathbf{J}$ in terms of Wronskians,

$$I_{i\beta} = -\frac{W(g_i, \psi_{i\beta})}{W(f_i, g_i)}$$

and

$$J_{i\beta} = -\frac{W(f_i, \psi_{i\beta})}{W(f_i, g_i)},$$

and this suffices to define either the reaction matrix $\mathbf{K} = \mathbf{I}\mathbf{J}^{-1}$ or the scattering matrix $\mathbf{S} = (\mathbf{I} + i\mathbf{J})(\mathbf{I} - i\mathbf{J})^{-1}$. The notation $\psi_{i\beta}$ refers to the projection of the solution ψ_β onto the i-th channel function at the appropriate matching surface.

The variational R-matrix method requires an explicit form for the potential energy function within the two-dimensional box. In principle, the potential energy of molecular

hydrogen as a bivariant function of r and R is quite complicated, reflecting short-range electron correlation effects that are challenging to define for the highly excited pseudo-continuum states that characterize the R-matrix eigenspectrum. Instead, we have opted to work with a simplified two-dimensional model potential that reproduces the features of the exact H_2 intermolecular potential to reasonable quantitative accuracy. A separate potential form is utilized for each Λ-space symmetry, with several parameters that may be optimized through a one-dimensional R-matrix procedure to reproduce the known body-frame quantum defects $\mu_\Lambda(R)$. For the Σ symmetry, this procedure yields (in atomic units)

$$V(r,R) = -\alpha_1 \left(1 - \tanh \frac{\alpha_2 - R - \alpha_3 R^4}{7}\right) \tanh\left(R/\alpha_4\right)^4 \frac{e^{-r^2/3}}{r} \tag{5.11}$$

where $\alpha_1 = 1.6435$, $\alpha_2 = 6.2$, $\alpha_3 = 0.0125$, and $\alpha_4 = 1.15$. For the Π symmetry, the optimization gives

$$V(r,R) = \alpha_1 \sqrt{R} \left(e^{-(R-\alpha_2)^2/\alpha_3}\right) \frac{e^{-r^2/3}}{r} \tag{5.12}$$

with $\alpha_1 = 0.480$, $\alpha_2 = 3.35$, and $\alpha_3 = 6.5$. The resulting model potential curves are shown in 5.2. Note that the model potential begins to break down for Σ states of low n, owing to the neglected energy dependence of the Σ quantum defect which is not described by this fitted potential. The shape of the 2Σ potential is not even qualitatively correct, a reflection of the inability of a $^1\Sigma_u^+$ state to dissociate into two ground state hydrogen atoms [40]. This is a problem common to all QDT techniques that use an energy-independent quantum defect, but since the n=2 state lies so low in energy as to be inactive for scattering or photoabsorption processes near the ionization threshold, this does not constitute a serious defect for the purpose of using the model as a test system.

As mentioned above, the R-matrix procedure is computationally expensive to re-

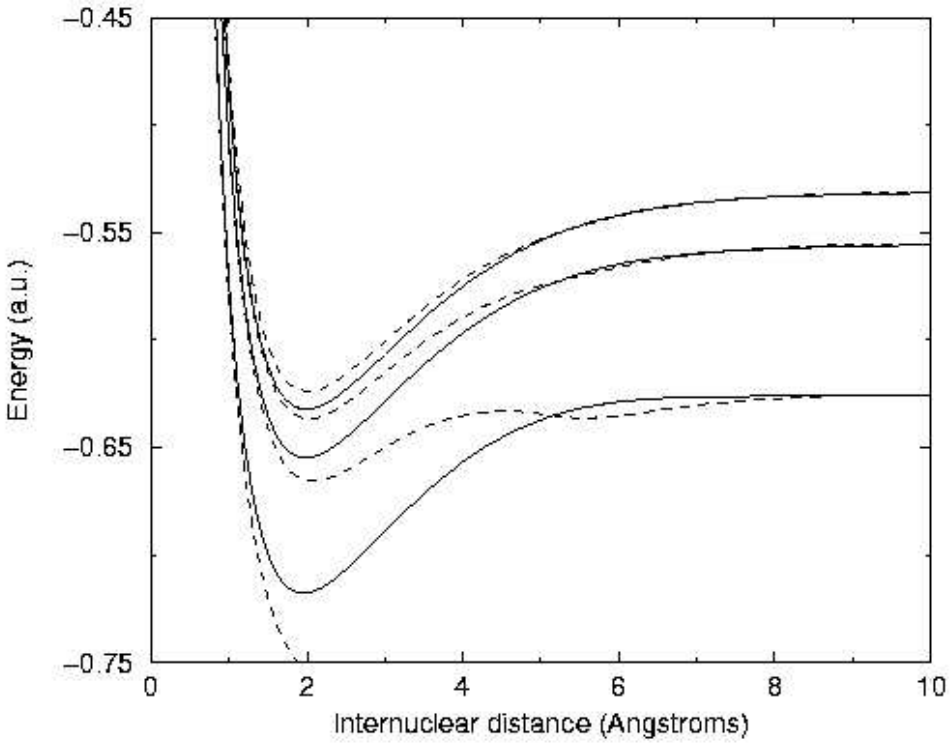

Figure 5.2: Potential curves generated from the model Hamiltonian using Eqs. 5.11 and 5.12. Potentials drawn with a dashed curve are of $^1\Sigma_u$ symmetry, and those with a solid curve are of $^1\Pi_u$ symmetry. (These may be compared with the exact curves for H_2 shown in Figure 2.1.)

peat at each new energy (unless the basis set is small enough to use the streamlined version). Fortunately, the quantities **I** and **J** are only weakly and smoothly energy dependent, and can be interpolated from data computed on a coarser energy grid. Because they incorporate relative phase information, and because the phase is ambiguous with respect to a shift of π, the eigenvector solutions are susceptible to branch discontinuities associated with the underlying trigonometric functions; these must be repaired before the interpolation is applied. Given the interpolated reaction matrix values, the only remaining step that must be performed at each energy is the elimination of closed channels according to the conventional channel elimination procedure. Note that this method results in the appearance of channels in the S-matrix that are explicitly labeled as either ionization or dissociation channels.

Results of the R-matrix calculation, and a comparison with experimental data, are summarized in Table 5.1 (aside from the $v^+ = 2$ resonance series, for which the peaks are exclusively ionized, and occur within a wavenumber or two of the correct position). The photoionization, photodissociation, and total cross-sections are shown in Figures 5.3, 5.4, and 5.5. The photoionization and photodissociation portions of the cross-section are separated by summation over only the appropriate physical channels. Note that since this calculation is based on a model potential, and resonance features are often highly sensitive to small variations in the form of the short-range potential, the comparison is not expected to be quantitative. A comparison with the Siegert method (below) using the same model potential, however, suggests that only errors in the positions (as opposed to widths or relative yields) of the peaks are likely to be a consequence of the failure of the model approximations. The inability of the relative yields to reproduce experiment in anything beyond a general qualitative correspondence is disappointing, and may reflect either a fundamental weakness of the technique, or some undetected error in the implementation. Moreover, the dissociation spectrum reveals an unassignable peak at 786 Å; this may be an artifact related to the anomalous

shape of the $2p\sigma$ and $3p\sigma$ potential curves. This method probably merits further study before any definite conclusions are drawn concerning its capabilities and limitations.

Table 5.1: Positions and fractional yields for select *ungerade* J=0 resonances in H_2.

		Model	Obs. (H_2)
$3p\pi, v = 8$	Position (cm^{-1})	127295.7	127248.2
	Width (cm^{-1})	3.9	3.4
	% Ionization	0.1	≤ 2
	% Dissociation	99.9	≥ 98
$5p\sigma, v = 4$	Position (cm^{-1})	127622.0	127599.4
	% Ionization	0.42	0.77
	% Dissociation	0.58	0.10 ± 0.10
$4p\pi, v = 5$	Position (cm^{-1})	127701.4	127667.6
	% Ionization	0.998	0.85
	% Dissociation	0.002	0.18 ± 0.05

The two-dimensional R-matrix method, unlike the MQDT approaches, works directly from the potential energy function, rather than incorporating that information through intermediate parameters such as the quantum defects. Its advantage is that it does not rely on the vibrational frame transformation method, and thus serves well as a benchmark calculation. In situations where the short-range potential can be described in full quantitative detail, it provides a "brute force" alternative to the more approximate quantum defect methods, with a controlled convergence behavior relative to the variation of geometric parameters like the number of channels and the box dimensions. This can be of potential utility for testing other methods, or studying representative model systems. For experimental spectra, however, the reproduction of accurate high-resolution spectra at the sub-wavenumber level is much more easily attained by the inclusion of semi-empirical parameter adjustments that naturally account for small correction effects.

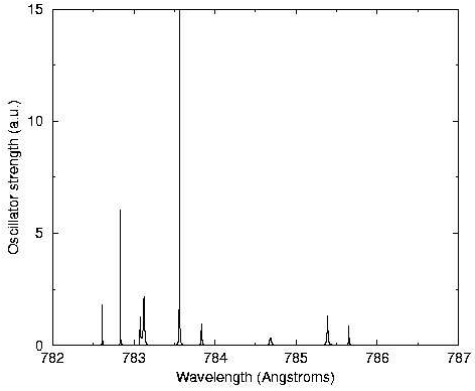

Figure 5.3: Infinite resolution photoionization cross-section calculated using the two-dimensional R-matrix technique.

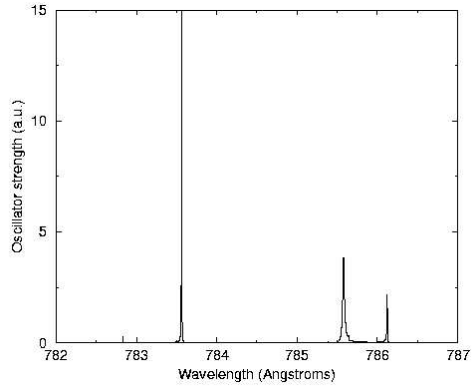

Figure 5.4: Infinite resolution photodissociation cross-section calculated using the two-dimensional R-matrix technique.

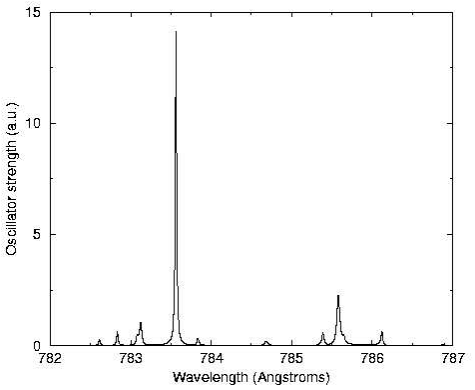

Figure 5.5: Infinite resolution total photoabsorption cross-section, taken from the summation of Figures 5.3 and 5.4.

5.3 Siegert pseudostates: Basic concepts

The difficulties of the Stephens-Greene box-averaging stems from its inability to represent a true outgoing wave solution. With the box averaging method, for example, the inner region solutions are fixed by normalization in such a way as to guarantee conservation of the probability within the box radius; the solution cannot have a finite flux at the boundary, but can only "bounce". As such, the shape of an averaged peak can be broadened, but the total integrated area can never be reduced. This is a necessary consequence of flux conservation. For methods that incorporate the dissociative channel as if it were an additional ionic channel, on the other hand, the solution forces flux to be conserved despite distribution over all channels; this neglects the possibility that the true solution may be coupled to both types of continua at once, implying a failure when the first threshold for dissociative ionization is crossed; it is simply not possible in these methods for flux to be outgoing in both channel types at once. Despite the ability of MQDT to provide, in principle, the true two-dimensional solution within a finite region of space, the use of a conventional basis fails to provide sufficient flexibility to characterize a wavefunction with outgoing wave form in both the asymptotic electronic coordinate (controlled by the assumed asymptotic form of the outer region solutions) and the finite-bounded nuclear coordinate simply in terms of a single set of channel states. Thus, methods such as the treatment of Ross-Jungen [121] must explicitly supplement the basis using additional sets of basis functions obeying non-Dirichlet boundary conditions, with the logarithmic derivative of each new set selected in a somewhat arbitrary and *ad hoc* manner.

The construction of outgoing-wave solutions for a given Hamiltonian can be accomplished by analytically generalizing the energy eigenvalue spectrum of that Hamiltonian into the complex plane. Because outgoing wave states behave asymptotically as exponential functions of a complex argument, they cannot be described in terms of the

usual boundary conditions encountered in Sturm-Liouville theory, since neither their values nor their first derivatives vanish at any point in space; thus, the hermiticity of the Hamiltonian operator is no longer sufficient to guarantee that the eigenvalues are confined to real axis. The physical interpretation of complex eigenenergies was first explored by Gamow [131], who recognized that the lifetime τ of a resonance state was inversely proportional to the imaginary part of its complex energy. Subsequent work by Wiesskopf and Wigner [132] related the lifetime τ to the linewidth parameter $\Gamma = 1/\tau$, at least at the level of the approximation of their theory.

The definition of resonance states in terms of the solutions of the Schrödinger equation may be approached from two somewhat different perspectives. The first theory, developed by Kapur and Peierls [133], was based on the partitioning of the Hamiltonian into an outer region (with a continuous spectrum) and and inner region (with a discrete spectrum), treated as two interacting coupled channels. The Kapur-Peierls eigenstates are defined as the eigenfunctions of an effective Hamiltonian defined by inverting the projection of the resolvent operator onto the inner channel. Since this is an energy-dependent operator, with the wavenumber of the outer channel continuum state as a free parameter of the Hamiltonian, the eigensolution set itself has a parametric dependence on the scattering energy. Although the Kapur-Peierls functions have the advantage of well-behaved orthogonality and completeness properties, they are inconvenient for use in any calculation which involves a range of scattering energies; because they have such a complicated parametric dependence on the energy, they are quite difficult to evaluate except by rediagonalizing the effective Hamiltonian at each new energy.

A alternate, parameter-free version of the resonance states was developed by Siegert [134]. Siegert states are defined, in a much more intuitive way, as the eigensolutions of the Hamiltonian that vanish at the origin and have pure outgoing wave character in the asymptotic limit $R \to \infty$. Siegert's derivation, notably, allowed for overlapping resonances of arbitrary width, giving a smooth background term in the

cross-section. Siegert eigenstates formally correspond to S-matrix poles in the complex plane. Sharply resonant features associated with bound states can be identified with poles lying on the real axis, while broad background scattering can be described by closely spaced eigenstates with finite imaginary parts that serve as a discretized approximation to the true continuum. The Siegert states offer several advantages over the Kapur-Peierls theory. First, they correctly describe long-lived resonances in the sense that they pass smoothly over into bound states; any states that lie lower in energy than the continuum threshold of a potential are guaranteed to correspond to the usual (real-valued) bound states. For the Kapur-Peierls formulation, this only occurs for a fortuitous selection of the partitioning radius. Moreover, the Siegert bound states are guaranteed to be correctly normalized and orthogonal. Second, the Siegert states are uniquely defined for a given Hamiltonian at any scattering energy. This allows them to serve as an expansion basis for other functions, including the Green's function. (A more detailed survey of the relations between the Siegert and Kapur-Peierls theories may be found in [135].) In addition to their identification as poles of the scattering matrix, one may note from the Siegert boundary conditions at 0 and ∞ that the Siegert eigensolutions are proportional to the Jost solution $f_{\pm}(k, R)$ [136], and the eigenvalues are equivalent to the zeroes of the Jost function $J_{\pm}(k) = f_{\pm}(k, 0)$ in the complex plane [137].

A renewed interest in Siegert functions during the 1970s was stimulated by the realization that they could be applied to the direct calculation of total [138] or partial [139, 140] linewidth parameters in many-electron multichannel systems. These methods do not calculate cross-sections, but extract the resonance eigenvalues directly as poles of the scattering matrix; they are closely related to the various complex coordinate scaling methods [141]. The utility of Siegert states for numerical calculations is compromised by their rapid exponential divergence for increasing r. One of several approaches for circumventing divergence-related instabilities was developed by Meyer and Walter [137],

who confined the range of the Siegert states to a finite radius, and solved for their eigenspectrum within an L^2 primitive basis set using variational calculus. That is, they replaced the exact Siegert boundary condition

$$\left(\frac{d}{dR} - ik\right)\phi(R)\Big|_{R=\infty} = 0 \tag{5.13}$$

with the finite range boundary condition

$$\left(\frac{d}{dR} - ik\right)\phi(R)\Big|_{R=R_0} = 0. \tag{5.14}$$

(As a historical note, it is the latter definition that actually corresponds to that of Siegert's original paper, which was only concerned with very short-range nuclear interaction potentials.) This method allowed a single formalism to yield all the bound, virtual, and resonance states of the potential, a significant accomplishment.

A complication of the method involves the necessity of differentiating the ''cut-off" resonances, a string of closely spaced poles in the complex plane arising from the truncation of the potential at a finite cut-off radius, from the true physical resonances. These are not artifacts, but rather the direct scattering states associated with that modified potential. They are highly sensitive to the shape of the potential tail and the location of the cut-off discontinuity, even if the tail is exponentially small in that region. This is a general peculiarity of the analytical properties of Siegert states in any infinite-range potential, even one that decays exponentially rapidly– they invariably display a pathological sensitivity to the asymptotic potential behavior, preventing all but a finite subset of the Siegert states for cut-off potentials (SSCPs) from converging to exact Siegert states. From the standpoint of rigorous mathematical formalism, it is important to consider all further discussion in light of this recognition. Since all realistic physical potentials have a tail behavior that decays more *slowly* than exponentially, the ultimate test of any Siegert method, including the elegant work of [142], is whether or not

the derived observable quantities (cross-sections and S-matrices) are numerically stable with respect to variation of the box radius parameters. Since scattering observables in atomic physics are in general *not* sensitive to weak long-range potential terms (except in sufficiently low energy scattering regimes that such terms can no longer be considered weak), however, the pathological behavior of the SSCPs is expected not to have physical significance for any realistic system; even with two very different eigenvalue spectrums, an expansion-based expression for an observable should converge to exactly the same value in both cases.

Even methods based on the SSCPs still suffer from the serious drawback of being computationally dependent on iterative procedures, either in diagonalizing the full matrix [138], or the secular equation resulting from a variational principle [137], or most recently, a partitioned submatrix reduced to the dimension of the open channels [143]. The solution must be iterated many times to converge on every individual eigenvalue. While this is potentially practical for "direct" methods, in which the only objective is the determination of a finite number of true resonant states and perhaps a representative topology of the surrounding scattering (cut-off) resonances, it would be impossible to calculate all the wavefunctions of the infinite series of SSCPs, which are necessary components of any complex basis vector expansion, such as would be used (for example) to construct the Green's function by means of the Mittag-Leffler expansion theorem. In principle, all of the information describing the continuum resonance features and state densities should be contained in these eigenvectors, thus bypassing the need for approximating any integrals over the continuum. Turning that promise into a computational reality requires a careful study of the relationship between the SSCPs, and their representation in any finite basis, as well as a way of finding *all* of the eigensolutions defined by that basis selection without the need for cumbersome and potentially unstable iterative searches for eigenvalues in the complex plane.

Both of these difficulties were resolved recently by Tolstikhin *et al.* in their study

of the Siegert pseudostates (SPSs) [144, 142], the set of N eigenstates the result from solving the Hamiltonian with Siegert boundary conditions on the interval [0,R_0] for an N-dimensional basis set. Tolstikhin *et al.* assume orthonormality of the basis functions, but most of their expressions can be straightforwardly generalized to a non-orthogonal basis, and we will lift that assumption except where otherwise noted. Regardless of orthogonality, the basis is in general not assumed to be complete except in the limit of $N \to \infty$. The SPS basis representation allows the derivation of completeness and normalization properties of the Siegert state functions to be replaced by linear algebra operations, which are then related to the true properties of the SSCPs by investigation of the $N \to \infty$ limiting behavior.

We seek a solution expanded in terms of some primitive basis set

$$\phi(R) = \sum_{j=1}^{N} c_j \, y_j(R), \qquad 0 \leq R \leq R_0. \tag{5.15}$$

Here N is the dimension of our basis, and we have selected a non-orthogonal b-spline basis [145, 146] for the $y_j(R)$. Inserting this into the Schrödinger equation, premultiplying by $y_{j'}$, integrating with an integration by parts, and employing the boundary value 5.14, we find a matrix equation for the coefficients c_j

$$\sum_{j=1}^{N} \Big(\tfrac{1}{2} \int_0^{R_0} \tfrac{dy_{j'}}{dR} \tfrac{dy_j}{dR} dR - \tfrac{ik}{2} y_{j'}(R_0) y_j(R_0) \tag{5.16}$$

$$+ \int_0^{R_0} y_{j'}(R) \mu [V(r) - E] y_j(R) dR \Big) \, c_j = 0. \tag{5.17}$$

$$\tag{5.18}$$

Note that we have used a Green's theorem identity before substituting in the boundary condition, and that the Hamiltonian has been multiplied through by the reduced mass μ. Written more concisely in matrix notation, we have a system of the form

$$(\tilde{\mathbf{H}} - ik\mathbf{L} - k^2\mathbf{O})\vec{c} = 0, \tag{5.19}$$

where $L_{j,j'}$ is the surface matrix $y_j(R_0)y_{j'}(R_0)$, $\tilde{H}_{j,j'}$ is the matrix $2\mu H_{j,j'}+y_j(R_0)\frac{d}{dr}y_{j'}(R_0)$, and $\mathbf{O}$ is the overlap matrix for the spline basis set.

This equation is manifestly nonlinear, but the method of Tolstikhin *et al.* allows it to be "linearized" by recasting it as a new eigensystem in a basis of doubled dimension. ([147, 148] discuss related techniques for solving differential equations where the eigenvalue appears in a boundary condition.) We continue by defining $d_i = ikc_i$, yielding a trivial second equation $ik\mathbf{O}\vec{c} = \mathbf{O}\vec{d}$. Substituting this into the original eigenequation now gives a linear equation in the doubled basis space

$$\begin{pmatrix} \tilde{\mathbf{H}} & 0 \\ 0 & -\mathbf{O} \end{pmatrix} \begin{pmatrix} \vec{c} \\ \vec{d} \end{pmatrix} = ik \begin{pmatrix} \mathbf{L} & -\mathbf{O} \\ -\mathbf{O} & 0 \end{pmatrix} \begin{pmatrix} \vec{c} \\ \vec{d} \end{pmatrix}. \tag{5.20}$$

This is an equation for the eigenvalue $\lambda = ik$, giving $2N$ solutions lying either on the (Re λ)-axis or in conjugate pairs in the right half of the complex λ-plane. The solutions (plotted here in the k plane, rather than the λ-plane) are shown in Figures 5.6 and 5.7.

An atypical feature of the SPS eigensystem should be noted here– the eigenvalue parameter is proportional to the wavenumber k, rather than the energy. Since the energy has a k^2 functional dependence, the energy spectrum itself will need to be mapped onto a two-sheet Riemann surface in order to become single-valued, with a branch point at the origin and the cut following the positive real semiaxis. States with k in the upper half-k-plane will be mapped onto the first sheet of the Riemann surface on which the energy eigenspectrum is defined, and those with k in the lower half-plane will map to the second sheet. Since the bound state eigenvalues (that is, those which exponentially decay as $R \to R_0$) lie on the first sheet, this will be termed the "physical" sheet. The only states that can lie on the physical sheet are bound states (although if a discrete state is embedded in the continuum, it will be located on top of the cut line). Thus, all resonance states, whether they are near the real energy axis and related to real observable resonances, or deeper in the complex plane and related to smooth background

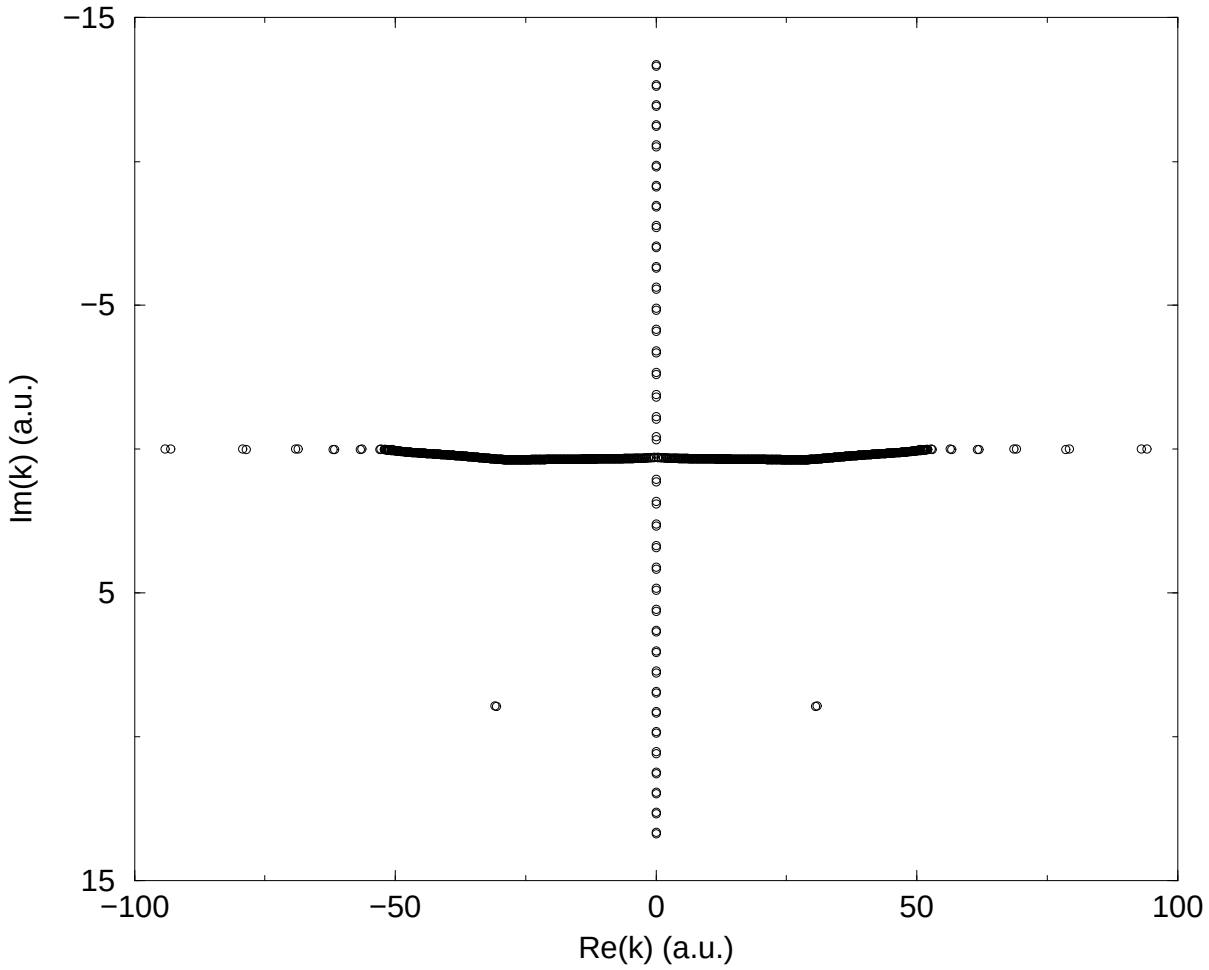

Figure 5.6: Siegert pseudostate eigenspectrum resulting from the solution of of Equation 5.20. Note that the eigenstates have been transformed from λ to k, corresponding to a rotation in the complex plane by 90 degrees. States above the real axis all lie on the imaginary axis, and are identified as the bound states of the potential. States on the complex axis below the real axis are unphysical antibound states.

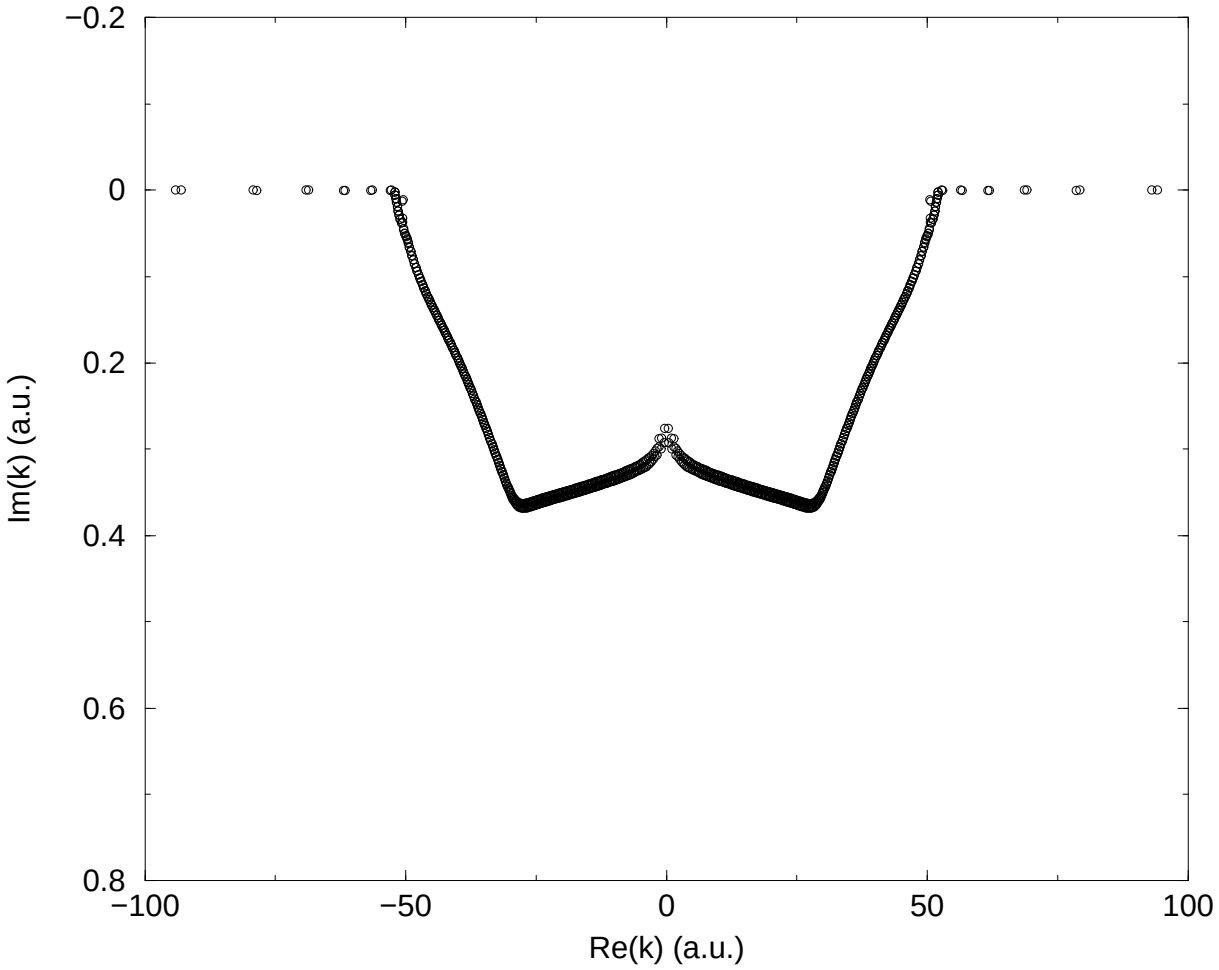

Figure 5.7: Enhanced detail of the spectrum in the vicinity of the real axis, showing states that correspond to the Seigert discretized continuum. Note that the "kink" in the spectrum occurs for values of k that oscillate too quickly to be represented in the primitive spline basis.

scattering, are exclusively on the unphysical sheet of the multisheet Riemann surface.

The Siegert states are known to obey unconventional orthogonality, normalization, and completeness relations, and this has historically been a source of controversy in the literature, with several competing schemes for regularizing the non-square-normalizable continuum-like states. In the SPSs, however, the origin of these questions become simpler to understand by working within the doubled dimension space. If the eigenvalues of Equation 5.20 are nondegenerate, then it may be easily shown (noting that the matrices are symmetric, not Hermitian) that the eigenvectors are symmetric with respect to the weighting matrix that appears on the right hand side,

$$\left(\vec{c}^{(n)T}\vec{d}^{(n)T}\right)\begin{pmatrix}\mathbf{L} & -\mathbf{O}\\ -\mathbf{O} & 0\end{pmatrix}\begin{pmatrix}\vec{c}^{(m)}\\ \vec{d}^{(m)}\end{pmatrix}=0,\quad \forall n\neq m. \tag{5.21}$$

The normalization condition may be derived by examining the behavior of the exponentially decaying bound states, and imposing unit normalization on them in the limit that R_0 is made sufficiently large that their amplitude on that boundary vanishes. We begin from the orthonormality expression with an undetermined normalization constant,

$$\left(\vec{c}^{(n)T}\vec{d}^{(n)T}\right)\begin{pmatrix}\mathbf{L} & -\mathbf{O}\\ -\mathbf{O} & 0\end{pmatrix}\begin{pmatrix}\vec{c}^{(m)}\\ \vec{d}^{(m)}\end{pmatrix}=\alpha\delta_{nm}. \tag{5.22}$$

By the definition of $\vec{d}$, this condition reduces to an equivalent version in the original N-dimensional basis,

$$-(\lambda_n+\lambda_m)\vec{c}^{(n)T}\mathbf{O}\vec{c}^{(m)T}+\vec{c}^{(n)T}\mathbf{L}\vec{c}^{(m)T}=\alpha\delta_{nm}, \tag{5.23}$$

or in the position-space representation,

$$-(\lambda_n+\lambda_m)\int_0^{R_0}\phi_n(R)\phi_m(R)dR+\phi_n(R_0)\phi_m(R_0)=\alpha\delta_{nm}. \tag{5.24}$$

For bound states in the limit $R_0 \to \infty$, where the surface term vanishes, we must recover the conventional unit normalization

$$\int_0^\infty \phi_n(R)\phi_m(R)dR = \delta_{nm}. \tag{5.25}$$

This requirement uniquely determines the normalization constant $\alpha = -(\lambda_n + \lambda_m)$ for all states. Note that since all the states on the unphysical sheet, the eigenfunction diverges exponentially for increasing R, and thus the normalization condition 5.24 amounts to a cancellation of two exponentially growing terms; this is a potential source of numerical instability as the box size increases.

The orthonormality relation 5.22 implies an associated completeness relation in the doubled dimension space,

$$\sum_{n=1}^{2N} \frac{1}{2\lambda_n} \begin{pmatrix} \vec{c}^{(n)} \\ \vec{d}^{(n)} \end{pmatrix} \left(\vec{c}^{(n)T} \vec{d}^{(n)T} \right) = \begin{pmatrix} -\mathbf{L} & \mathbf{O} \\ \mathbf{O} & 0 \end{pmatrix}^{-1}, \tag{5.26}$$

which yields a set of multiple completeness relations upon reduction to the original N-dimensional basis:

$$\sum_{n=1}^{2N} \frac{1}{\lambda_n} c^{(n)} c^{(n)T} = 0 \tag{5.27}$$

$$\sum_{n=1}^{2N} c^{(n)} c^{(n)T} = 2\,\mathbf{O}^{-1} \tag{5.28}$$

$$\sum_{n=1}^{2N} c^{(n)} c^{(n)T} = 2\,\mathbf{O}^{-1}\mathbf{L}\mathbf{O}^{-1} \tag{5.29}$$

In fact, an infinite list of such completeness relations, generated by changing the power of λ_n in the weighted sum, may be derived on the basis of a recursion relation based on the Schroödinger equation 5.19, as shown in [142].

5.4 Siegert pseudostates: Single channel Green's function method

For a single-channel system with a finite-range potential, the SPS eigenstates serve as a complete expansion set for the Mittag-Leffler expansion theorem. Unlike the true Siegert states, for which convergence of this representation is problematic (see More and Gerjuoy [135] for an extended discussion), the SPS Green's function is guaranteed to converge, owing to the completeness relations given above. The derivation proceeds entirely by linear algebra [142], and requires no assumptions about the analytical properties of the exact Green's function in the limit $N \to \infty$.

The form of the Green's function depends on the choice of boundary conditions. The Green's function is required in all cases to vanish at the origin,

$$G(0, R'; k) = 0. \tag{5.30}$$

For a conventional (i.e. eigenvalue-independent) outer boundary condition, the Schrödinger Green's function equation

$$(H - E)G(R, R'; k) = \delta(R - R') \tag{5.31}$$

yields the solution

$$G(R, R'; k) = \sum_{n=1}^{2N} \frac{\phi_n(r)\phi_n(r')}{k_n^2 - k^2}. \tag{5.32}$$

This function is identifiable as the principle value Green's function; it displays neither incoming nor outgoing wave character on the boundary. On the other hand, the Siegert boundary condition

$$\left(\frac{d}{dR} - ik\right) G(R, R'; k)\Big|_{R=R_0} = 0 \tag{5.33}$$

has the same quadratic matrix equation representation as 5.19, and gives the alternate solution form

$$G(R,R';k) = \sum_{n=1}^{2N} \frac{\phi_n(r)\phi_n(r')}{k_n(k_n-k)}. \tag{5.34}$$

This is the outgoing wave Green's function. Both forms are solutions to the same Hamiltonian, and differ only by a homogeneous solution of the Schrödinger equation.

These Green's functions require *all* $2N$ SPS solutions to be included in the summation; the omission of even one state (or pair of states) will give a totally incorrect solution. Since some of the pseudostates lie very far from the axis, their exponential growth at the outer boundary may be extremely rapid. This is a potential cause of serious numerical instability, as noted first in [149]; because the normalization of the Siegert pseudostates 5.24 involves a cancellation of an exponentially large integral with an exponentially large surface term, an exponential growth factor that exceeds the inverse of the machine precision will effectively destroy any orthonormality of the basis set, and thus the completeness relations on which the derivation of the Green's function depends.

Fortunately, the scattering matrix may be analytically derived directly from the Green's function expansion, giving either a "sum formula"

$$S(k) = e^{2ikR_0}\left[\, 1 + ik\sum_{n=1}^{2n} \frac{[\phi_n(R_0]^2}{k_n(k_n-k)}\right] \tag{5.35}$$

or the "product formula"

$$S(k) = -e^{2ikR_0}\prod_{n=1}^{2N} \frac{k_n+k}{k_n-k}. \tag{5.36}$$

The second result, rather remarkably, allows the S-matrix to be written entirely in terms of the eigenvalues; this completely bypasses the difficulty of numerical instability associated with the rapid exponential breakdown of the orthonormality relation for increasing value of R_0, as discussed in [149].

The partitioning of configuration space into inner and outer regions for the SPS

eigenvalue and the subsequent symmetrization of the Hamiltonian by use of the Bloch operator are both reminiscent of the eigenvalue R-matrix method. Further, the derivation of the sum and product formulas shown above involves the surface value of the Green's function, $G(R_0, R_0; k)$, which is known to be proportional to the R-function (the one-dimensional R-matrix) [124]. This suggests that there should be some natural relationship between the SPS formulation and the R-matrix formulation. In fact, Baye *et al.* [149] have shown that for the same finite basis set representation, the methods are formally equivalent. [2] This homology provides an alternate expression for the S-matrix based on R-matrix theory, working directly from the primitive basis and the matrices in its representation without any need to find the complete set of SPS eigenstates. Of course, it may still be useful to find SPSs that correspond to the true physical Siegert states, for the sake of extracting their width and shape parameters, but for only a few states this can be easily accomplished by using the iterative approach. For the task of constructing the scattering matrix, the usefulness of the SPS formalism appears to be subsumed by the more general applicability of the R-matrix formalism; the latter is not susceptible to the Siegert states' noted susceptibility to long-range potential tails, and the multichannel version of R-matrix theory is far simpler than that for the Siegert state case.

Although the Green's function SPS theory is completely rigorous, it is severely restricted in utility. The limitations discussed in the last two sections of this chapter may be summarized: First, the SPS technique is best suited for single channel problems. An extension to even two-channel problems presents considerable challenge, and depends on the motivated selection of a fortuitously simple uniformization transformation [150]. Such a transformation is necessary to map the multi-valued function defined on the entire multisheet Riemann surface into a single-valued (but potentially quite complicated)

[2] This is already anticipated in the discussion of Lane and Thomas, who note that the Wigner-Eisenbud theory is "absolutely equivalent" to the Kapur-Peierls resonance theory [124], which in turn is related to the Siegert theory by the renormalization procedure suggested by More and Gerjuoy [135].

function of some new variable. For a two-channel system, the Riemann surface has four sheets (arising from two branch cuts, with branch points at each of the threshold energies) and the uniformized matrix eigenequation is quartic in the transformed variable. More generally, a N-channel problem will have a 2^N-sheet Riemann surface, and there is no known method for uniformization beyond the two-channel case.

Second, the derivation of the SPS Green's function expressions shown above is considered only for one dimensional model systems in the work of Tolstikhin *et al.* It remains a matter of untested conjecture whether or not there exists a multidimensional generalization of the requisite completeness relations, or whether the derivation yields a comparably simple closed form. At the approximate level, one might imagine an expansion in hyperspherical coordinates [151]; this treatment is only of utility, however, if the fragmentation modes are qualitatively similar. For the solution of competing ionization and dissociation channels, involving the coupling between fundamentally distinct degrees of freedom, an entirely different approach is necessary. This problem is further compounded by the possibility that one set of channels (e.g., the ionization channels in the hydrogenic system) may have Coulombic long-range interaction or a centrifugal effective potential term associated with finite angular momentum. In this case, the SPS formalism is not simply non-rigorous, but involves increasingly complicated corrections to the boundary condition that must be expressed at the level of a Taylor expansion.

In the conclusion of their work, Tolstikhin *et al.* hinted at the possibility of an entirely different philosophy for application of the Siegert states to scattering physics: "The SPS formulation also has advantages as a method of discretization of the continuum." Their suggestion called for the use of the SPSs as a basis for a time-dependent close-coupling calculation, with the recognition that this would "enable one to distinguish between the excitation of a resonance state and the underlying continuum scattering." This idea was implemented shortly thereafter by Yoshida and coworkers [152, 153] to describe the reflectionless loss of wavepacket probability by flux across a bounding

surface.

In fact, the ability of Siegert states to serve as a finite basis approximation to the continuum had already been demonstrated some time earlier in the work of Seideman and Miller [154], in the context of exploring the semiclassical analysis of transition state theory in nonperturbative regimes. If the wavefunction describing reaction dynamics in the vicinity of a harmonic transition state are expanded in terms of the normal mode frequencies, with the reaction coordinate naturally acquiring an imaginary frequency, then the Hamiltonian expanded in normal mode coordinates becomes complex symmetric. If this Hamiltonian is solved by direct diagonalization, instead of perturbative corrections to the semiclassical solution, then the spectrum contains a set of complex eigenvalues identifiable as Siegert states. These states do not represent resonant complex formation, but are instead the discretization of the reaction coordinate continuum, and give smooth and structureless contributions to the transition probability. Ryaboy and Moiseyev [155] showed that this set of states could be equivalently generated by a complex coordinate scaling in which the "white" (non-resonant) continuum was rotated off into the complex plane to uncover the Siegert eigenvalues and make their states square integrable in the scaled coordinates.

In the next section, we follow the approach of Siedeman and Miller, rather than the more rigorous theory of Tolstikhin *et al.*, and begin from the hypothesis that the Siegert pseudostates can be usefully appropriated as a basis set for representing the discretized continuum of a channel expansion. In effect, this creates an additional (potentially infinite) set of complex-energy channels that extend arbitrarily high into the vibrational continuum. As Ryaboy and Moiseyev note, so long as these channels are associated with poles of the scattering matrix that are separated in the complex plane by "distances" (i.e., the difference between the real parts of the eigenvalues) that are smaller than the corresponding widths (i.e., the sum of the imaginary parts of the eigenvalues), the contribution to the observable scattering parameters (phase shift,

cross-section, etc.) can be sufficiently smooth to completely represent the background elastic scattering. In effect, the coupling to the continuum has been broken up into a sequence of broad, overlapping Lorentzian resonances which may be summed together to give a slowly varying baseline that reflects direct coupling to the continuum. If any physical resonance states are present, they will normally have poles much closer to the real axis, and thus their Siegert eigenstate widths will be much sharper and narrower, and their contribution to the spectrum will be manifestly resonant.

5.5 Extending MQDT to a Siegert pseudostate basis: Theory

Since the Siegert pseudostate basis consists of two branches of narrowly-spaced continuum-like complex eigenstates, in addition to the same rovibrational eigenstates they share with a more conventional basis with fixed logarithmic derivatives on the box boundary, they appear at first glance to include exactly the basis set contribution needed to give the wavefunction outgoing flux across that boundary. In principle, we would like to have a solution state located at precisely the energy of the vibrational continuum state into which the molecule is dissociating at that energy, with an imaginary part corresponding to the width of the predissociating resonance. In practice, if we have an artificial discretized continuum of sufficiently dense pseudostates with the property of being complete (or at least, complete with respect to the subset of continuum states one is attempting to represent), then the lack of a state at exactly the right energy and width is immaterial, and accommodated at the level of a complex basis expansion. This is quite different from the original method Jungen described above, where producing a pseudo-continuum state at precisely the correct energy (by varying a parameter iteratively in [53]) was of paramount importance for the success of the solution. (It is more similar to the later method of Ross and Jungen, which augments the basis by including additional sets that do not vanish, although even in this case the choice of additional sets must be optimized by the choice of a boundary condition resembling the boundary

condition of the real solution wavefunction. This cannot typically be known in advance, but must be optimized by hand for different resonances for best results, whereas the Siegert method avoids the need to readjust any parameters throughout an entire energy region.) There are, to be sure, numerical concerns to be addressed before this approach should be naively trusted, especially in light of the known peculiarities of the Siegert states, including their exponential divergence for increasing argument (on the "unphysical" sheet of the Riemann surface) and their innate overcompleteness. For the sake of devising a useful basis, however, it suffices that these concerns be resolved merely to the level of numerical accuracy (i.e., convergence of the calculated cross-section) under certain specified parameters that reflect relevant real-world conditions. This is a much weaker requirement than the one necessary for implementation by the more rigorous approach of Tolstikin *et al.*.

For resonance series corresponding to high electronically excited intermediates (Rydberg states) of diatomic molecules, the most natural description of the system is one with quantum defect parameters defined in terms of a fixed internuclear distance R and a well-defined projection of the orbital angular momentum Λ onto the axis of symmetry. This is because the electron spends most of its time far from the nuclear core, and when it does penetrate into the core, it gains enough speed from falling through the Coulomb potential that the nuclei are essentially frozen on the time scale of its motion. The quantum defect functions $\mu_\Lambda(R)$ in this representation, the so-called "body-frame", may either be calculated from highly accurate *ab initio* techniques, or extracted from a semi-empirical fitting of experimental data [121]. In order to connect them with the true asymptotic ionization channels defined in terms of Siegert pseudostates of the residual core, $j = \{v^+, N^+\}$, a *frame transformation* must be performed [45, 37], where N^+ is the ionic rotational momentum, and v^+ is the vibrational quantum number of the pseudostates. In the Siegert MQDT procedure, it is necessary to directly evaluate the S-matrix by the frame transformation integral

$$S_{j,j'} = \sum_\Lambda \langle N^+|\Lambda\rangle \int_0^{R_0} \phi_j(R) e^{2i\pi\mu_\Lambda(R)} \phi_{j'}(R)\, dR\, \langle\Lambda|N^{+'}\rangle + i\sum_\Lambda \langle N^+|\Lambda\rangle \frac{\phi_j(R_0) e^{2i\pi\mu_\Lambda(R_0)} \phi_{j'}(R_0)}{k_j + k_{j'}} \langle\Lambda|N^{+'}\rangle. \tag{5.37}$$

The surface term in 5.38 is new, but it is included because also arises in the orthonormality relation [142]. A similar transformation converts the body-frame transition dipole elements $D_\Lambda(R)$ into reduced dipole matrix elements in the same S-matrix representation,

$$D_j^S = (2J+1) \sum_\Lambda \langle\Lambda|J_0\rangle^{(J)} \langle\Lambda|N^+\rangle \times \int_0^{R_0} \phi_0(R) D_\Lambda(R) e^{i\pi\mu_\Lambda(R)} \phi_j(R)\, dR. \tag{5.38}$$

Here $\phi_0(R)$ is the initial vibrational wavefunction, and J_0 and J are the total angular momenta of the initial and final states of the system, respectively. (Note that the surface term is omitted here because $\phi_0(R)$ is assumed to be negative on the surface.)

Note that the Siegert pseudostates are *never* conjugated in these expressions, even when they formally belong to the dual ("bra") space. In particular, this means that the quantity labeled as $\vec{D}^{S\dagger}$ below is calculated by conjugating only $e^{i\pi\mu_\Lambda(R)}$ in the definition above, and not the dipole matrix elements directly. The unconventional nature of the inner product in a Siegert basis may be understood from a somewhat more intuitive perspective by means of an appeal to the symmetry properties of the Green's function in the complex k plane, as first presented by More and Gerjuoy [135]. To briefly sketch this argument, we begin by noting that the Green's operator formed by eigenvector expansion over a resonance state basis such as the Siegert pseudostates obeys the identity

$$G^\dagger(k) = G(-k^*). \tag{5.39}$$

This relation follows rigorously from the fact that the Green's operator is real for negative energies (i.e., for pure imaginary values of k), via the Schwartz reflection principle. (This is in contrast to the more usual case of the reflection principle, defined for functions which are real when their argument is real.) This nonstandard symmetry also applies to the left eigenvector states $\tilde{\phi}_j$ and right eigenvector states ϕ_j

$$\tilde{\phi}_j(R;k) = \phi_j(R;-k^*) = \phi_j^*(R;k). \tag{5.40}$$

In other words, if $\langle\tilde{\phi}_j|$ is a left eigenvalue of the Green's operator $G(k)$, then $|\tilde{\phi}_j\rangle$ is a right eigenvalue of $G(-k^*)$. Since both the transformation between left and right eigenvectors *and* the transformation between the bra and ket space representations both involve a conjugation, the net effect is that the functions of the dual space are unconjugated.

At this stage of the calculation no information about the long-range behavior of the channels has yet been included, and since the body-frame quantum defects are nearly energy independent, the resulting S-matrix is typically a smooth and fairly weak function of energy. The method of *channel elimination* [156, 44] systematically eliminates flux in all electronic channels below the energy threshold for electron escape (the "closed-channel subspace") to form a "physical" S-matrix $\mathbf{S}^{phys}$, by taking the proper linear combination of short-range solutions that ensures exponential decay at infinity. For a long-range Coulomb potential, this procedure gives

$$\mathbf{S}^{phys} = \mathbf{S}_{oo} - \mathbf{S}_{oc}(\mathbf{S}_{cc} - e^{-2i\beta})^{-1}\mathbf{S}_{co}. \tag{5.41}$$

Here, β is a diagonal matrix of the usual Coulomb long-range phase parameter $\pi\nu_j$ where ν_j is the (possibly complex) effective quantum number in the jth channel, $\mathbf{S}$ is the scattering matrix, and the subscripts indicate partitions of the matrices into closed and open subspaces [44].

For a Siegert state basis, this physical scattering matrix is in general *not* unitary,

but rather subunitary, reflecting the loss of flux at the boundary R_0 via coupling to the Siegert pseudo-continuum states. It can be used to calculate the total cross-section for dissociative recombination by means of conventional formulas, but with the departure from unitarity, $1 - \sum_j |\mathbf{S}^{phys}_{j,j'}|^2$, identified as the probability $|\mathbf{S}^{phys}_{d,j'}|^2$ for scattering into the dissociative continuum. This method also provides all quantities necessary to find the partial photoionization cross-section into any open channel, σ_j; see Eq. 2.59 of [44] for further details. The contributions from all open channels can then be summed to give the total cross-section for photoionization.

Alternatively, the total photoabsorption cross-section may be found directly from a *"preconvolution" formula* first derived by Robicheaux to handle the energy smoothing of densely spaced resonances [48], but expressed here in the equivalent but more symmetrical form of Granger [157, 158],

$$\sigma_{total}(E) = \frac{4\pi^2 \alpha\omega}{3(2J_0+1)} \mathrm{Re}\, \vec{\mathrm{D}}^{\mathrm{S}\dagger} \left[\mathbf{1} - \mathbf{S}\mathbf{e}^{\mathbf{2i}\beta}\right]^{-1} \left[\mathbf{1} + \mathbf{S}\mathbf{e}^{\mathbf{2i}\beta}\right] \vec{\mathrm{D}}^{\mathrm{S}} \tag{5.42}$$

where Re signifies taking the real part of everything that follows, and the † here conjugates only the operator, not the entire matrix element. The diagonal matrix written as $e^{-2i\beta}$ has a nontrivial definition in terms of the quantum defect parameters, it may be approximated quite well by taking $\beta_j = \pi\nu_j$ for "closed" channels with $E < \mathrm{Re}\,\mathrm{E_j}$, and $\beta_i = i\infty$ for "open" channels with $E > \mathrm{Re}\,\mathrm{E_j}$. Here E is the total energy of the system, E_j is the threshold energy for channel j, and $\nu_j = 1/\sqrt{2(E_j - E)}$ on the branch where Im $\nu > 0$. The utility of this expression lies in recognizing that the value of the cross-section at a complex energy in the above formula is equivalent to the cross-section at a real energy, smoothed over a channel-dependent width $\Gamma_j = 2\,\mathrm{Im}\,\epsilon_\mathrm{j}$. Within the Siegert state formulation, the electron energy $\epsilon_j = E - E_j$ will naturally take on a complex value in any channel where the channel eigenenergy E_j is itself complex, while E remains real.

Given $\mathbf{S}$ and ϵ_j, either of the two cross-section formulas above can be evaluated, with appropriate allowances for the possibility of complex energy eigenvalues. Note that the first procedure simply gives a sum over the flux into specific ionization channels, while the second gives a single value for the total photoabsorption cross-section. This means that the latter will contain information about the solution wavefunction along the $R = R_0$ boundary not contained in any of the open ionization channels. In general, the value of σ_{total} will be equal to *or greater than* the sum over the individual σ_j, and any difference may be attributed to the effect of coupling to high-lying Siegert states in the continuum. Thus, the difference between these two formulae at any energy provides the photodissociation cross-section.

In order to test the validity of this hypothesis, we will start by defining a set of Siegert pseudostates for the H_2^+ internuclear potential. The eigensolutions fall into three classes, as shown in Figure 5.8. Those lying along the positive (Im k)-axis are associated with negative eigenenergies on the physical sheet of the E-plane, the bound states of the potential. These are the channel thresholds to which the Rydberg autoionization series of the ionization spectrum converge, and so we include all of their states. The solutions along the negative (Im k)-axis lie on the unphysical energy sheet, and we reject them as antibound states arising from the doubling of the dimension space. The remainder of the solutions fall above and below the (Re E)-axis, corresponding to conjugate solution pairs of the eigenvalue parameter $\lambda = ik$. We select only those with negative Im E_j, a decision that can be justified conceptually on the grounds that these states display a time dependence in which total probability decreases over time, corresponding to decay into the continuum. (For a much more sophisticated discussion of this topic, see the extensive discussion of [159, 160, 161], which arrives at the same conclusion for complex expansions of the Green's function using far more rigorous formal arguments.) For MQDT matrix elements it is also acceptable to reject states lying very high in the continuum, since their Franck-Condon overlap with the bound states is negligible.

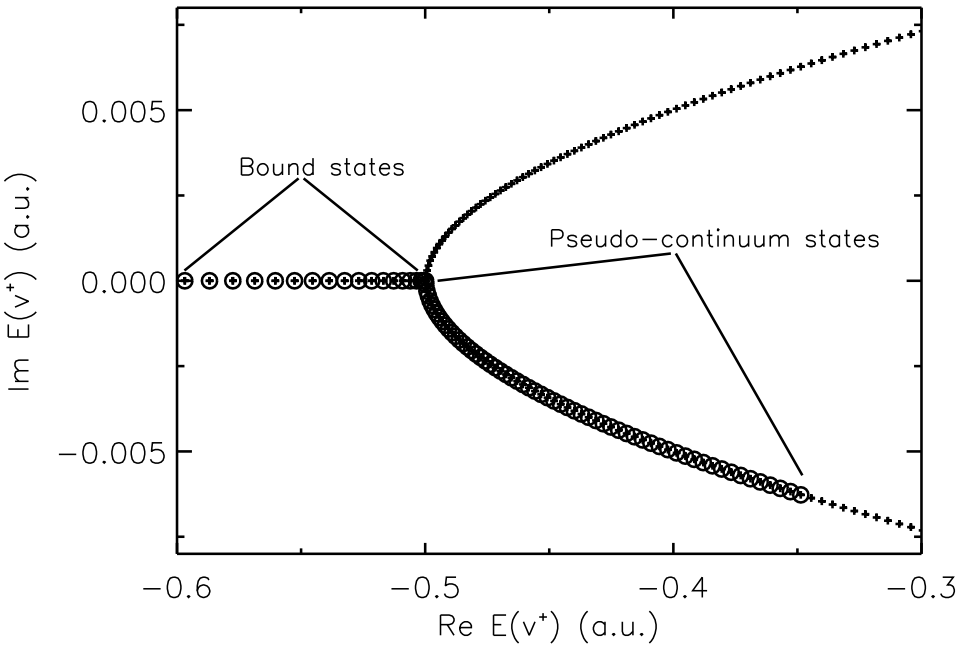

Figure 5.8: Distribution of H_2^+ vibrational Siegert pseudostate energies in the complex energy plane for angular momentum N^+=1. Only the circled states are included as channels in the scattering matrix.

Tolstikhin *et al.* discuss the unusual completeness relation obeyed by the full set of Siegert pseudostates, which has an additional factor of 2. Our restricted subset of Siegert pseudostates does not, of course, obey that doubled completeness relation. We have confirmed through numerical tests, however, that this restricted subset behaves like a complete set, to at least 10^{-12} accuracy, for representing either L^2 functions confined within the boundary or functions with purely outgoing wave character at the boundary. The ability to represent L^2 functions diminishes somewhat for extremely narrow functions, for which the primary contribution must come from shorter wavelength pseudocontinuum functions. For example, when expanding in terms of a truncated set with a maximum Re(k) of about 50 a.u., only features broader than $\frac{1}{7}k$=0.02 a.u. in width can be well- represented. When using this truncated set numerically, a Gaussian of the form $e^{-\alpha(R-R_{eq})^2}$ can be only represented to 10^{-6} accuracy when α=100 (i.e., a Gaussian of width 0.14 a.u.), has a relative error of over 10% for α=1000 (i.e., a Gaussian of width 0.045 a.u.), and fails entirely for α=10000 (i.e., a Gaussian of width 0.014 a.u., smaller than the wavelength of the highest excited state included in the basis). For an impressive demonstration (in a somewhat different context) of the convergence properties of a similarly truncated Siegert basis also used to describe smooth continuum physics, see [154].

5.6 Extending MQDT to a Siegert pseudostate basis: Results and discussion

In the region of the ungerade H_2 spectrum between 127200 and 127800 cm^{-1} there are several strongly predissociated resonances, members of the $np\pi, v^+ = 8$ and $np\pi, v^+ = 5$ series. In each case, our calculated spectrum correctly reproduces them in the total absorption cross-section, but shows them as weak or absent in the ionization cross-section. Comparisons of our results with other theoretical and experimental values [55, 121] for the relative yields of selected resonances appear in Table 5.2. Note particu-

larly that this method is able to correctly describe the strong rotational dependence of the $4p\pi, v^+ = 5$ branching ratio, a nontrivial consequence of subtle channel interactions.

Table 5.2: Photoionization and photodissociation yields for select *ungerade* resonances in H_2 for which the relative yields have been experimentally observed [55].

State	Source	Energy	% Ion.	% Diss.
$3p\pi, v = 8, R(0)$	Observed	127248.2	10(5)	95(5)
	Theory[121]	127246.9	1	99
	Present	127242.2	1	99
$5p\sigma, v = 4, R(0)$	Observed	127599.4	90(10)	10(10)
	Theory[121]	127602.2	88	12
	Present	127606.8	76	24
$4p\pi, v = 5, R(0)$	Observed	127667.6	82(5)	18(5)
	Theory[121]	127665.4	93	7
	Present	127666.6	97	3
$4p\pi, v = 5, R(1)$	Observed	127599.4	30(10)	70(10)
	Theory[121]	127758.4	17	83
	Present	127759.5	29	71

As a test of the method in an entirely different energy regime we considered the problem of dissociative photoionization, a three-body breakup channel accessible only at much higher energies. Experimental measurements of the ratio between pure ionization and dissociative ionization have been performed since the 1970s by a number of researchers [162, 163, 164], along with at least one early theoretical calculation [165]. Since our ionization spectrum is a sum over individual channels, one can easily distinguish between contributions from channels above and below the dissociative threshold. Our results, plotted against those of past experiment and theory, are presented in 5.9.

Finally, we have performed a model calculation demonstrating the utility of our method for treating dissociative recombination, particularly in systems where indirect channels (those involving scattering into intermediate autodissociating Rydberg states) play an important role. 5.10 shows the dissociative recombination spectrum of a simplified H_2 model potential (neglecting rotation and with R-independent quantum defects), compared with the familiar approximation of O'Malley for smooth background scatter-

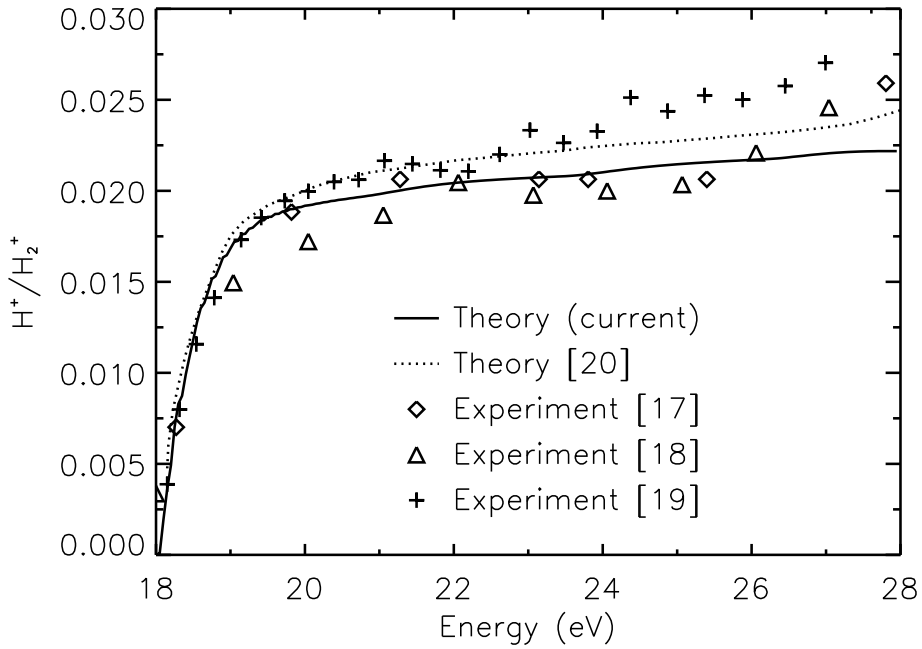

Figure 5.9: Dissociative photoionization cross-section, as a ratio to the total photoionization cross-section. The solid line is the current theory, the dotted line is an earlier theory [165], and the points are data from various experimental measurements [162, 163, 164].

ing by direct processes [166]. This spectrum accurately reproduces the background, and also describes complex interference effects from the series of resonances converging to each Rydberg threshold.

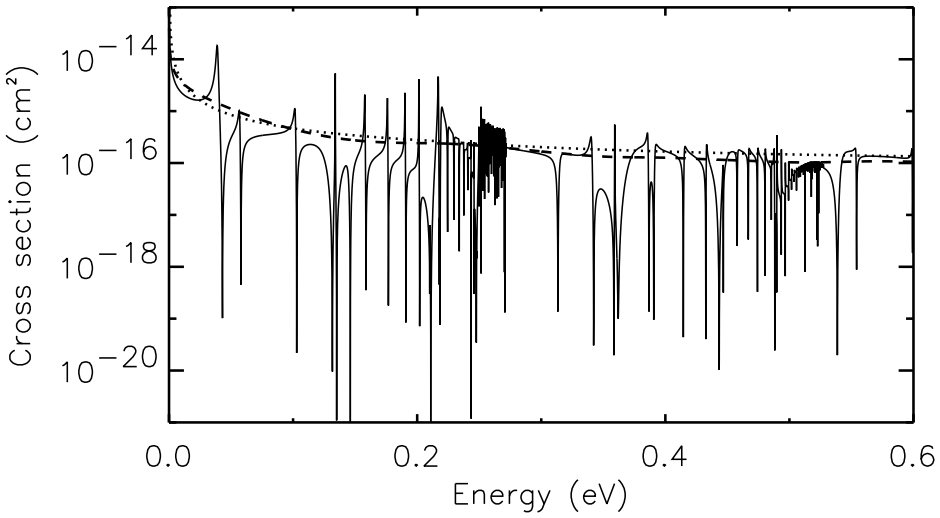

Figure 5.10: Dissociative recombination cross section for the model potential, unconvolved (solid) and convolved with a Lorentzian of width 0.1 eV (dashed), compared to that resulting from the O'Malley formula (dotted).

The extension of the Siegert MQDT method to polyatomic systems might be attempted in several ways. First, by transforming the nuclear coordinates to a hyperspherical coordinate system, a multidimensional problem is effectively reduced to a single scattering coordinate (the hyperradius), allowing the formulas above to be adapted with minimal alteration. This has already been demonstrated for the dissociative recombination of H_3^+ [28], with results that appear to correctly reproduce broad features in the experimental spectrum, although the theory appears not to be sufficiently precise to describe detailed resonance structures. Alternatively, it might be possible to recast the Siegert eigenproblem in a generalized form that admits arbitrary dimension. Even if the completeness relations and matrix inversion identities required for the derivation

of the Green's function (as in the Tolstikhin papers) were no longer possible to write out analytically in multiple dimensions, the ability to construct a "locally complete" representation of the multidimensional continuum would still be sufficient to provide appropriate channel states for the MQDT channel expansion.

Chapter 6

Conclusion

On a practical level, this dissertation has considered the physical properties of two highly excited diatomic systems, one commonplace, and naturally occurring throughout the universe, and one exotic, and likely to be observed under only carefully controlled laboratory conditions. On a conceptual level, however, these studies share a common philosophical framework with respect to the way in which they approach the process of scattering for Rydberg electrons in quantum mechanical systems.

From the standpoint of classical mechanics, scattering is understood as a discrete event or series of events associated with the changing trajectories of a set of particle or bodies or bodies. A pair of scattering billiards, for example, will move along a flat surface in straight line until they hit one another, experience an instantaneous redistribution of their total energy and momentum (perhaps with some dissipation due to inelasticity), and then continue away along altered trajectories. A satellite undergoing a close encounter with a planet will slingshot rapidly through its gravitational field in a hyperbolic orbit, emerging along a new asymptotic trajectory with a modified direction and velocity. Scattering, by nature, is a *localized* process. It takes a strong interaction the occurs during a short period of time and is confined to a limited region of space, and reduces it to an overall effect in terms of the alteration of a system's trajectories in free space.

In quantum mechanics, the picture of particles traveling along trajectories and

undergoing isolated events must typically be abandoned. The solution to tunneling through a barrier, the first quantum scattering calculation that any young physicist is likely to encounter, is solved entirely in terms of wavefunctions and matching conditions; the solution in each region is solved separately, and the solutions are joined together by the conditions of continuity and smoothness across the boundaries. This picture is entirely *delocalized*. The solutions are continuum solutions that extend from negative infinity to positive infinity, and there is no "event" associated with the calculation. A sufficiently large number of solutions may be superposed, of course, to give a localized wavepacket, and propagating that wavepacket according to the time-dependent Schrödinger equation will recover a dynamical behavior recognizably similar to the classical case. But the preparation of such a packet will necessarily involve states with a range of energies, whereas many interesting quantum mechanical measurements are associated with experiments for which the preparation of such wavepackets is difficult or impossible. A common situation is that of experimental continuous-wave spectroscopy, where a monoenergetic photon source (like a laser) excites an atomic or molecular system with a single, well-defined energy.

The challenge of highly excited quantum mechanical systems, such as Rydberg atoms and molecules, is that they occupy an intermediate status between the quantum and classical understandings of scattering. On one hand, they are clearly scattered by localized interactions. The total volume through which a Rydberg electron moves is typically quite large compared to the volume in which it has a complicated interaction with a scattering body. One is logically motivated to find some way of exploiting the spatial confinement of this interaction in order to simplify the task of solving the Schrödinger equation. On the other hand, the interactions themselves are clearly quantum mechanical in nature, such that it would be disastrous to attempt to treat an electron scattering from a molecule as if it were something like a marble scattering from a set of bowling balls connected by springs. The exchange of energy and momentum between a scattering

electron and a molecule is a function of inherently quantum mechanical properties such as phase, wavelength, spin, quantized orbital angular momentum, and quantized molecular excitation modes. The solution must therefore be quantum mechanical in form. The possibility of successfully combining advantageous features of both perspectives is realized by quantum defect theory, which interprets complex short-range interactions in terms of their net effect on long-range parameters like the quantum defects or phase shifts.

In Chapter 2, quantum defect theory was introduced as a paradigm for thinking about the effect of core scattering on a Rydberg state. The electron moves mostly in a region far separated from the core, under the influence of a long-range Coulomb potential, and therefore has a solution that resembles the hydrogenic wavefunctions; the only effect of the core is to shift the energy of these wavefunctions in a way that is dependent on the orbital angular momentum, but at least to a good approximation is independent of the electron's long-range behavior. In the wavefunction itself, this manifests as a phase parameter that mixes the regular and irregular Coulomb functions. In effect, the quantum defect formalism divides the problem into a short-range solution region and a long-range solution region, and describes the effect of the short-range physics on the long-range solution in terms of the minimum number of necessary parameters. For a problem with multiple scattering channels, the scattering matrix suffices to specify the probability amplitude for inelastic scattering from one type of channel to another. Although this is fully quantum mechanical, the classical picture of scattering as a localized event that modifies particle trajectories has been restored. In semiclassical terms, the electron occupies a closed orbital that, once per orbital period, scatters from the core in such a way as to accumulate an additional phase shift, and transfer incoming probability flux in one channel to outgoing flux in the others. The efficacy of this approach was demonstrated for the diatomic system HD, but the method generalizes naturally to any Rydberg system, atomic, diatomic, or polyatomic. With respect to the problem of

describing overlapping Rydberg series of resonances in the electronic continuum, there is presently no other method that rivals the capabilities of quantum defect methodology to efficiently reproduce resonant features in the scattering cross-section.

In Chapter 3, a single long-lived Rydberg stationary state is created, and the effect of perturbation by the presence of a second particle that physically impinges on the Rydberg wavefunction is considered. This situation is similar to that of Rydberg excitation in the previous chapter, in the respect that electron-core interaction may still be described most efficiently by quantum defects, but the second scattering center creates an additional set of boundary conditions that must be satisfied. Just as the modification of a Coulomb potential could be expressed in terms of phase-like quantum defect parameters, so also the short-range scattering of the electron by a neutral perturber can be fully described in terms of an overall phase shift in each channel. These phase shifts provide the basis for a zero-range pseudopotential approximation that performs with accuracy comparable to the more conventional approach of diagonalizing the Hamiltonian in an L^2 basis. In classical terms, one might think about the difference between a detailed modeling of the local interaction between two colliding billiard balls, with infinitesimal deformations during the moment of contact accounting for the exchange of impulse, and an hard sphere approximation that treats the collision as truly instantaneous. The first level of detailed analysis might be necessary to account for slight inelasticity of the collision, or the transfer of translational motion into rotation for off-center collisions, but once the functional dependence of these effects was known, they could be incorporated directly into the hard-sphere model as various corrections and coefficients without the need to repeated the detailed calculation. The parameterization of Rydberg-neutral scattering in terms of phase shifts that depend only on the energy and angular momentum of the electron accomplishes a similar reduction of the detailed short-range behavior in terms of its collective asymptotic effect.

Chapter 4 implements the separation between the scattering region and the exter-

nal free-electron region in an even more literal sense, by using the Coulomb Green's function to write an exact integral equation solution in the outer region, and match it onto the phase-shift adjusted short-range solution close to the perturber. Since the Green's function serves as a propagator in the energy representation, this may be viewed quite literally as repeatedly colliding the electron with the perturber, and using the boundary matching condition to select out the stable closed orbit trajectories of the motion. In fact, modern semiclassical theory allows this picture to be implemented directly, with a coherent summation over the two closed Coulomb orbits that pass through a given point and begin and end on a small sphere bounding the perturber. The constructive interference between the paths is responsible for the distinctive nodal pattern of the wavefunction that accounts for its resemblance to the ridged shell of a trilobite.

The Rydberg state localized-scattering picture is certainly powerful with respect to the task of describing highly excited and continuum electronic states. This raises the question of whether on can retain the advantages of this philosophy, while at the same time including the nuclear continuum states that arise in the context of dissociation. Chapter 5 provides a demonstration of several approaches to extending multichannel quantum defect theory or R-matrix theory to systems with such a double continuum, including one that is entirely original, the method of Siegert channel states.

This dissertation has refined and extended a set of existing tools from the fields of resonance theory, quantum defect theory, and multichannel spectroscopic analysis in order to describe two rather dissimilar diatomic systems that arise from Rydberg electron excitation. From this foundation, there are many directions that could be pursued with respect to verifying, improving, or applying these ideas. In some cases, this may simply mean coming to a better understanding of the limitations of these methods. The machinery of quantum defect theory, for example, as powerful as it often proves to be, leaves no obvious procedure for improvement of accuracy. Unlike perturbation theory, there are no "higher level terms" available in the theory to systematically improve the

convergence of a solution, and unlike variational methods, there is no guarantee of a lower or upper bounding of the calculated values. The incorporation of effects arising from energy dependence of the quantum defect parameters, for example, or symmetry breaking effects like the loss of *gerade-ungerade* symmetry in HD and Jahn-Teller couplings in triatomics, must usually be added to the model on a somewhat *ad hoc* basis. This increases the importance of confirming the results of such calculations, either by more rigorous computational methods, or by direct experimental observation.

For the long-range Rydberg bound states, the first crucial test of the theory would involve experimentally confirming their existence by means of some spectroscopic signature. At present, the most difficult aspect of preparing these states lies in the creation of a high-enough density cold dilute gas sample. Most modern magneto-optical traps are capable of generating densities in the range of 10^{10}-10^{11} atoms per cm^{-3}; the population of nearest-neighbor pairs with the correct separation to form resonance-induced bound states (e.g., at 500-1000 Bohr radii for n=30-70) would be greatly enhanced at densities only a few orders of magnitude larger than this. As a possible alternative, the existence and structure of molecular potential curves might be deduced from the observation of satellite lines even at temperatures above those favorable for the formation of bound states. On the theoretical end, further refinement of the theory in this paper (particularly with regard to the handling of fine and hyperfine structure) would be advantageous.

If the existence of such states is confirmed, other opportunities for application-oriented theoretical study could be investigated more thoroughly. The large permanent dipole moments attached to these states makes the prospect for alignment-based applications particularly appealing. For example, if a sample of Rydberg molecules were prepared and oriented along a common axis, and a beam of slow electrons passed through the sample in the direction of that axis, one might imagine the electrons displaying a diffraction pattern suggestive of the intricate nodal structure of the electronic wavefunc-

tion. Another possibility, prompted by the observation that (to a good approximation) the effect of the perturber is simply to mix atomic states, might be the creation of a similarly shaped electronic wavefunction in the absence of any perturber at all, perhaps by the use of pulsed multipole electric fields [167]. A third idea might involve the study of Rydberg-state induced dissociation of diatomic or polyatomic perturbers *via* dissociative attachment, as initially proposed in the work of Dubov and Rabitz [65, 66] in the context of considering laser-assisted exchange reactions.

As noted in the conclusion to Chapter 5, the utility of the Siegert state method has already been demonstrated beyond the case of molecular hydrogen. The most direct route to generalize the method to polyatomic molecules is probably that used in [28], based on a transformation of the nuclear motion to hyperspherical coordinates. One might also envision finding a technique for calculating multidimensional Siegert pseudostates, with the possibility of outgoing flux on several different surfaces or hypersurfaces in a multidimensional volume. In the two-dimensional case, for example, it could provide a new approach to the handling of two-electron systems with an accessible double ionization continuum, perhaps in conjunction with R-matrix methodology. Even more complicated molecules might be analyzed by isolating a subset of particularly "active" normal modes, and defining the Siegert spectrum in the normal mode coordinates directly.

The study of resonant effects in near-threshold electron-molecule scattering processes may provide the first step toward a greater understanding of resonant effects in larger molecules with similar local structure. The work of Burrow and coworkers, for example, has described resonant scattering properties of electrons from both chloroalkanes and DNA bases using a model that assumes a single electronically active bond, with subsequent vibrational coupling to the other bonds of the molecule [168, 169]. And the work of Gianturco and Lucchese has suggested that one of the most important contributions to DNA radiation-induced decay channels involves the creation of photoionized elec-

trons that undergo low-energy dissociative attachment, a process that depends vitally on energy redistribution between electronic and nuclear excitation modes [170, 171].

Bibliography

[1] J. J. Balmer, Ann. Phys. Chem. **25**, 80 (1885).

[2] J. R. Rydberg, Kgl. Svenska Akad. Handl. **23**, 1 (1889).

[3] G. Onida, L. Reining, and A. Rubio, Rev. Mod. Phys. **74**, 601 (2002).

[4] J. C. Boyce, Rev. Mod. Phys. **13**, 1 (1941).

[5] G. Herzberg, J. Mol. Spectrosc. **33**, 147 (1970).

[6] P. M. Dehmer and W. A. Chupka, J. Chem. Phys. **65**, 2243 (1976).

[7] E. Reinhold, W. Hogervorst, and W. Ubachs, Phys. Rev. Lett. **78**, 2543 (1997).

[8] E. Reinhold, W. Hogervorst, and W. Ubachs, Chem. Phys. Lett. **296**, 411 (1998).

[9] E. McCormack and E. Eyler, Phys. Rev. Lett. **66**, 1042 (1991).

[10] E. McCormack, S. T. Pratt, P. M. Dehmer, and J. L. Dehmer, J. Chem. Phys. **98**, 8370 (1993).

[11] M. D. Lukin *et al.*, Phys. Rev. Lett. **87**, 037901 (2001).

[12] M. D. Lukin, Rev. Mod. Phys. **75**, 457 (2003).

[13] S. Haroche, Fortschr. Phys. **51**, 388 (2003).

[14] C. Rangan, J. Ahn, D. N. Hutchinson, and P. H. Bucksbaum, Phys. Rev. A **66**, 022312 (2002).

[15] J. Ahn, T. C. Weinacht, and P. H. Bucksbaum, Science **287**, 463 (2000).

[16] T. Gallagher, P. Pillet, M. P. Robinson, B. Laburthe-Tolra, and M. W. Noel, J. Opt. Soc. Am. B **20**, 1091 (2003).

[17] T. C. Killian, M. J. Lin, S.Kulin, R. Dumke, S. D. Bergeson, and S. L. Ralston, Phys. Rev. Lett. **86**, 3759 (2001).

[18] S. Kulin, T. C. Killian, and S. D. Bergeson, Phys. Rev. Lett. **85**, 318 (2000).

[19] T. C. Killian, S. Kulin, S. D. Bergeson, L. A. Orozco, C. Orzel, and S. L. Ralston, Phys. Rev. Lett. **83**, 4776 (1999).

[20] J. R. R. Verlet, V. G. Stavros, R. S. Minns, and H. H. Fielding, Phys. Rev. Lett. **89**, 263004 (2003).

[21] W. C. Magno, R. B. Prandini, P. Nussenzveig, and S. S. Vianna, Phys. Rev. A **63**, 063406 (2001).

[22] C. Boisseau, I. Simbotin, and R. Côté, Phys. Rev. Lett. **88**, 133004 (2002).

[23] A. L. de Oliveira, M. W. Mancini, V. S. Bagnato, and L. G. Marcassa, Phys. Rev. Lett. **90**, 143002 (2003).

[24] F. Merkt, Chimia **54**, 89 (2000).

[25] B. H. Bransden and C. J. Jochain, Physics of Atoms and Molecules (Longman Group Limited, Essex, 1983).

[26] H. Friedrich, Theoretical Atomic Physics (Springer-Verlag, Berlin, 1990).

[27] C. H. Greene and C. Jungen, Adv. At. Mol. Phys. **21**, 51 (1985).

[28] V. Kokoouline and C. H. Greene, Phys. Rev. A **68**, 012703 (2003).

[29] W. Kolos and L. Wolniewicz, J. Chem. Phys. **41**, 3674 (1964).

[30] W. Kolos and L. Wolniewicz, J. Chem. Phys. **49**, 404 (1968).

[31] D. M. Bishop and L. M. Cheung, Phys. Rev. A **16**, 640 (1977).

[32] L. Wolniewicz and J. D. Poll, J. Chem. Phys. **73**, 6225 (1980).

[33] W. Kolos and K. Szalewicz, J. Chem. Phys. **84**, 3278 (1986).

[34] B. D. Esry and H. R. Sadeghpour, Phys. Rev. A **60**, 3604 (1999).

[35] L. Wolniewicz, J. Chem. Phys. **78**, 6173 (1983).

[36] W. Kolos and L. Wolniewicz, J. Chem. Phys. **48**, 3672 (1968).

[37] C. H. Greene and C. Jungen, Phys. Rev. Lett. **55**, 1066 (1985).

[38] H. Gao and C. H. Greene, J. Chem. Phys. **91**, 3988 (1989).

[39] H. Gao and C. H. Greene, Phys. Rev. A **42**, 6946 (1990).

[40] C. Jungen and O. Atabek, J. Chem. Phys. **66**, 5584 (1977).

[41] R. M. More, Phys. Rev. A **3**, 1217 (1971).

[42] R. M. More, Phys. Rev. A **4**, 1782 (1971).

[43] C. Greene, U. Fano, and G. Strinati, Phys. Rev. A **19**, 1485 (1979).

[44] M. Aymar, C. H. Greene, and E. Luc-Koenig, Rev. Mod. Phys. **68**, 1015 (1996).

[45] U. Fano, Phys. Rev. A **2**, 353 (1970).

[46] M. Raoult and C. Jungen, J. Chem. Phys. **74**, 3388 (1980).

[47] C. Jungen and D. Dill, J. Chem. Phys. **73**, 3338 (1980).

[48] F. Robicheaux, Phys. Rev. A **48**, 4162 (1993).

[49] P. M. Dehmer and W. A. Chupka, J. Chem. Phys. **79**, 1569 (1983).

[50] N. Y. Du and C. H. Greene, J. Chem. Phys. **85**, 5430 (1986).

[51] E. L. Hamilton and C. H. Greene, Phys. Essays **13**, 265 (2000).

[52] H. Gao, C. Jungen, and C. H. Greene, Phys. Rev. A **47**, 4877 (1993).

[53] C. Jungen, Phys. Rev. Lett. **53**, 2394 (1984).

[54] J. A. Stephens and C. H. Greene, J. Chem. Phys. **103**, 5470 (1995).

[55] M. Glass-Maujean, J. Breton, and P. M. Guyon, Z. Phys. D **5**, 189 (1987).

[56] G. M. Greetham, U. Hollenstein, R. Seiler, W. Ubachs, and F. Merkt, Phys. Chem. Chem. Phys. **5**, 2528 (2003).

[57] E. Fermi, Nuovo Cimento **11**, 159 (1934).

[58] E. Fermi, Ric. Scientifica **7**, 13 (1936).

[59] M. H. Mittleman, Phys. Rev. **162**, 81 (1967).

[60] N. Allard and J. Kielkopf, Rev. Mod. Phys. **54**, 1103 (1982).

[61] I. L. Beigman and V. S. Lebedev, Phys. Rep. **20**, 95 (1995).

[62] L. P. Presnyakov, Phys. Rev. A **2**, 1720 (1970).

[63] Y. N. Demkov and V. N. Ostrovskii, Zero-Range Potentials and Their Applications in Atomic Physics (Plenum Press, New York, 1988 (USSR, 1975)).

[64] G. K. Ivanov, Opt. Spectrosc. (USSR) **37**, 361 (1974).

[65] V. S. Dubov, J. Chem. Phys. **97**, 7342 (1992).

[66] V. Dubov and H. Rabitz, J. Chem. Phys. **104**, 551 (1996).

[67] E. de Prunelé, Phys. Rev. A **35**, 496 (1987).

[68] G. K. Ivanov, Opt. Spectrosc. (USSR) **43**, 617 (1977).

[69] N. Y. Du and C. H. Greene, Phys. Rev. A **36**, 971 (1987).

[70] N. Y. Du and C. H. Greene, J. Chem. Phys. **390**, 6347 (1989).

[71] C. H. Greene, A. S. Dickinson, and H. R. Sadeghpour, Phys. Rev. Lett. **85**, 2458 (2000).

[72] J. Léonard, M. Walhout, A. P. Mosk, T. Muller, M. Leduc, and C. Cohen-Tannoudji, Phys. Rev. Lett. **91**, 073203 (2003).

[73] B. E. Granger, E. L. Hamilton, and C. H. Greene, Phys. Rev. A **64**, 042508 (2001).

[74] A. A. Khuskivadze, M. I. Chibisov, and I. I. Fabrikant, Phys. Rev. A **66**, 042709 (2002).

[75] A. Omont, J. Phys. (Paris) **38**, 1343 (1977).

[76] C. Bahrim, U. Thumm, and I. I. Fabrikan, Phys. Rev. A **63**, 042710 (2001).

[77] C. Bahrim and U. Thumm, Phys. Rev. A **64**, 022716 (2001).

[78] C. Bahrim, U. Thumm, and I. I. Fabrikant, Phys. Rev. A **61**, 022722 (2000).

[79] E. L. Hamilton, C. H. Greene, and H. R. Sadeghpour, J. Phys. B: At. Mol. Opt. Phys. **35**, 199 (2002).

[80] W. E. Cooke and T. F. Gallagher, Phys. Rev. A **21**, 588 (1980).

[81] J. Pascale, Phys. Rev. A **28**, 1632 (1983).

[82] J. Brust and C. H. Greene, Phys. Rev. A **56**, 2005 (1997).

[83] D. B. Khrebtukov and I. I. Fabrikant, Phys. Rev. A **51**, 4675 (1995).

[84] L. Hostler and R. H. Pratt, Phys. Rev. Lett. **10**, 469 (1963).

[85] L. Hostler, J. Math. Phys. **5**, 591 (1964).

[86] L. Hostler, J. Math. Phys. **8**, 642 (1967).

[87] Y. N. Demkov and G. F. Drukarev, Sov. Phys. JETP **20**, 614 (1964).

[88] Y. N. Demkov and G. F. Drukarev, Sov. Phys. JETP **22**, 271 (1965).

[89] Y. N. Demkov and G. F. Drukarev, Sov. Phys. JETP **54**, 650 (1981).

[90] S. P. Andreev, B. M. Karnakov, V. D. Mur, and V. A. Polunin, Sov. Phys. JETP **59**, 506 (1984).

[91] B. M. Karnadov and V. D. Mur, Sov. Phys. JETP **60**, 657 (1984).

[92] L. D. Landau and E. M. Lifshitz, Course of Theoretical Physics (Pergamon Press, London, 1959).

[93] S. V. Tkachenko, Sov. Phys. JETP **61**, 1149 (1985).

[94] M. I. Chibisov, A. M. Ermolaev, F. Brouillard, and M. H. Cherkani, Phys. Rev. Lett. **84**, 451 (2000).

[95] M. I. Chibisov, A. A. Khuskivadze, and I. I. Fabrikant, J. Phys. B: At. Mol. Opt. Phys. **35**, L193 (2002).

[96] F. I. Dalidchik and G. K. Ivanov, Teor. Eksp. Khim. **8**, 9 (1972).

[97] V. A. Davydkin, B. A. Zon, N. L. Manakov, and L. P. Rapoport, Sov. Phys. JETP **133**, 70 (1971).

[98] U. Fano, Phys. Rev. A **24**, 619 (1981).

[99] D. Harmin, in Atoms in Strong Fields, NATO ASI, edited by C. Nicolaides (Plenum Press, New York, NY, 1988).

[100] D. J. Armstrong and C. H. Greene, Phys. Rev. A **50**, 4956 (1994).

[101] E. Luc-Koenig, S. Liberman, and J. Pinard, Phys. Rev. A **20**, 519 (1979).

[102] M. P. Strand and W. P. Reinhardt, J. Chem. Phys. **70**, 3812 (1979).

[103] P. D. Robinson, Proc. Phys. Soc. London **71**, 828 (1958).

[104] C. A. Coulson and P. D. Robinson, Proc. Phys. Soc. London **71**, 815 (1958).

[105] B. R. Judd, Angular Momentum Theory for Diatomic Molecules (Academic Press, New York, 1975).

[106] S. M. Sung and D. R. Herschbach, J. Chem. Phys. **95**, 7437 (1991).

[107] A. Sommerfeld, Atomic Structure and Spectral Lines (Methuen and Co. Ltd., London, 1934).

[108] H. A. Erikson and E. L. Hill, Phys. Rev. **75**, 29 (1949).

[109] Y. Duan and J. M. Yuan, Eur. Phys. J. D **6**, 319 (1999).

[110] M. C. Gutzwiller, Chaos in Classical and Quantum Mechanics (Springer-Verlag, New York, 1990).

[111] A. M. O. de Almeida, Hamiltonian Systems: Chaos and Quantization (Cambridge University Press, Cambridge, 1988).

[112] B. I. Schneider, Phys. Rev. A **11**, 1957 (1975).

[113] B. I. Schneider and P. J. Hay, Phys. Rev. A **13**, 1923 (1976).

[114] P. G. Burke, I. Mackey, and I. Shimamura, J. Phys. B: At. Mol. Opt. Phys. **10**, 2497 (1977).

[115] B. I. Schneider, M. LeDourneuf, and P. G. Burke, J. Phys. B: At. Mol. Opt. Phys. **12**, L365 (1979).

[116] A. Giusti, J. Phys. B: At. Mol. Opt. Phys. **13**, 3867 (1980).

[117] F. H. Mies, J. Chem. Phys. **80**, 2514 (1984).

[118] C. H. Greene, A. R. P. Rau, and U. Fano, Phys. Rev. A **22**, 149 (1982).

[119] J. Burke, C. H. Greene, and J. L. Bohn, Phys. Rev. A **81**, 3355 (1998).

[120] U. Fano and C. M. Lee, Phys. Rev. Lett. **31**, 1573 (1973).

[121] C. Jungen and S. C. Ross, Phys. Rev. A **55**, R2503 (1997).

[122] S. C. Ross, C. Jungen, and A. Matzkin, Can. J. Phys. **79**, 561 (2001).

[123] E. P. Wigner and L. Eisenbud, Phys. Rev. **72**, 29 (1947).

[124] A. M. Lane and R. G. Thomas, Rev. Mod. Phys. **30**, 257 (1958).

[125] G. Raşeev and H. L. Rouzo, Phys. Rev. A **27**, 268 (1983).

[126] W. Kohn, Phys. Rev. **74**, 1763 (1948).

[127] C. H. Greene, Phys. Rev. A **28**, 2209 (1983).

[128] H. L. Rouzo and G. Raşeev, Phys. Rev. A **29**, 1214 (1984).

[129] C. H. Greene, in Fundamental Processes of Atomic Dynamics, edited by J. S. Briggs, H. Kleinpoppen, and H. O. Lutz (Plenum Publishing Corporation, Essex, 1988).

[130] F. Robicheaux, U. Fano, M. Cavegnero, and D. A. Harmin, Phys. Rev. A **35**, 3619 (1987).

[131] G. Gamow, Z. Phys. **51**, 204 (1928).

[132] V. Weisskopf and E. P. Wigner, Z. Phys. **63**, 54 (1930).

[133] P. Kapur and R. Peierls, Proc. R. Soc. London A **166**, 277 (1938).

[134] A. J. F. Siegert, Phys. Rev. **56**, 750 (1939).

[135] R. M. More and E. Gerjuoy, Phys. Rev. A **7**, 1288 (1973).

[136] R. G. Newton, Scattering Theory of Waves and Particles (Academic, New York, 1966).

[137] H.-D. Meyer and O. Walter, J. Phys. B: At. Mol. Opt. Phys. **15**, 3647 (1982).

[138] J. N. Bardsley and R. R. Junker, J. Phys. B: At. Mol. Opt. Phys. **5**, L178 (1972).

[139] R. Yaris and H. S. Taylor, Chem. Phys. Lett. **66**, 505 (1979).

[140] C. W. McCurdy and T. N. Rescigno, Phys. Rev. A **20**, 2346 (1979).

[141] W. P. Reinhardt, Ann. Rev. Phys. Chem. **33**, 223 (1982).

[142] O. I. Tolstikhin, V. N. Ostrovsky, and H. Nakamura, Phys. Rev. A **58**, 2077 (1998).

[143] H. W. Jang and J. C. Light, Phys. Rev. A **51**, 1277 (1995).

[144] O. I. Tolstikhin, V. N. Ostrovsky, and H. Nakamura, Phys. Rev. Lett. **79**, 2026 (1997).

[145] H. Bachau, E. Cormier, P. Decleva, J. E. Hansen, and F. Martín, Rep. Prog. Phys. **64**, 1815 (2001).

[146] C. de Boor, A Practical Guide to Splines (Springer, New York, 1978).

[147] B. Friedman, Principles and Techniques of Applied Mathematics (John Wiley & Sons, Inc., New York, 1956).

[148] D. L. Huestis, J. Math. Phys. (N.Y.) **16**, 2148 (1975).

[149] D. Baye, J. Goldbeter, and J.-M. Sparenberg, Phys. Rev. A **65**, 052710 (2002).

[150] G. V. Sitnikov and O. I. Tolstikhin, Phys. Rev. A **67**, 032714 (2003).

[151] C. D. Lin, Phys. Rep. **257**, 1 (1995).

[152] S. Yoshida, S. Watanabe, C. O. Reinhold, and J. Burgdorfer, Phys. Rev. A **60**, 1113 (1999).

[153] S. Tanabe *et al.*, Phys. Rev. A **63**, 052721 (2001).

[154] T. Seideman and W. H. Miller, J. Chem. Phys. **95**, 1768 (1991).

[155] V. Ryaboy and N. Moiseyev, J. Chem. Phys. **98**, 9618 (1993).

[156] M. Seaton, Rep. Prog. Phys. **46**, 167 (1983).

[157] B. E. Granger and C. H. Greene, Phys. Rev. A **62**, 012511 (2000).

[158] B. E. Granger, Ph.D. thesis, University of Colorado at Boulder, 2001.

[159] A. Bohm, S. Maxson, M. Loewe, and M. Gadella, Physica A **236**, 485 (1997).

[160] R. de la Madrid, A. Bohm, and M. Gadella, Fortschr. Phys. **50**, 185 (2002).

[161] A. Bohm, N. L. Harshman, and H. Walther, Phys. Rev. A **66**, 012107 (2002).

[162] R. Browning and J. Fryar, J. Phys. B: At. Mol. Opt. Phys. **6**, 364 (1973).

[163] C. Backx, G. R. Wright, and M. J. van der Wiel, J. Phys. B: At. Mol. Opt. Phys. **9**, 315 (1976).

[164] Y. M. Chung, E.-M. Lee, and J. A. R. Samson, J. Chem. Phys. **99**, 885 (1993).

[165] A. L. Ford, K. K. Docken, and A. Dalgarno, Asrophys. J. **195**, 819 (1975).

[166] T. F. O'Malley, Phys. Rev. **150**, 14 (1966).

[167] K. B. MacAdam and C. S. Hwang, Rev. Sci. Instr. **74**, 2267 (2003).

[168] K. Aflatooni, G. A. Gallup, and P. D. Burrow, J. Phys. Chem. A **102**, 6205 (1998).

[169] P. D. Burrow *et al.*, J. Phys. B: At. Mol. Opt. Phys. **31**, L1009 (1998).

[170] F. A. Gianturco and R. R. Lucchese, Int. Rev. Phys. Chem. **15**, 429 (1996).

[171] F. A. Gianturco and R. R. Lucchese, Phys. Rev. A **64**, 32706 (2001).